AD NUMBER
AD390481
CLASSIFICATION CHANGES
TO: unclassified
FROM: confidential
LIMITATION CHANGES
TO: Approved for public release, distribution unlimited
FROM: Distribution authorized to U.S. Gov't. agencies and their contractors; Critical Technology; FEB 1968. Other requests shall be referred to Air Force Rocket Propulsion Laboratory, Research and Technolgoy Division, Attn: RPPR/STINFO, Edwards AFB, CA 93523. NOFORN.
AUTHORITY
AFRPL ltr 30 Jul 1973; AFRPL ltr 30 Jul 1973

SECURITY MARKING

The classified or limited status of this report applies to each page, unless otherwise marked.
Separate page printouts MUST be marked accordingly.

THIS DOCUMENT CONTAINS INFORMATION AFFECTING THE NATIONAL DEFENSE OF THE UNITED STATES WITHIN THE MEANING OF THE ESPIONAGE LAWS, TITLE 18, U.S.C., SECTIONS 793 AND 794. THE TRANSMISSION OR THE REVELATION OF ITS CONTENTS IN ANY MANNER TO AN UNAUTHORIZED PERSON IS PROHIBITED BY LAW.

NOTICE: When government or other drawings, specifications or other data are used for any purpose other than in connection with a definitely related government procurement operation, the U. S. Government thereby incurs no responsibility, nor any obligation whatsoever; and the fact that the Government may have formulated, furnished, or in any way supplied the said drawings, specifications, or other data is not to be regarded by implication or otherwise as in any manner licensing the holder or any other person or corporation, or conveying any rights or permission to manufacture, use or sell any patented invention that may in any way be related thereto.

AFRPL-TR-68-76

LPC REPORT NO. 720-F
COPY NO.

(unclassified title)

FINAL REPORT KINETICS OF DECOMPOSITION OF SOLID OXIDIZERS

FINAL REPORT AFRPL-TR-68-76

FEBRUARY 1968

Lockheed Propulsion Company
A Division of Lockheed Aircraft Corporation
Redlands, California

SPECIAL HANDLING REQUIRED
NOT RELEASABLE TO FOREIGN NATIONALS

GROUP – 4
Downgraded at 3 year intervals;
declassified after 12 years

FOREIGN NATIONAL. EMPLOYEES OF THE CONTRACTOR OR SUBCONTRACTOR(S), INCLUDING THOSE POSSESSING CANADIAN OR UNITED KINGDOM RECIPROCAL CLEARANCE, ARE NOT AUTHORIZED ACCESS TO CLASSIFIED INFORMATION RESULTING FROM, OR USED IN THE PERFORMANCE OF, THIS CONTRACT UNLESS AUTHORIZED IN WRITING BY THE PROCURING CONTRACT ACTIVITY.

AIR FORCE ROCKET PROPULSION LABORATORY
RESEARCH AND TECHNOLOGY DIVISION
AIR FORCE SYSTEMS COMMAND
UNITED STATES AIR FORCE
EDWARDS, CALIFORNIA

(unclassified title)

FINAL REPORT
KINETICS OF DECOMPOSITION OF SOLID OXIDIZERS

SPECIAL HANDLING REQUIRED
NOT RELEASABLE TO FOREIGN NATIONALS

GROUP – 4
Downgraded at 3 year intervals;
declassified after 12 years

This document contains information affecting the national defense of the United States, within the meaning of the Espionage Laws, Title 18, U.S.C., Sections 793 and 794. Its transmission or the revelation of its contents in any manner to an unauthorized person is prohibited by law.

FOREIGN NATIONAL EMPLOYEES OF THE CONTRACTOR OR SUBCONTRACTOR(S), INCLUDING THOSE POSSESSING CANADIAN OR UNITED KINGDOM RECIPROCAL CLEARANCE, ARE NOT AUTHORIZED ACCESS TO CLASSIFIED INFORMATION RESULTING FROM, OR USED IN THE PERFORMANCE OF, THIS CONTRACT UNLESS AUTHORIZED IN WRITING BY THE PROCURING CONTRACT ACTIVITY.

In
docu
t
b

APPR/REQUESTINFO
Edwards, Calif 93523

FOREWORD

This is the final report on work performed under Air Force Contract No. AF 04(611)-11385, "Kinetics of Decomposition of Solid Oxidizers," covering the period from 1 December 1965 through 31 January 1968. The contract is assigned to LPC, Redlands, California, and is monitored by Lt. R. Foscante, AFRPL, Edwards, California.

Technical effort under this contract was performed by Dr. G.E. Myers, Y.A. Tajima, Dr. J.A. Hammond, W.G. Stapleton, and W. Koehler. Mrs. B. Knight assisted in the data reduction. Dr. R. Plock, of the University of Redlands was consultant to the program, developing the computer program for calculating ribbon thermal profiles. R.A. Lane of the LPC Mathematical Sciences group performed the computer calculations under the direction of Dr. Plock. Dr. W.E. Baumgartner acted as Program Manager.

This report contains information regarding the structure and reactions of specific NF oxidizers and is therefore classified CONFIDENTIAL.

Publication of this report does not constitute Air Force approval of the report's findings and conclusions. It is published only for the exchange and stimulation of ideas.

William Ebelke
Colonel, USAF
Chief, Propellant Division

UNCLASSIFIED ABSTRACT

The thermal decomposition of high energy oxidizers and binders has been studied in order to derive data which can be used to relate molecular structures, chemical kinetic rate data, and thermal decomposition mechanism to explosive sensitivity, shelflife, and combustion behavior. Fast vacuum pyrolysis techniques were combined with a Bendix Time-of-Flight mass spectrometer for the study of the initial reactions occurring during thermal decomposition in INFO-635, PFABDE, PBEP, NC, and HP_2. Primary decomposition mechanisms were postulated, and activation energies calculated. Indications for a heating rate dependence of the decomposition mechanisms were found for INFO-635, PFABDE, and PBEP.

GLOSSARY

(U) A	The Arrhenius Pre-exponential Frequency Factor from the kinetic rate equation
(U) B	An arbitrary mass spectrometer system constant
(U) CRT	Cathode Ray Tube
(U) DSC	Differential Scanning Calorimetry
(U) DTA	Differential Thermal Analysis
(U) E	Activation energy
(U) FMTA	Flash Mass Thermal Analysis
(U) HP_2	Hydrazinium Diperchlorate
(U) INFO-635P	2-Tris (difluoramino) methoxy ethylammonium perchlorate
(U) k	Reaction rate constant
(U) m/e	Mass to charge ratio of ions in the mass spectrometer, commonly used for mass identification
(U) MTA	Mass Thermal Analysis
(U) NC	Nitrocellulose
(C) PBEP	Poly 1, 2-bis(difluoramino) 2, 3-epoxy propane
(C) PFABDE	Poly 1, 4-bis[tris(difluoramino) methoxy butene oxide-2, 3]
(U) SCR	Silicon-controlled rectifier
(U) TGA	Thermo Gravimetric Analysis
(U) TOF	Bendix Time-of-Flight Mass Spectrometer
(U) UJT	Unijunction Transistor
(U) ECH	Epichlorohydrin
(U) PECH	Polyepichlorohydrin

(The reverse is blank)

TABLE OF CONTENTS

TABLE OF CONTENTS (Continued)

LIST OF ILLUSTRATIONS

LIST OF ILLUSTRATIONS (Continued)

LIST OF ILLUSTRATIONS (Continued)

(The reverse is blank)

LIST OF TABLES

(This Page Unclassified)

SECTION I

SUMMARY

(U) A new method of mass spectral thermal analysis (MTA) was developed and applied to determine the energetics and kinetics of the initiating reactions in the decomposition of solid propellant ingredients and propellants. The technique involves the pyrolysis of very small quantities of the test material in the close vicinity of the electron beam of a time-of-flight mass spectrometer for recording at high time resolution the time-dependent composition of the primary pyrolysis species as the sample is pyrolyzed under programmed temperature-time conditions. The resulting data are used to derive the Arrhenius rate parameters, thereby providing a basis for relating thermal stability, explosive sensitivity, and ballistic behavior to chemical structure.

(U) Microgram quantities of the materials are deposited upon a small platinum ribbon that is heated ohmically by battery current or by condenser discharge. Using battery current, a linear heating rate is obtained that can be varied from 10^0C/sec to 1000^0C/sec (dynamic heating). With the condenser discharge, the sample temperature is brought instantaneously (~10 microseconds) to a predetermined temperature that is maintained for ~50 milliseconds (isothermal heating). Computer programs were derived for evaluating time-dependent sample temperatures across the ribbon.

(U) The heating process is monitored by a specially designed Wheatstone Bridge circuit, and is synchronized with the spectral timing sequence of the mass spectrometer. Signals are fed by various techniques into oscilloscopes for cinematographic recording.

(U) To verify accuracy of the data obtained, test runs were performed with materials possessing decomposition kinetics that had been studied by other workers employing different techniques. Good agreement was obtained with respect to the observed mechanism of decomposition and the activation energies involved. With nitrocellulose as the test material, the MTA method gave an activation energy of ~95 Kcal/mole for the initiating reaction as compared to the value of 100 Kcal/mole obtained by R. Musso using an Argon sweep over the burning material; for hydrazinium diperchlorate (HP_2), the values were 23 Kcal/mole for the initiating reaction by the MTA method as compared with 23.5 Kcal/mole obtained by Grelecki and Cruice, using time-to-acceleration of heated samples contained in sealed, evacuated bulbs.

(U) The method then was applied to relate the explosive sensitivity of NF oxidizers to chemical structure. The materials that were studied included INFO-635, PFABDE, and PBEP.

(U) INFO-635 thermal decomposition was shown to proceed by the loss of perchloric acid, followed by scission of the remaining fragment at the oxygen-methylene bond.

(C) The isothermal decomposition of PFABDE appears to be initiated by the loss of a complete tris-(difluoramino)methoxy side-chain unit. Under dynamic heating conditions, on the other hand, PFABDE first loses difluoramino radicals, followed by a temporary stabilization, probably by cyclization. Pyrolysis then proceeds by elimination of the remainder of the (difluoramino) methoxy group. The data provide an activation energy of ~77 Kcal/mole for the initiating reaction. This is a comparatively high value, and it is presumed to be responsible for the high explosive sensitivity of this material.

(C) PBEP was shown to decompose by a free-radical-induced chain unzipping mechanism. This mechanism appears to be initiated by structural defects, end groups or impurities present; it involves an activation energy of ~18 Kcal/mole, as compared with ~77 Kcal/mole for PFABDE, which could explain the lesser sensitivity to impact of PBEP. In working with this latter material, significant differences in the decomposition patterns were observed between samples representing different molecular weight fractions or production lots. Efforts were initiated to apply the MTA method as a quality control technique.

(U) Because sample heating rates could be varied from 100^0C/sec to 10^7 ^{0}C/sec, and because the TOF mass spectrometer provides the necessary high analytical response for studying very rapid decomposition (10^4 spectra/second), it was possible to study the effects of heating rates upon the mechanism of sample pyrolysis. Distinct changes in the spectral decomposition patterns were observed with various materials, implying changes in decomposition mechanism as the heating rates were increased. The data suggest that heating rate could be an important parameter affecting the mechanism and the energetics of explosives decomposition, and that kinetic measurements performed under low heating rates may be of limited significance in rationalizing explosive sensitivity and interior ballistic behavior. A more careful investigation of the effects of heating rates is indicated.

SECTION II

INTRODUCTION

1. OBJECTIVE

The objective of this program was to obtain correlations between impact sensitivity and molecular structure of high energy oxidizer materials through a study of their thermal decomposition kinetics resulting from isothermal and rapid heating.

2. BACKGROUND

Despite the considerable amount of effort that has been and is being devoted to the study of oxidizer sensitivity, understanding of the molecular basis for their sensitivity is poor. Solid fluorine oxidizers, for example, possess sensitivities appearing to be at variance with their reasonable thermal stabilities and differing in an as yet unexplained fashion with molecular structure, physical form, and mode of excitation (impact, friction, and spark).

Basically, inability to rationalize the behavior of these materials arises from lack of knowledge as to the molecular events occurring during the detonation process. The usual picture of impact detonation, for example, assumes localization of the impact energy within microscopic volume elements, with consequent initiation of thermal decomposition. Exothermic reactions in the decomposition process produce further localized adiabatic heating and very rapid escalation of reaction rate to the point of detonation. Obviously, therefore, a complete understanding of detonation sensitivity requires a detailed understanding of the thermal decomposition kinetics and mechanism at temperatures and times corresponding to detonation processes, i.e., at temperatures of several hundreds of degrees centigrade and times approximately between 0.05 and 50 milliseconds. The dependence of sensitivity upon molecular structure, for example, can be expected to differ if the explosive chain set up in the "hot spot" is strictly a thermal one or is additionally complicated by chemical chains, e.g., free radicals.

Simulation of detonation conditions in such a fashion that confident kinetic conclusions may be drawn is a formidable experimental task. In point of fact, it is unlikely that any one experimental approach will elucidate completely all facets of the process. Ideally, the following experimental requirements should be met:

- Isothermal kinetic measurements during time periods between 0.05 and 50 milliseconds after initiation
- Heat-up of sample to a known temperature in times short as compared with the above, i.e., heat-up in microseconds; this, plus the above, necessitates very small samples in intimate contact with a thermostat.

- Identification of reaction products and intermediates (free radicals, ionic species)

- Quantitative measurements of rates of decomposition of starting material, rates of production of intermediate species and products, and lifetimes of intermediate species

It w the purpose of this program to apply a newly developed technique, fl.sh mass thermal analysis (FMTA), to study the chemical phenomena underlying NF oxidizer explosive sensitivity. Initially, emphasis was to be placed upon the study of solid NF oxidizer decomposition kinetics and energetics. However, because of the change in emphasis toward NF polymers, e.g., PBEP, plans were modified to provide for a more intensive study of phenomena (structure, impurities) controlling the sensitivity and stability of these polymeric NF materials.

3. EXPERIMENTAL APPROACH

One technical approach expected to meet the experimental requirements of this program involves the very rapid pyrolysis of very thin sample films deposited upon a heating element, the latter being inserted adjacent to the ionization region of a time-of-flight mass spectrometer. This general technique was developed previously (Ref. 1), and the results obtained provided confidence that this method, with some modifications, would serve the purpose of this program. This technique combines the following potential advantages:

- Ability to achieve programmed, high sample heating rates

- Ability to detect at high analytical sensitivity the primary decomposition species

- Ability to operate at high time resolution relying upon the high spectral frequency (10^4 spectra per second) of a mass spectrometer operating on the time-of-flight principle

The early experimental arrangement was as follows: Microgram quantities of the solid material were coated on a platinum (Pt) wire heated in microseconds to several hundred degrees centigrade by a capacitor discharge. Th e coated Pt wire was located within approximately two centimeters of the ionizing electron beam in a Bendix Time-of-Flight mass spectrometer. Gaseous decomposition products therefore were detected and measured every 100 microseconds. Wire temperatures were measured by incorporating the wire in a Wheatstone Bridge circuit that became imbalanced as the wire temperature (resistance) rose. Simultaneously with the capacitor discharge, a battery current was imposed upon the bridge that provided a known bridge input for temperature measurement, and also helped to maintain the wire at constant temperature as the capacitor current dissipated. The mass spectra were recorded using photographs of the oscilloscope tube face upon which the mass spectra were displayed. Recording of the mass spectra every one hundred microseconds was accomplished using either high-speed cinematography, or the Z-axis modulation procedure

(Ref. 2), in which each mass peak is presented on an oscilloscope as a time-dependent series of dots with intensity proportional to concentration.

The Bendix Time-of-Flight mass spectrometer was used as the instrument with which to analyze the gaseous products from the decomposing/reacting materials because it is capable of acquiring data at a rate fast enough to keep pace with the pyrolysis reactions at high temperatures/heating rates. The mass spectrometer operates with the sample in a vacuum, so that only the primary decomposition species are studied. Close proximity of the sample to the ionizing electron beam assures that the primary species undergo no collisions before analysis, i.e., no secondary reactions. The mass spectra also are sensitive to the structure of the gaseous species, so that identification of the thermal fragment structure is possible. The mass spectrometer also is capable of continually analyzing the products from many simultaneous reactions, so that the relative importance of different reaction mechanisms at different temperatures can be evaluated.

The electrically heated platinum filament was selected for use as sample holder/heater for very small samples in order to heat the samples at rates simulating those encountered in detonation and combustion processes. The well-known linear temperature dependence of the electrical resistance of Pt permits use of the heater as its own thermometer, thus eliminating errors associated with attaching thermocouples or other heat sensing devices. The small sample size (10 to 20 micrograms) assures the close compliance of the sample temperature to the filament temperature. The low thermal mass of the filament and sample permit the use of simple techniques, such as capacitor or battery discharge to achieve the desired heating rates.

The Pt filament used was originally a wire, but this was changed to a ribbon to facilitate, and to improve, accuracy of sample preparation and to improve the geometric factors involved in the sampling of the gases leaving the surface of the filament during pyrolysis.

To study the effects of heating rate on the kinetic mechanisms, the capacitor discharge circuit was replaced by a 24-volt battery. This dropped the heating rate from millions of degrees centigrade per second to hundreds of degrees per second, stretching the duration of an experiment to as much as two seconds. Consequently, high-speed cinematography was capable of achieving such suitable time and temperature resolution of the pyrolysis species mass spectra that the tasks of data reduction and reaction mechanism determination were facilitated.

The use of the mass spectrometer for mass analysis during sample heating is known as Mass Thermal Analysis (MTA). In the current work, the terminology has been extended, for convenience, to isothermal FMTA and dynamic FMTA. The F stands for "flash" heating. Compared with other methods, the current heating rates are fast enough to justify the use of the term, flash heating, and by combination with the mass thermal analysis technique, the process is best described as Flash Mass Thermal Analysis, or FMTA. The two methods of sample heating during pyrolysis are exactly analogous to those used in thermogravimetric studies. Hence, isothermal FMTA refers to the study of reactions occurring when the sample is flash heated to an isothermal condition, and held there during the experiment. Dynamic FMTA refers to the study of reactions occurring during a linearly programmed temperature rise.

(The reverse is blank)

SECTION III

EXPERIMENTAL MEASUREMENTS

1. SUMMARY

Thermal decomposition rates of propellants/propellant ingredients can be extremely high. The instruments and techniques used to study the pyrolysis of these compounds should, therefore, be capable of acquiring data at rates characteristic of the processes. The mass thermal analytical technique developed for such investigations at LPC uses the fast scan speed of the Bendix TOF mass spectrometer. Figure 1 shows a schematic of the experiments. The sample, weighing 5 to 20 micrograms, is coated on a resistive platinum ribbon located 2 millimeters from the ionizing electron beam of the mass spectrometer. The ribbon and sample are heated by a battery discharge for slow heating rates or a capacitor discharge for fast heating rates. The ribbon forms one arm of a Wheatstone bridge that determines the temperature-time profile of the ribbon and sample. For slow heating rates, the mass spectra displayed on an oscilloscope are monitored continuously by fast cinematography. For fast heating rates, the mass spectra are recorded photographically using the Z-axis modulation of the oscilloscope display. Alternatively, individual m/e peaks may be monitored as a function of time.

This section contains the details of the experimental arrangement, including mechanical modifications to the Bendix TOF mass spectrometer, the electrical circuitry required for the sample heating, and the electronic circuitry necessary to acquire meaningful data. Because the pyrolysis ribbon temperature measurement is intimately connected with its heating, the mathematical models necessary to obtain temperature data from the observed electrical parameters are derived. A computer-predicted temperature profile of the ribbon agrees well with the experimental value.

2. APPARATUS

a. The Bendix Time-of-Flight (TOF) Mass Spectrometer

The TOF instrument consists basically of three sections: the ionization chamber, the flight tube, and the detector multiplier. In the normal mode of operation, ions are produced by a beam of electrons of controlled energy every 50 to 100 microseconds. (A 100-microsecond cycle can be easily achieved.) Immediately after the electron pulse, voltage pulses are applied, accelerating into the flight tube positive ions with identical kinetic energies per unit charge. Because the flight tube is field-free, the ions travel at velocities proportional to $\sqrt{e/m}$ (e and m are charge and mass, respectively) and thus arrive at the detector at different times. The detector multiplies the signal resulting from each group of ions at given arrival times, yielding an intensity--arrival time (m/e) spectrum of the ions produced in the ionization chamber. When the voltage and electron pulses are applied every 100 microseconds, a complete spectrum (in the m/e range of interest here) is obtained every 100 microseconds.

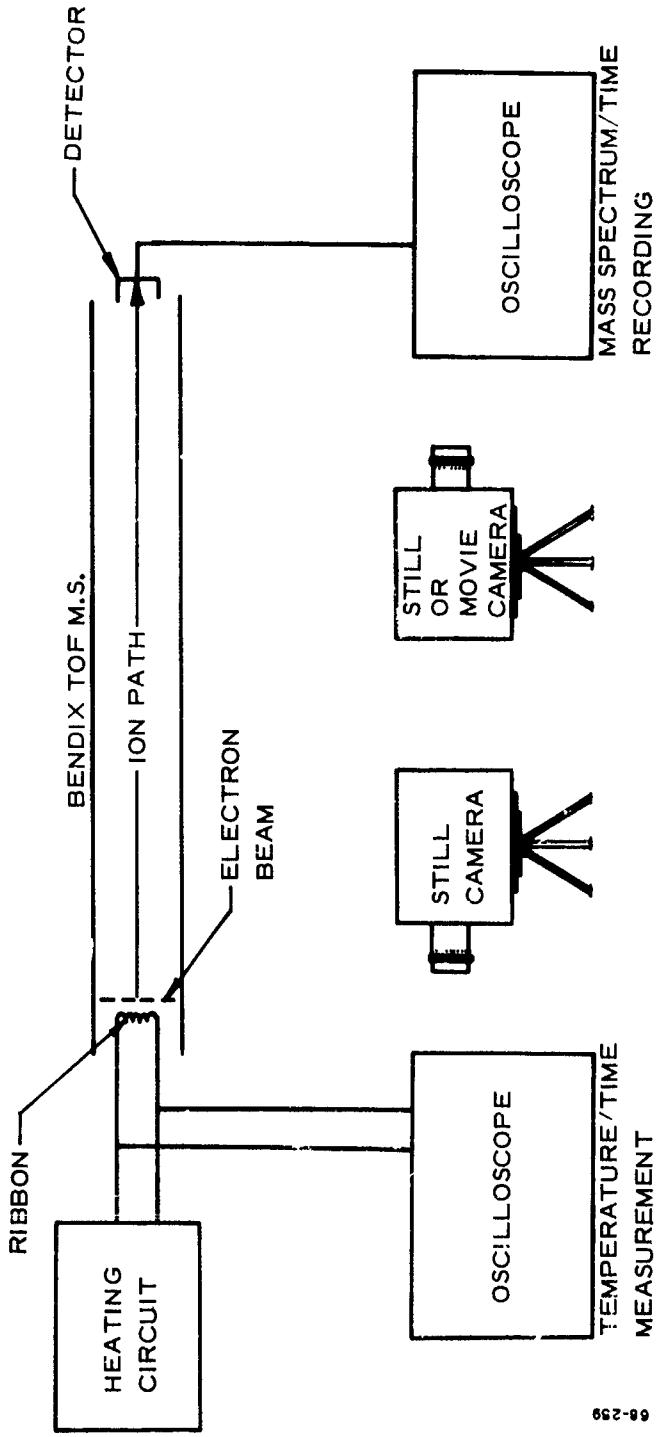

Figure 1 MTA Experiment Schematic

Mass resolution of the Bendix spectrometer is such that no more than a one-percent peak height contribution exists between adjacent peaks (one mass unit apart) in the Hg spectrum at m/e of 200.

b. TOF Modifications

(1) The Sample Holder

To achieve high heating rates, it is essential that the sample holder be of low mass (low heat content). Because it is desirable to heat the sample electrically, the geometry must ensure a reasonable electrical resistance for ohmic heating. The sample holder must also be constructed of a relatively non-reactive metal. All these constraints dictated the use of a platinum ribbon sample holder. The wide, flat ribbon (15 by 1.02 by 0.025 mm) permits distribution of the small sample over a large area, resulting in a thin film that ensures good thermal contact and close compliance of sample temperature to the ribbon temperature.

(2) Direct Inlet Sample Probe

In the early studies it was necessary to remove the ion source and the lower header plate leading into the spectrometer ionization region to introduce a sample. To improve efficiency of operation, a Bendix Direct Inlet Probe, Model 843A, was installed. A schematic of the probe inserted through its vacuum lock is shown in Figure 2. The sample mount and heater received with the probe were replaced by one appropriate for this program (Figure 3). Location of the probe and assembly within the spectrometer is depicted in Figure 4, showing that the sample can be located immediately adjacent to the electron beam or can be pulled back as much as five inches. The actual distance between sample and electron beam can, of course, be calibrated. The probe assembly requires its own high vacuum pumping station.

When the probe is positioned so that the sample is approximately 2 mm from the ionizing electron beam, a higher intensity spectrum results than would be possible for a system in which the sample were located at greater distances from the electron beam. Also, short-lived products may be detected before decay to secondary species.

(3) Cold Traps

The ionization chamber is cryogenically pumped with two specially designed liquid nitrogen cold traps (Figures 5 and 6). Their function is two-fold: (a) the residual H_2O background is reduced to virtually zero, and (b) pyrolysis products that escape from the ionization region are trapped before they can rebound from the walls and re-enter the ionization region. This ensures that most of the products being analyzed are detected while in a high energy state and have not collided with sampling system walls.

A viewing port also was incorporated into the upper trap assembly to permit visual observation during the delicate insertion of the sample mount up to the electron beam and for possible radiometer observations during actual firings.

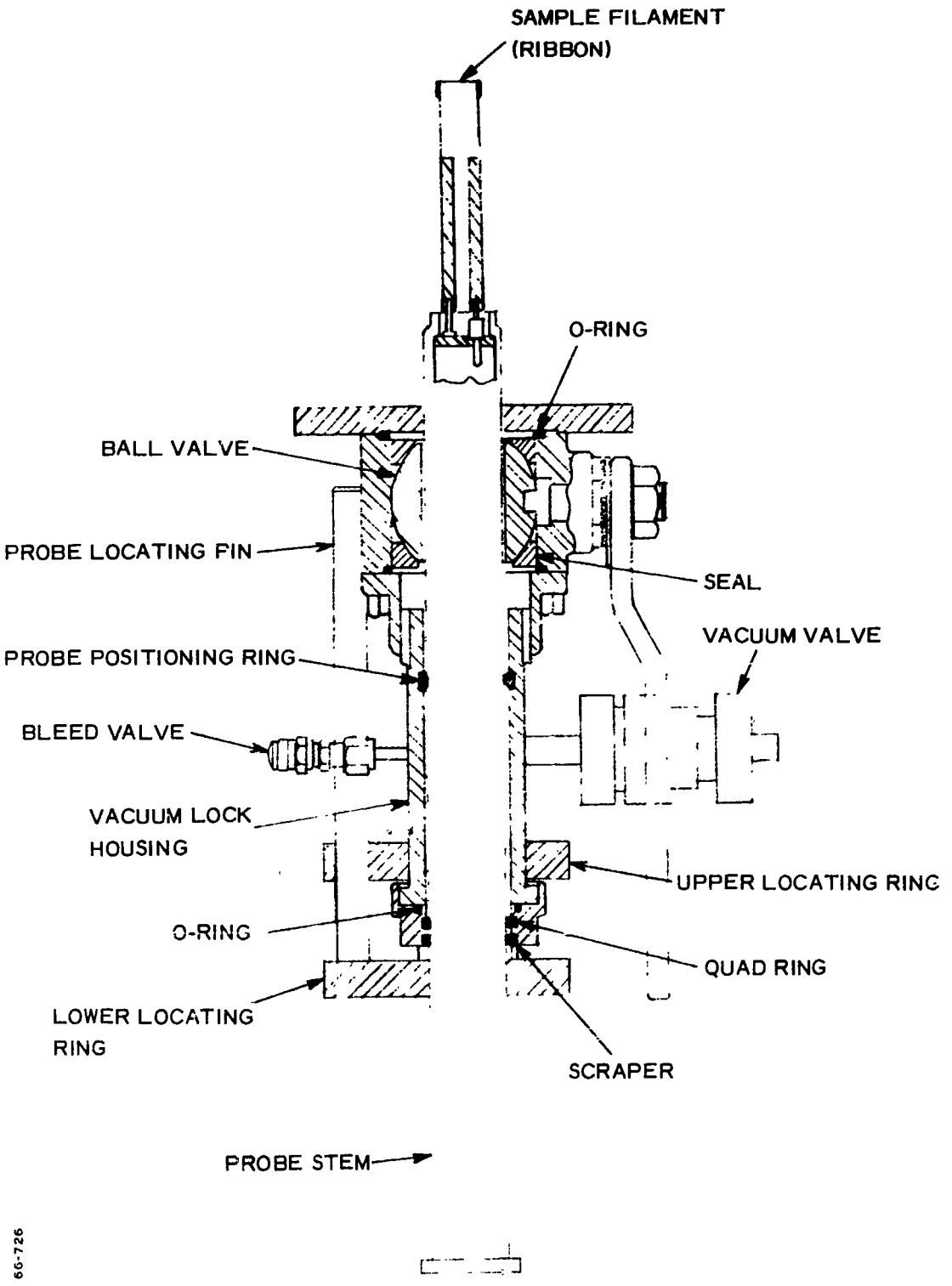

Figure 2 Bendix Direct Inlet Sample Probe

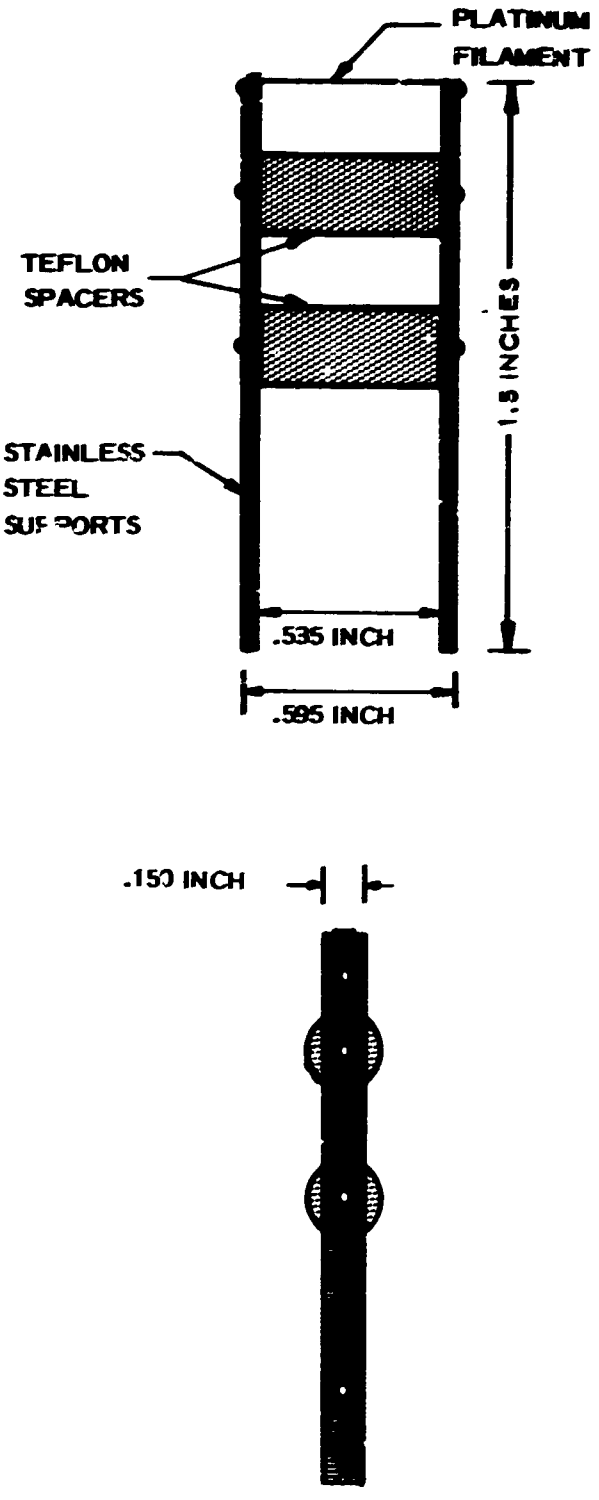

Figure 3 Filament Mount

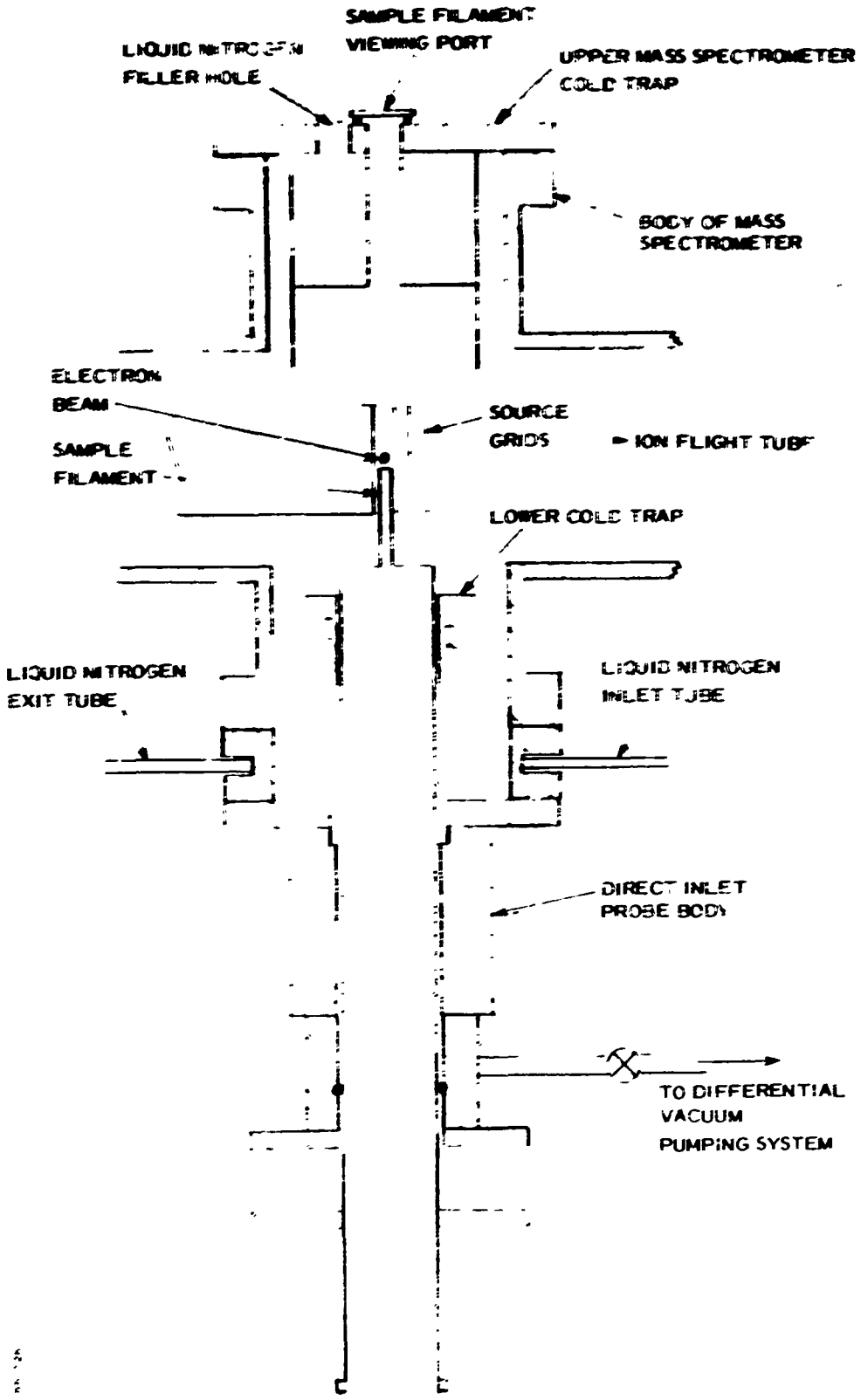

Figure 4 Complete Sample Probe and Trap Assembly in Spectrometer Ionization Region

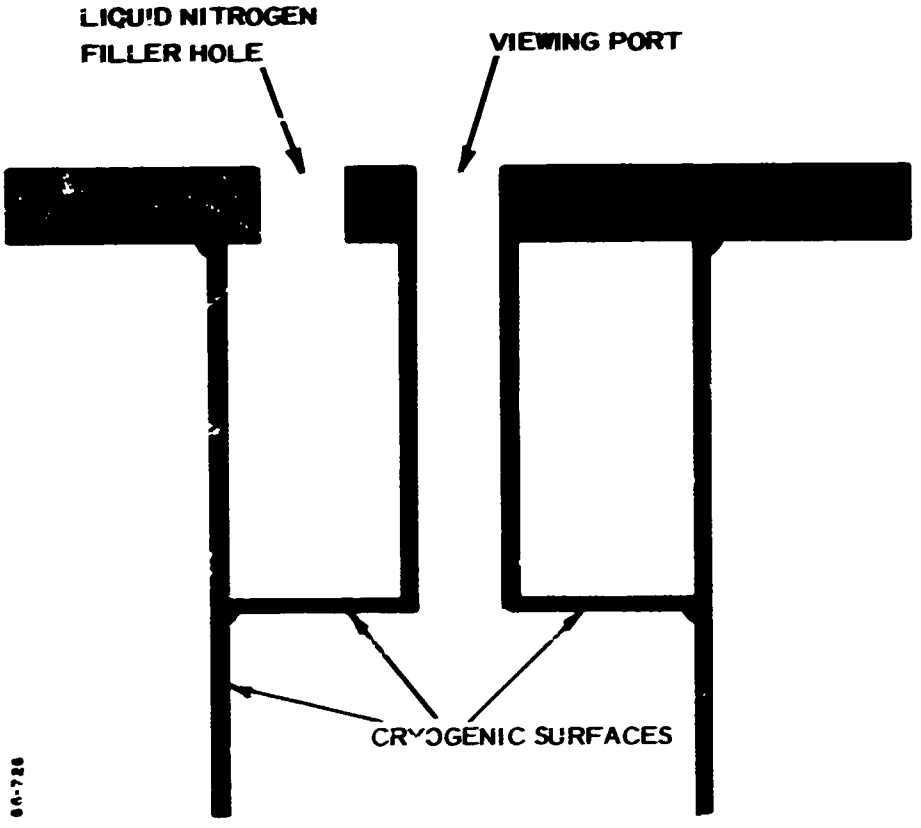

Figure 5 Upper Cold Trap for Spectrometer Ionization Region

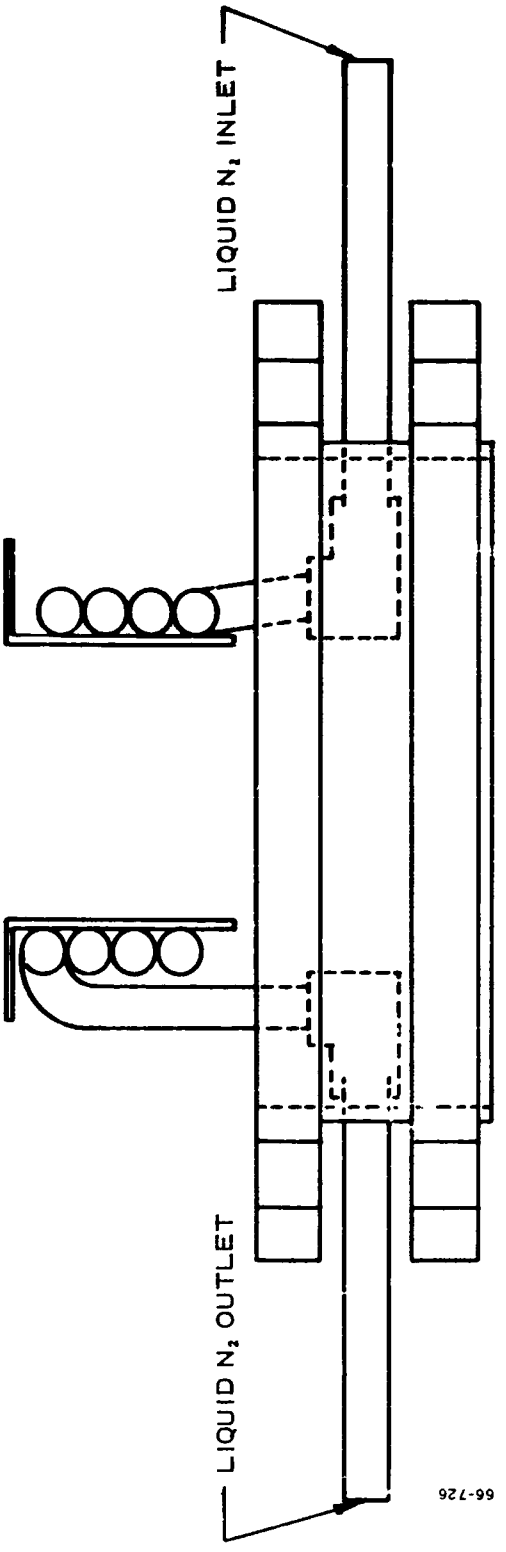

Figure 6 Lower Cold Trap for Spectrometer Ionization Region

c. Electronic and Electrical Circuitry

(1) Introduction

In the LPC experiments, the sample may be heated in two different modes: (a) flash heating (3×10^7 ^{0}C/second) to an isothermal condition (isothermal FMTA) and (b) a slower temperature rate of increase that was varied from 100 to 200^{0}C/second (dynamic FMTA). In either case, the platinum filament constitutes one arm of a Wheatstone bridge. Before each sample run, the bridge is nulled. As the ribbon is heated, its resistance changes and the bridge becomes unbalanced. The output signal of the bridge is fed to an oscilloscope and is recorded photographically.

(2) Isothermal FMTA

Because the method requires precise coordination in timing of the sample pyrolysis (capacitor discharge) with the spectral recording (time resolution) and temperature recording (bridge imbalance), considerable time was spent in designing and modifying circuits. Specifically, early measurements showed the capacitor discharge to be unacceptably slower than expected, causing a serious interference with the bridge imbalance measurement (temperature definition). Circuitry modifications drastically reduced this discharge decay to within acceptable limits (90 percent complete in 10 microseconds). Other circuitry modifications included:

- Installation of a second firing circuit, to be activated a predetermined time after the first capacitor discharge and producing a significantly higher ribbon temperature. This second discharge is intended to pyrolyze all remaining test material for the purpose of obtaining a material balance.

- Installation of a scope blanking circuit for controlling the spectral recording time.

The general sequence of events in a pyrolysis experiment is shown in Figure 7. The process is initiated manually, thus activating the firing relay. This, in turn, accomplishes three steps simultaneously:

- Activation of the firing relay discharges the first capacitor (previously charged to a known high voltage) through a thyratron and into the bridge, one arm of which is the sample filament. The resultant bridge imbalance is displayed on an oscilloscope. As may be observed in the discharge circuit detail, the actual discharge through the thyratron is triggered by a 24-volt battery impressed upon the thyratron grid. The battery also supplies voltage to the bridge to maintain the filament temperature and for a bridge imbalance input after dissipation of the capacitor (perhaps 10 microseconds). The heated filament produces gaseous decomposition products, some of which pass into the

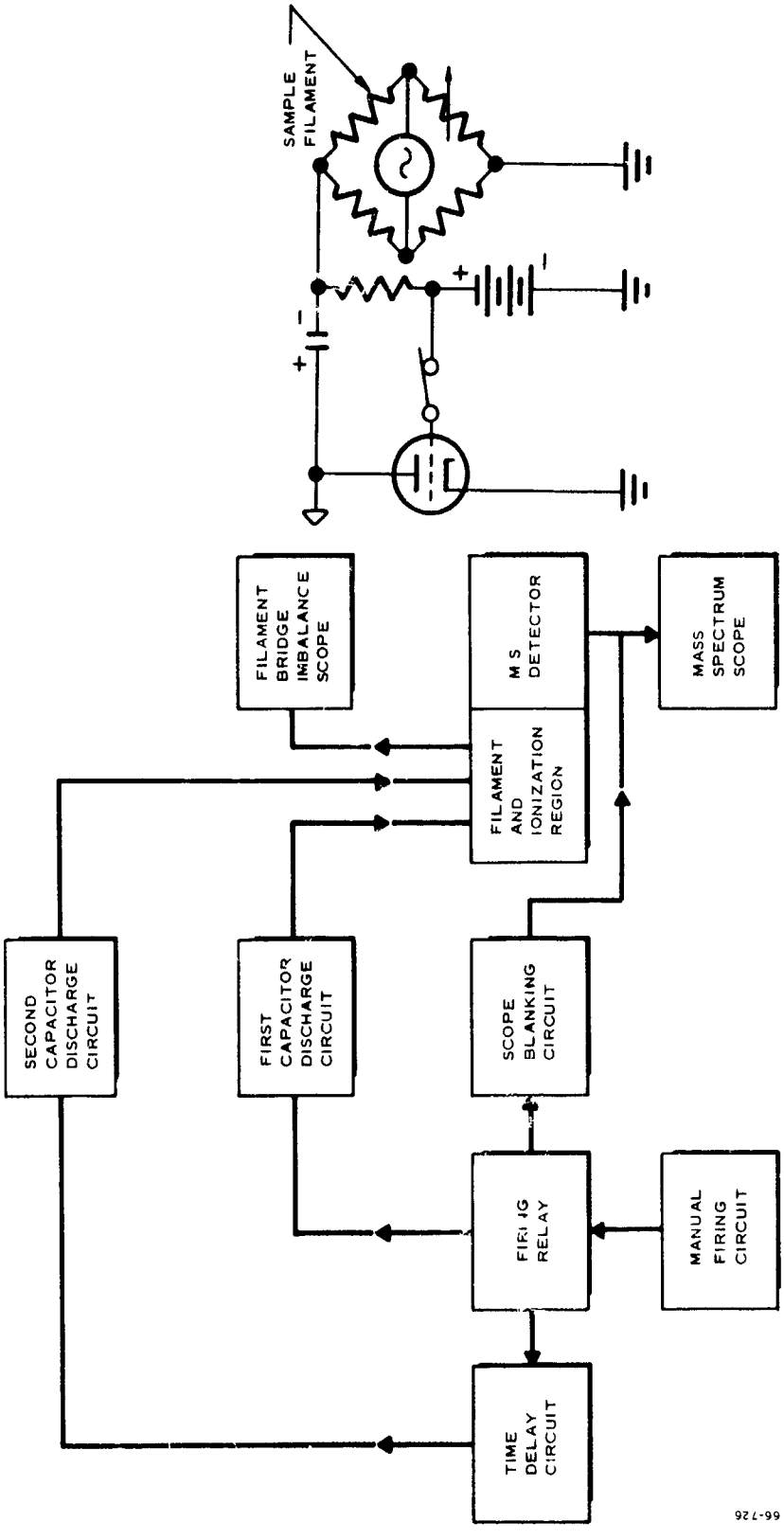

Figure 7 Block Diagram of Firing Sequence and Control

the electron beam, are ionized, and are pulsed down the flight tube every 50 (or 100) microseconds. The resultant spectra appear on the mass spectrum scope.

- The relay activates a time delay circuit (Figure 8) that will initiate a second capacitor discharge, if desired, after a known time interval. This is the discharge for "flashing" off all remaining sample for mass balance purposes.

- Finally, the relay activates the scope blanking circuit that controls the time during which the mass spectra are actually displayed on the oscilloscope, thus eliminating complications because of background spectra before discharge or to gaseous reactions occurring after the time period of real interest.

Details of the oscilloscope blanking circuit are shown in Figure 9. This circuit is divided into two functional sections: on the left of the vertical dotted line is a DC amplifier functioning as an electronic switch, and on the right there is a variable time delay circuit. The two transistors in the left section are designed to prevent the 20-KHz spectrometer trigger pulse from passing through to the oscilloscope until such time as the +24-volt switched circuit is activated, i. e., until the firing relay (Figure 7) is triggered. At that time, the transistor switch is opened, the 20-KHz pulse triggers the oscilloscope sweep, and hence the spectral data presentation, and the capacitor begins charging in the time-delay circuit. After the capacitor has become charged to a certain percentage of its total capacity, the transistor in the time-delay circuit switches on, causing the 20-KHz trigger pulse to be by-passed to ground and preventing any additional spectral data presentation on the oscilloscope. By use of the variable resistor in the time delay circuit, the time delay may be varied between approximately 100 microseconds to 10 milliseconds.

The time delay circuit for the second capacitor (Figure 8) is virtually identical to that in the blanking circuit except for the presence of a pulse transformer that becomes activated after the time delay and immediately triggers the thyratron of the second discharge circuit.

(a) Time-Resolved Data Acquisition

As indicated, the feasibility of resolving the separate mass spectra obtained at each cycle of the spectrometer has been demonstrated by either the Z-axis modulation technique or by high-speed cinematography. Because the former is only semiquantitative and the later relatively inconvenient, the possibility of spectral data acquisition with high-speed magnetic tape was investigated. It appears, however, that this application would entail an advancement in present technology requiring considerable expense and development effort. Hence, the Z-axis modulation and cinematographic techniques were pursued.

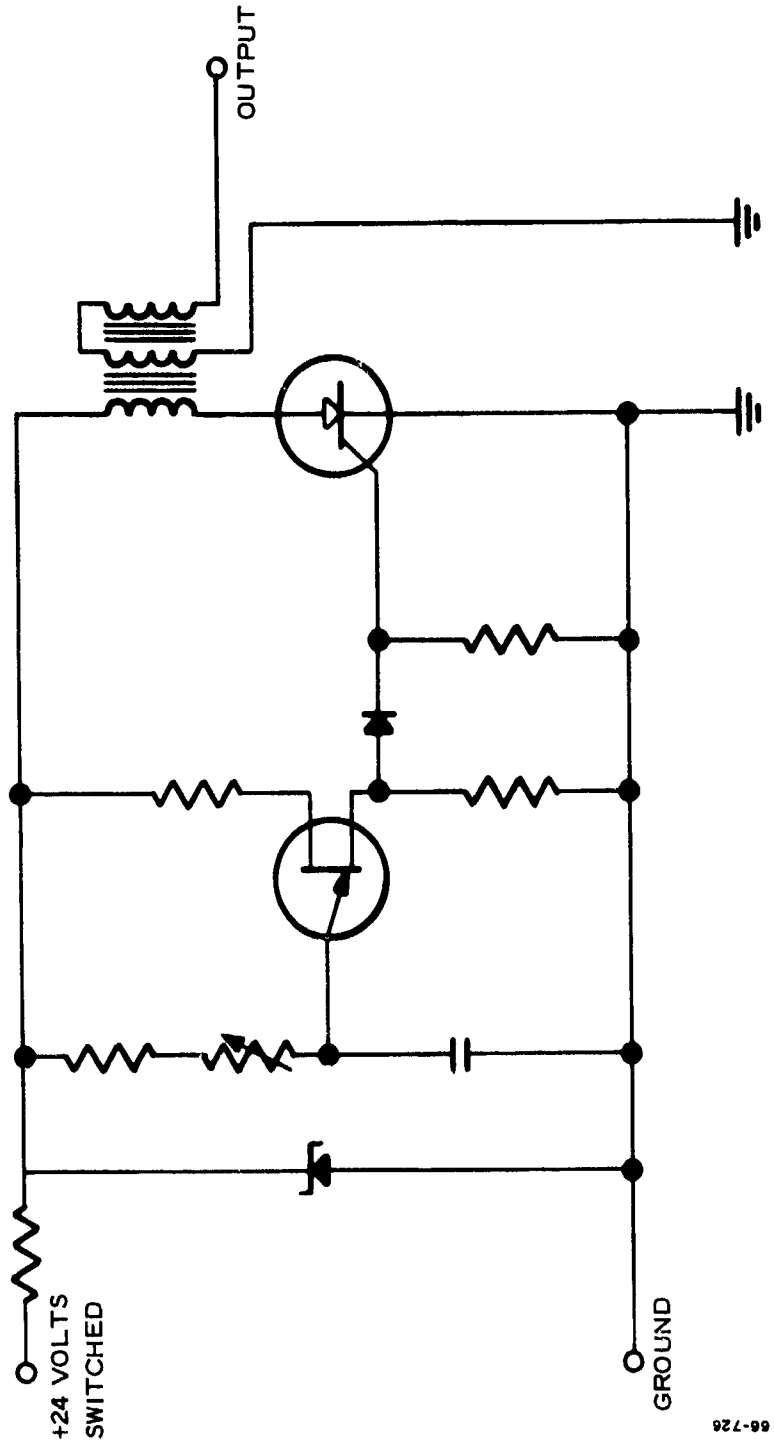

Figure 8 Time Delay Circuit for Second Capacitor Discharge

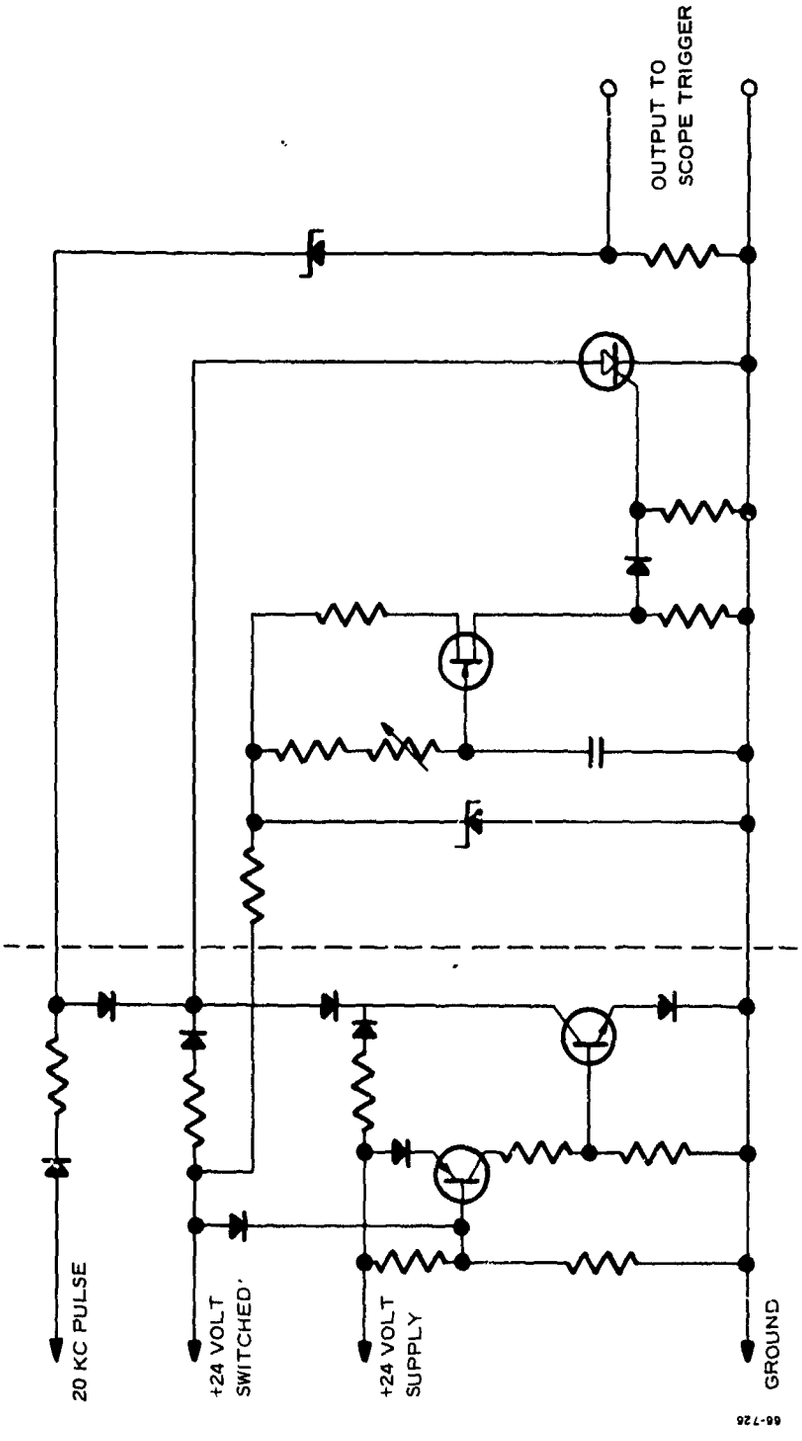

Figure 9 Variable Delay Oscilloscope Blanking Circuit

(b) Detection of Transient Species

One of the great advantages of the hot filament-mass spectrometer technique for elucidating reaction mechanisms is its ability to detect small amounts of transient species if their lifetimes approximate 50 microseconds or greater. It also is possible, in principle, to determine if such species are neutral, free radicals, or ionic.

Free radicals, for example, may be detected if the energy of the ionizing electron beam is maintained above the ionization potential of the suspected free radical but below the appearance potential of its parent molecule.

Alternate methods have been considered for detecting ionic species. Bendix has developed a complex system employing charged deflection plates for removing--and therefore detecting--ions present in flames or plasmas (Ref. 3). A modification of this technique originally was contemplated for use in this program. However, further consideration indicates that straight-forward pyrolysis experiments with and without the ionizing electron beam would provide a simpler and more sensitive method for detecting ionic intermediates.

(3) Dynamic FMTA

The Dynamic FMTA heating of the ribbon is produced by disconnecting the capacitor discharge circuit and inserting a 24-volt battery connected in series with the bridge. The rate of heating may be varied with a rheostat, also in series with the bridge. A schematic of the circuitry is presented in Figure 10.

For the slow heating experiments, a high-speed framing camera was employed to photograph the spectrum oscilloscope trace at a speed of 200 frames/second or 1 frame each 5 milliseconds. In general, the heating rate was 100°C/second. With the small sample, the pyrolysis event usually was completed within 2 seconds (Figure 11). To synchronize the temperature trace oscilloscope with the spectrum oscilloscope, a flashlamp was triggered simultaneously with the beginning of current input to the ribbon. The flash overexposes the first few frames on the spectrum oscilloscope, thereby marking the beginning of heating. The same trigger pulse that fires the flashlamp also is used to trigger the sweep of the temperature trace oscilloscope.

3. TEMPERATURE DEFINITION AND MEASUREMENT

Meaningful kinetic and mechanistic conclusions regarding the rapid thermal decomposition processes will necessitate accurately known, uniform sample temperatures. Two complementary approaches were employed in this program. First, a complete mathematical analysis of the thermal processes occurring in the filament and sample has been performed and is programmed for computer calculations. In conjunction with the measured voltage input to the filament, this analysis, in principle, should yield a complete time-position-temperature profile. Secondly, the spatial average

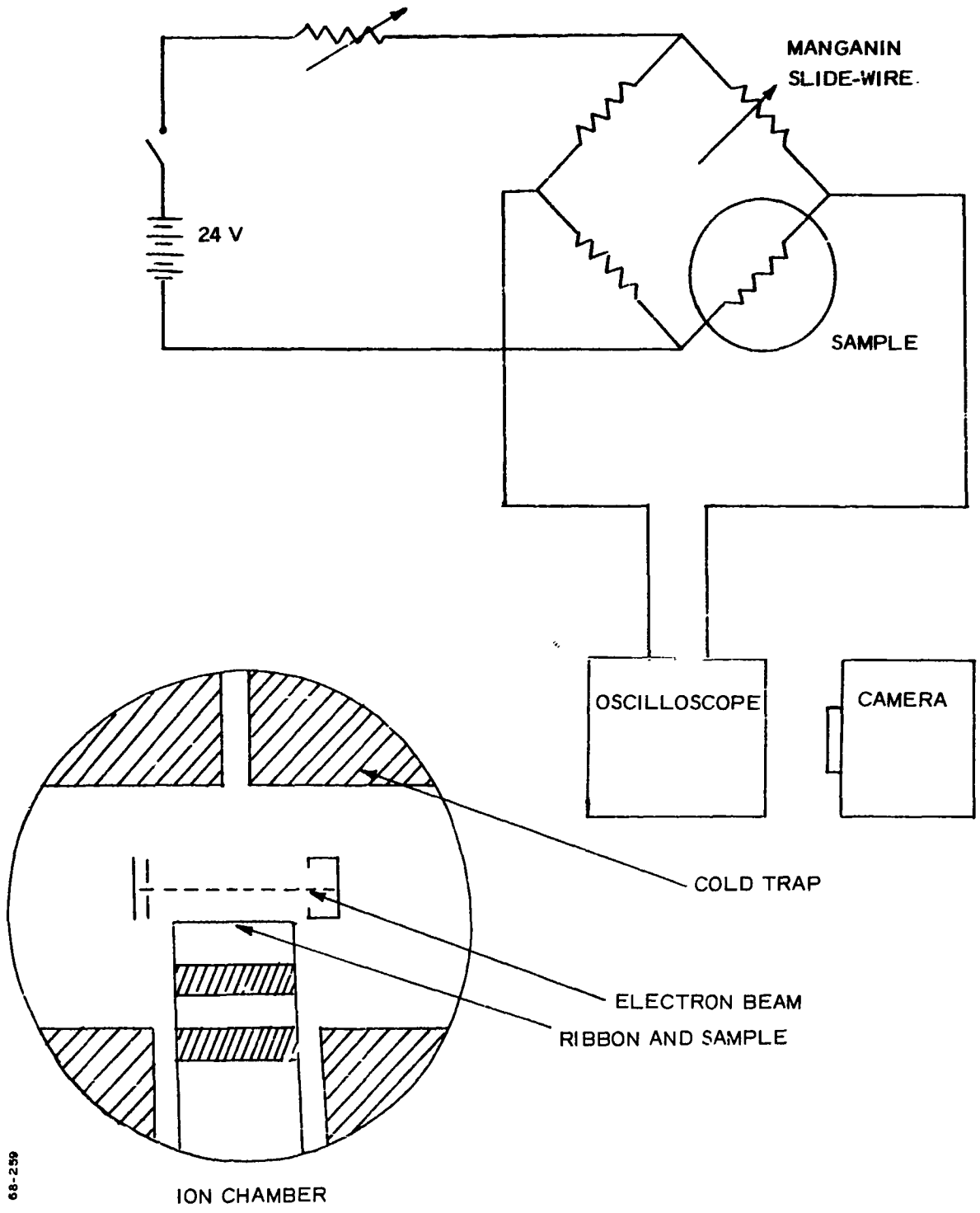

Figure 10 Dynamic FMTA Schematic

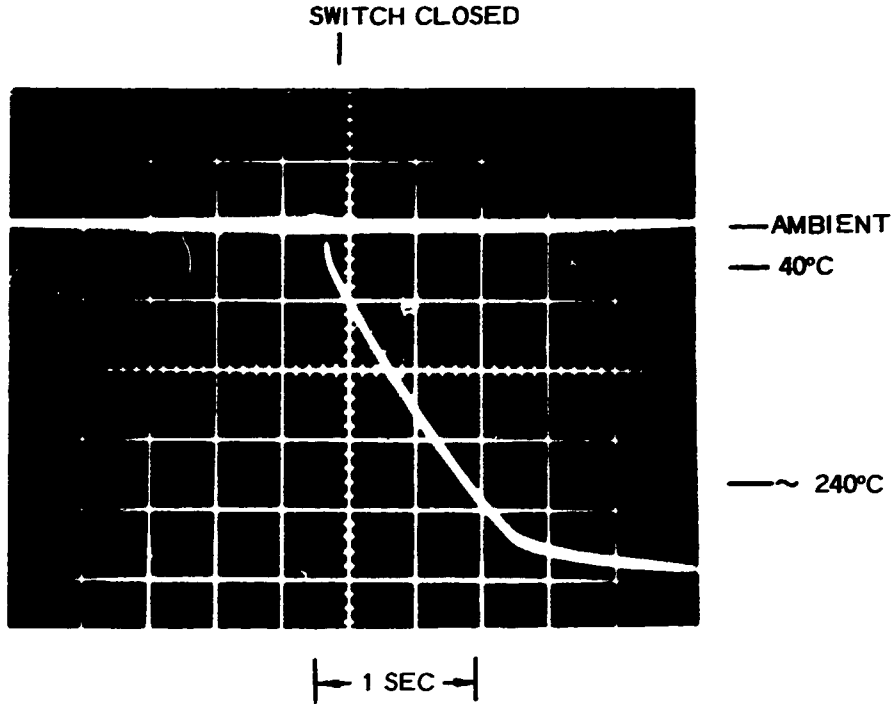

Figure 11 Heating Rate Determination, Dynamic FMTA

temperature of the filament is being determined as a function of time from measurements of input and output voltage to the bridge in which the filament forms one arm.

a. Filament Heating Without Sample

Briefly, the physical situation is the following. A platinum (Pt) ribbon (2 mm by 0.025 mm in cross section) is attached at each end to connecting posts of relatively large mass (Figure 3). The ribbon length is approximately 1.5 cm, and forms one arm of a Wheatstone bridge. A capacitor discharge is triggered through the ribbon by impressing the output of a 24-volt battery upon the grid of a thyratron (Figure 7). The battery also supplies current to the ribbon through a variable series resistor, thus helping to maintain the ribbon temperature after the rapid dissipation of capacitor current. In addition, the battery provides a known input voltage to the bridge imbalance (caused by ribbon temperature rise) that may be measured and the average (over-the-length) ribbon temperature calculated.

The general differential equation describing the time and position (length) dependence of temperature for the ribbon is

$$\frac{\partial T}{\partial t} = \frac{K}{\rho C}\left(\frac{\partial^2 T}{\partial x^2}\right) + \frac{I^2(t)R'(T)}{4.18\,\rho CA} - \frac{\sigma E S (T^4 - T_o^4)}{\rho C A} \qquad (1)$$

where ρ and C are density and specific heat of the metal, A is the cross section of wire and ribbon, K is the metal thermal conductivity, σ E represents surface emissivity, S is surface area per unit length. I is current, and R′ is resistance per unit length. The first term on the right side of Equation 1 represents the effects of heat conduction along the metal, the second term represents the ohmic heating, and the third represents heat losses because of surface radiation to surroundings at ambient temperature T_o.

For each of the wires the initial and boundary conditions are the following:

- $T = T_o$ at $t = 0$ for all x
- $T = T_o$ at all t for x - o, i.e., heat conduction at binding posts assumed large enough to maintain them at ambient temperature
- At x = l (junction of wire and ribbon. or ribbon and post)

$$\left[A\frac{\partial T}{\partial x}\right]_{wire} = \left[A\frac{\partial T}{\partial x}\right]_{ribbon}$$

For the ribbon, the initial and boundary conditions include (a) above, (c) at both ends, and (d) $\frac{\partial T}{\partial x} = 0$ at midpoint of ribbon, i.e., the filament is symmetrical. Hopefully, of course, $\partial T/\partial x$ will be zero along all or most of the ribbon length.

Equation (1) apparently has not been solved analytically even when I and R are assumed constant (Ref. 4). In the present case, the ohmic heating term is a relatively complicated one, involving the algebraic sum of currents (or voltages) from capacitor and battery with the former being a known exponential function of time. The resistance is a known linear function of temperature.

b. Thermal Analysis of Ribbon and Pyrolyzing Sample

The presence of sample on the ribbon obviously complicates the situation. Radiation losses will differ from top and botton ribbon surfaces because of the sample coating on the top surface. Heat will be required to raise the sample temperature, to produce decomposition, and to "boil off" decomposition products. On the other hand, heat will likely be produced by certain decomposition reactions and such heat hopefully will be absorbed by the ribbon to maintain isothermal conditions within the sample.

Rohm & Haas (Ref. 5) carried out an approximate thermal analysis for the closely related Wenograd technique wherein detonation sensitivity is determined by discharging a capacitor through a steel needle enclosing the material of interest. The quantity actually measured there is the time delay to explosion initiated by the combined heat transferred from the needle and that produced more or less adiabatically within the decomposing material. The equations describing that heating process may be adapted to the hot filament technique.

Consider a ribbon λ cm. long, α cm. wide, and δ_r cm. thick (y direction). The upper ribbon surface ($y = \delta_r$) is coated uniformly with sample δ_s cm thick. δ_r is approximately 25 microns while $\delta_s \simeq 0.1$ micron.

For the ribbon, assuming no temperature gradient along its length:

$$\frac{\partial T_m}{\partial t} = \frac{K_m}{\rho_m C_m} \frac{\partial^2 T_m}{\partial y^2} + \frac{I^2 R''}{4.18 \alpha \lambda \rho_m C_m} \qquad (2)$$

Where m refers to metal ribbon, K_m, ρ_m, C_m, and I have their previous significance, and R'' is the metal resistivity k(T) divided by $\alpha\lambda$. I, of course, has the same behavior discussed with relevance to Equation (1).

The initial and boundary conditions include the following:

- $T_m = T_o$ at $t = 0$ for all y
- At $y = 0$ (bottom surface) and all t

$$K_m\left(\frac{\partial T_m}{\partial y}\right) = \sigma \varepsilon_m (T_m^4 - T_o^4) \Big]_{y=0}$$

- At $y = \beta_r$ and all t

$$K_m\left(\frac{\partial T_m}{\partial y}\right) = -h\,(T_m - T_s) \Big]_{y=\beta_r}$$

and $$K_s\left(\frac{\partial T_s}{\partial y}\right) = -h\,(T_m - T_s) \Big]_{y=\beta_r}$$

where s refers to sample and h is the thermal contact resistance coefficient.

For the sample:

$$\left(\frac{\partial T_s}{\partial t}\right) = \frac{K_s}{\rho_s C_s}\left(\frac{\partial^2 T_s}{\partial y^2}\right) - \frac{Q_s}{C_s}\left(\frac{\partial f}{\partial t}\right) \qquad (3)$$

where Q_s is the heat per g of sample reacting and f is the fraction of original sample which is present at any given time.

Rohm & Haas in their analysis let

$$\frac{\partial f}{\partial t} = -f^n Z_1 \exp\left[\frac{-E_1}{RT}\right] - f(1-f) Z_2 \exp\left[\frac{-E_2}{RT}\right] \qquad (4)$$

where n is the order of the decomposition reaction, and Z_1, and E_1 are the pre-exponential factor and the activation energy for that reaction. The second term represents the contribution of an autocatalytic reaction. Within the bounds of our knowledge of heats of reaction and the terms of Equation (4), Q_s can be assumed to include any heat required for evaporation of decomposition products.

Obviously interaction occurs among Equations (1), (2), and (3). In fact, a combined two-dimensional (x and y) analysis was found to be necessary for the ribbon and its sample.

c. Numerical Solution to Ribbon Temperature Profile

After considering several approaches to the solution--computation of Equations (1) and (2), it was concluded that the most feasible procedure was to conduct an iterative computation upon Fourier series forms of the equations. This is demonstrated briefly in the following steps for computing T(x t) for the filament.

First, transform the equations into their parametric forms.

For the ribbon and wire:

$$\frac{\partial T}{\partial t} = D \frac{\partial^2 T}{\partial x^2} + f(x, t, T) \qquad (1')$$

where T is the temperature above ambient T_o and $D = \frac{K}{\rho C}$, the other symbols possess their usual identities. The function f (x, t, T) is defined by

$$f(x,t,T) \equiv \frac{I^2(t) R'(T)}{4.18 \rho CA} - \frac{\sigma ES[(T+T_o)^4 - T_o^4]}{\rho CA}$$

The boundary conditions for Equation (1') are the same as before.

For the sample in the direction perpendicular to the ribbon surface:

$$\frac{\partial T_s}{\partial t} = D_s \frac{\partial^2 T}{\partial y^2} - g(y,t,T_s) \qquad (3')$$

Where g is given by $\frac{Q_s}{C_s} \frac{\partial f}{\partial t}$ the boundary conditions for Equation (3') are:

$T_s = 0. \quad t = 0$

$$K_s \left(\frac{\partial T_s}{\partial y}\right)_i = K_m \left(\frac{\partial T_m}{\partial y}\right) = h(T_m - T_s), \; y = 0$$

i. e., at ribbon/sample interface.

$$\frac{\partial T_s}{\partial y} = \frac{\sigma E_s}{K_s} [(T_s + T_o)^4 - T_o^4], \; y = a,$$

i. e., at surface of sample.

Step 1: Assume T initially zero, yielding

$$f^{(o)}(x,t) = f(x,t, T=0)$$

Step 2: Compute

$$f_j^{(o)}(t) = \frac{1}{b} \int_{-b}^{b} f^{(o)}(x,t) \cos \frac{(2j+1)\pi x}{2b} \, dx$$

Step 3: Compute

$$T_j^{(1)}(t) = e^{-D\left[\frac{(2j+1)}{2b}\pi\right]^2 t} \int_0^t f_j^{(o)}(\xi) \, e^{D\left[\frac{(2j+1)\pi}{2b}\right]^2 d\xi}$$

Step 4: Compute

$$T^{(1)}(x,t) = \sum_{j=1}^{\infty} T_j^{(1)}(t) \cos \frac{(2j+1)}{2b} \pi x$$

Step 5: Repeat steps 1 to 4 until

$$T^{(n+1)}(x,t) = T^{(n)}(x,t) = T(x,t)$$

Computer calculations of the solution to the equations were carried out for the following case:

Pt ribbon, 1.50-cm long x 40 mil wide x 1-mil thick

$K/\rho C = 0.25$

$Q = I_o^2 R'/4.18 \rho CA = 2.28 \times 10^8$

$\alpha = 2/\tau = 4.54 \times 10^5$

x = 0 at midpoint of ribbon

x = 0.75 at ends of ribbon

T (°C) = 0 at x = 0.7. i.e., mounting posts massive relative to ri. on

The resultant temperatures are shown for various times in Figure 12). It should be noted that in the absence of any conductive heat losses ($\partial^2 T/\partial x^2 = 0$) the quantity Q/α employed will produce a ribbon temperature of 501°C after nearly 10 microseconds have elapsed. The results demonstrate that this exact temperature is attained shortly after 10 microseconds and is maintained, for example, over more than 80-percent of the ribbon for 5 milliseconds, more than 67-percent of the ribbon for 10 milliseconds, and more than 33-percent of the ribbon for 50 milliseconds.

This finding has great significance for this rapid pyrolysis technique. It means that a simple ribbon filament will suffice to provide constant sample substrate temperatures for up to 10 microseconds as long as the sample is restricted to the middle two-thirds of the ribbon. In actual fact, this time period probably could be extended because a constant DC

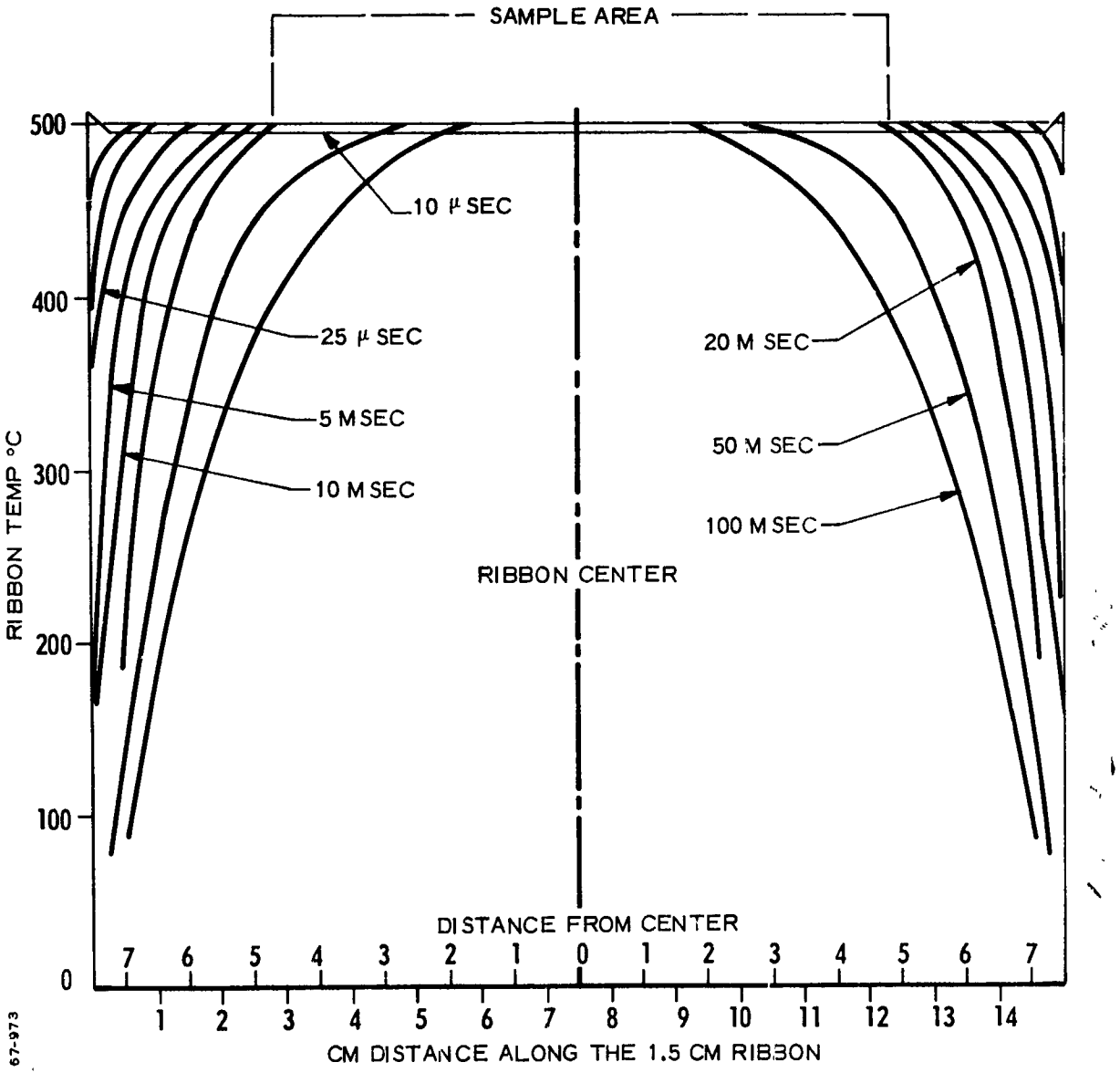

Figure 12 Computer-Predicted Ribbon Temperature Profile

voltage also is applied to the bridge containing the filament for the primary purpose of determining bridge imbalance and filament temperature (Figure 13). The ability to employ a ribbon filament greatly simplifies the preparation of filaments and increases the accuracy of temperatures calculated by the bridge imbalance technique. In addition, it will simplify the computer calculations of Equation (1) that still are desirable primarily for elucidating the influence of thermal contact resistance (sample/ribbon) and reaction heats upon actual sample temperatures.

During the course of these studies, the computer program was set up for solution of Equation (3), but was not completely debugged, so that no calculations were with respect to the sample/ribbon temperatures during pyrolysis.

d. Temperatures by Bridge Imbalance Measurement

The increase in filament resistance, and hence filament temperature, is determined during pyrolyses by measuring the imbalance of a bridge in which the filament forms one arm. This imbalance voltage must be measured after the capacitor is fully discharged, at which time a known, applied DC voltage becomes the sole source of power (small) to the bridge. Alternatively, during Dynamic FMTA measurements, the 24-volt DC battery is the sole heating source, so that the entire bridge imbalance/time curve can be transformed into temperature/time coordinates. In either event, the equations derived for the conversion are the same:

$$R_f = \frac{ER_3 + 2VR_s + 2VR_3 + \dfrac{R_s R_3 V}{R_1}}{E - 2V - \dfrac{VR_s}{R_1}}$$

in which R_f is the ribbon resistance, E is the source voltage, R_3 is the variable arm of the bridge, R_S is the series resistance, R_1 and R_2 are the remaining known arms of the bridge and V is the bridge output voltage. The temperature of the ribbon is in turn calculated from:

$$T_{pt} = \frac{R_{ft} - R_{fi}}{3.89 \times 10^{-4}} + T_i$$

in which T_{pt} is the temperature at time t, R_{ft} is the resistance of the ribbon at time t, R_{fi} is the initial resistance of the ribbon, and T_i is the room temperature. Triplicate heating experiments on the same ribbon indicate less than 5^0C deviation at 200^0C. It is believed that the equations and accompanying experimental quantities yield temperatures accurate to within 10^0C at the highest temperature so far reached $\sim 500^0$C.

Two attempts were made to obtain a separate experimental verification of temperature uniformity. The first involved the use of extremely fine thermocouples (No. 40) welded at several positions along the

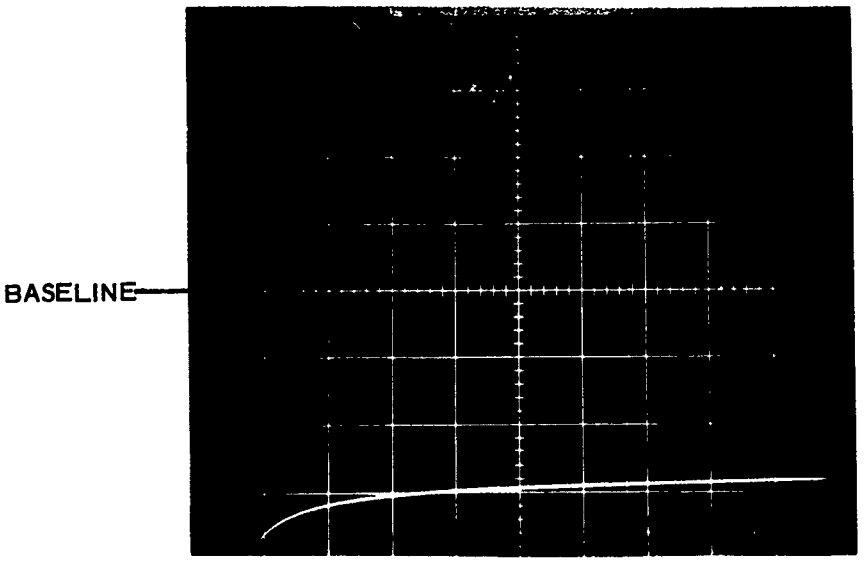

WITH BATTERY CONNECTED

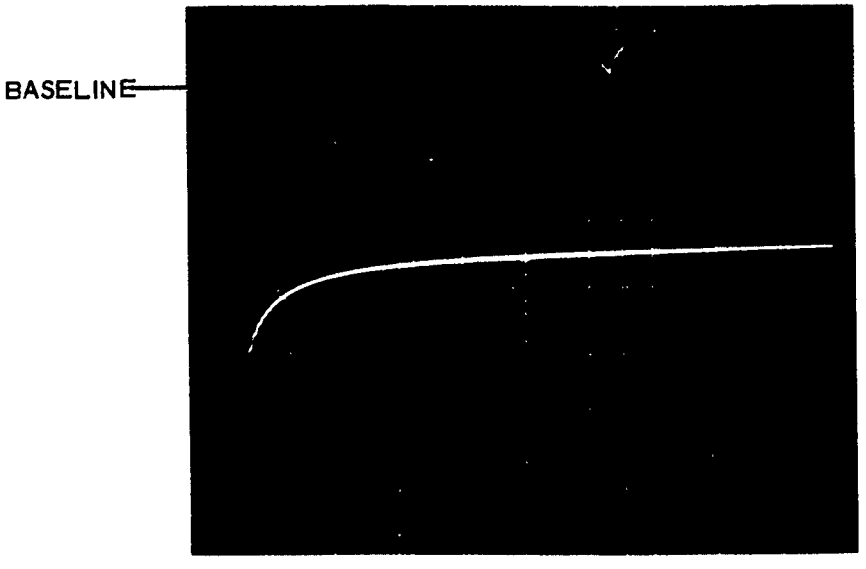

BATTERY DISCONNECTED

Figure 13 Bridge Imbalance Trace with Ribbon Filament

ribbon. Not surprisingly, even this fine a thermocouple produced heat sinks sufficiently great to distort the ribbon temperature profile under steady-state current.

The second attempt involved an infrared radiometer reputed to possess both time and area resolution suitable for determining the ribbon temperature profile during capacitor discharge heating. Unfortunately, the apparatus did not meet expectations.

To circumvent these difficulties, the equipment finally was calibrated by kinetic measurements using suitable reference materials.

4. SAMPLE PREPARATION AND MEASUREMENT

Very thin sample coatings upon the ribbon are a prerequisite for obtaining good kinetic data within the time span of interest (~50 microseconds to a few microseconds) for only then can the sample be heated up uniformly in a time that is short compared to the total experimental time. During the course of the program, two methods were used successfully for applying the samples to the ribbon. The following paragraphs give details on each method.

a. Spray Coating

Samples of INFO-635 were prepared successfully by spraying a solution of INFO-635 in nitromethane from an artist's air brush (Thayer-Chandler Model A) onto filaments mounted on the perimeter of the slowly revolving wheel, shown in Figure 14.

A wide latitude is available for the amount of sample coating and the particle size of the coating by varying the nozzle settings, air pressure, distance between brush and filament, and wheel speed. Microscopic examination of coated ribbons and glass slides indicates that average particle size of INFO-635 can be made at least as small as 2 microns. Additional optimization may reduce that size. Figure 15 is a photomicrograph of one of the better preparations and demonstrates that this technique will produce coatings of satisfactory uniformity.

b. Microsyringe Application

Although the spray coating method produced satisfactory samples, it was cumbersome and unsuited to preparation of single samples. A technique therefore was developed to apply 5 to 20 microgram samples to the ribbon by means of a microsyringe.

Weighed samples are dissolved in a suitable solvent to yield a solution concentration of 1 microgram per microliter. This solution then is applied, in a dry box, carefully to the center 0.5 cm of the ribbon using a Hamilton microsyringe of suitable capacity. With practice, it is possible to reproduce a sample coating to within ± 5 percent of the desired value. The solvent is allowed to evaporate, in the dry box, then transferred, in a dry bag, to either the mass spectrometer or to a bell jar and subjected to vacuum for 2 to 20 hours to remove the last traces of solvent. Dergazarian

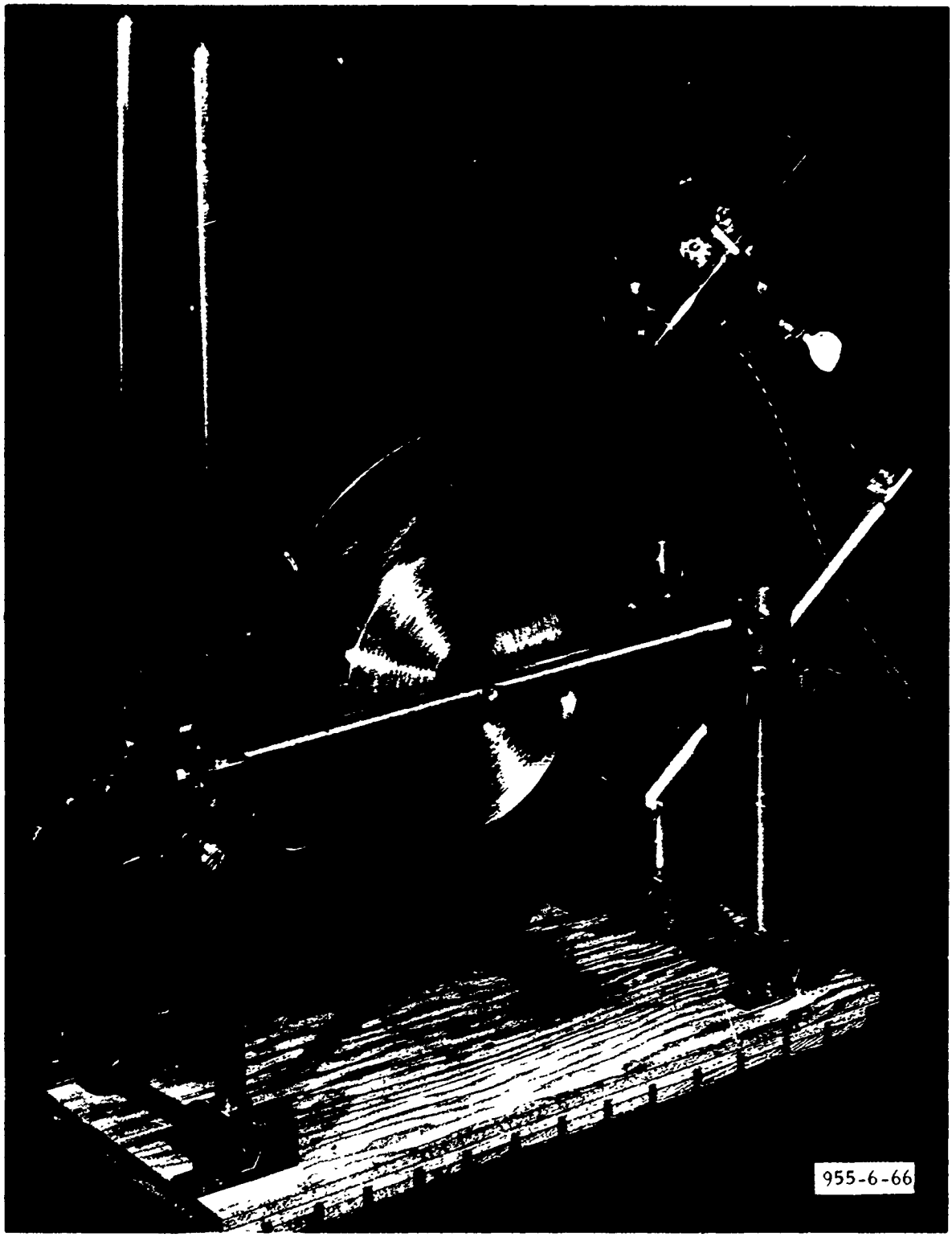

Figure 14 Filament Spraying Apparatus

Figure 15 Photomicrograph of INFO-635 Coating

at Dow (Ref. 6) has been unable to remove all solvent from 50 to 100 milligram samples of PBEP, and this residual solvent seriously affects the mass spectra of the pyrolysis species. The use of microgram samples in the present work results in complete solvent removal; no part of the mass spectra of PBEP pyrolysis species contains evidence for residual solvent. The sample, on the ribbon and holder, then is affixed to a probe, and is inserted into position inside the mass spectrometer through the vacuum lock. The sample then is heated by the capacitor discharge for isothermal studies, or by the battery discharge for dynamic FMTA studies.

c. Direct Determination of Sample Weight

Although it is possible to obtain quantitative kinetic data from the uncalibrated mass spectrometer system, it is also of great value, as a validity check, to measure the absolute quantities of materials involved in the pyrolysis experiments.

The task involves accurately measuring microgram quantities of material on a support that may weigh from 200 milligrams to 4 grams. At the beginning of the program, no commercially available balance possessed the required sensitivity at the required load. The capabilities of quartz helix microbalances were investigated using two different helices. Although the helices provided sufficient sensitivity, the load capacity was severely limited, so this approach was dropped.

However, within the past six months, two balances meeting the requirements have appeared on the market--manufactured by CAHN and by Mettler. Their utility will be investigated in future work.

5. DATA RECORDING TECHNIQUES

a. Introduction

Time-of-flight mass spectrometry lends itself well to fast pyrolysis studies because of its rapid sampling rate (10 to 20 KHz) over the spectrum of 0 to 250 mass units. This rapid rate permits the use of small samples and small heat sources that characteristically possess low heat capacities and therefore require less energy for a given temperature increase.

Rapid analysis coupled with extremely short periods in which the pyrolysis products are available for detection present some stringent requirements for recording data. In these experiments, the time range of interest may be as short as a hundred microseconds or, at most, two seconds. Obviously, the data must be recorded photographically from an oscilloscope trace. The photographic recording can be either time-resolved or time-integrated. Time-resolved refers to the separate oscilloscope presentation and photographic recording of each scan at 100 microsecond intervals over a particular m/e range. Time-integrated refers to the superposition upon one photograph with a single base line of all the separate scans occurring in the time range of interest.

b. Isothermal FMTA

With the Isothermal FMTA method, three techniques of data acquisition were used.

(1) Time-Integrated Spectra

In the first method, the spectrum is recorded on a single exposure with a Polaroid camera. Because the mass species of interest are generated in the first two milliseconds after rapid heating is begun, it is necessary to blank out the oscilloscope trace after that period so that the build-up of gaseous products is recorded only over the time period of interest. Thereafter, the ion concentration quickly becomes high enough to saturate the multiplier electronic circuit making useless the resultant spectrum. To achieve this, the 10 KHz recurrent mass spectrometer trigger pulse is fed continuously to the spectrum oscilloscope, causing the trace to sweep continuously. When the sample firing switch is activated, the positive 24-volt DC source is applied to the anode of the Silicon Controlled Rectifier (SCR). The 10 KHz trigger signal voltage then falls sharply to a value that will no longer trigger the spectrum oscilloscope. An advantage of this method over mechanical camera shutters is that the blanking time can be continuously varied and also precisely synchronized with the beginning of the rapid heating.

(2) Time Resolution by Z-Axis Modulation

In the second method, a roughly semiquantitative procedure described by Lincoln (Ref. 2) was used. The method is called Z-axis data display. The data are displayed on an oscilloscope in which each sweep is displaced vertically upward from the preceding sweep. The mass units are displayed as a series of dots along each sweep, and the dot intensity is a function of the signal strength of each mass peak. The experimental arrangement, that requires two oscilloscopes and three amplifiers, is shown in Figure 16.

Oscilloscope No. 1 is triggered externally from the sample firing switch and is set for single sweep operation. Any single peak of interest in the spectrum may be selected to be displayed on the oscilloscope by feeding the time-variable analogue gate pulse from the mass spectrometer to the Cathode Ray Tube (CRT) input. Because the sweep speed of this oscilloscope is slow compared to the analogue pulse sampling rate, as many as 5000 samples of the selected mass peak may be displayed during the single sweep.

Oscilloscope No. 2 is triggered in the usual manner for observing the mass spectrum. The vertical input is a linearly increasing ramp voltage derived from the sweep generator of oscilloscope No. 1. The sweep rate of oscilloscope No. 2 is 500 times faster than oscilloscope No. 1, and consequently the ramp voltage is sampled stepwise and is displayed as a series of nearly horizontal lines, starting in time at the bottom of the CRT and progressing to the top. The mass spectrum signal which is originally fed into oscilloscope No. 1 is taken from the "vertical signal out" terminal of oscilloscope No. 1, amplified and inverted by three wide-band amplifiers and

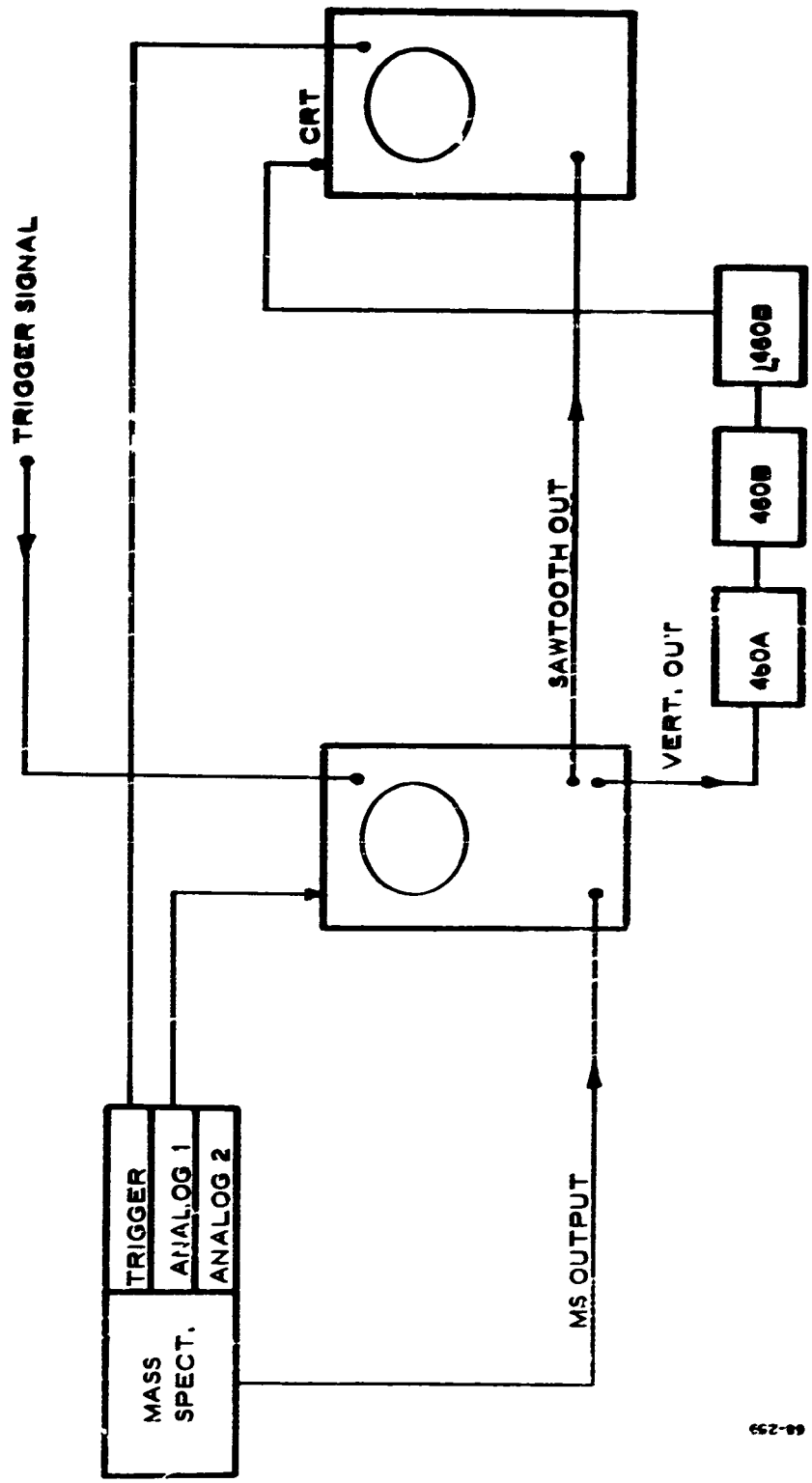

Figure 16 Z-Axis Experimental Arrangement

is fed into the CRT terminal of oscilloscope No. 2. The trace of oscilloscope No. 2 is brightened by the mass peak pulses and appears as a series of dots instead of vertically deflected peaks. The intensity of the dots is proportional to the mass peak height. Because the vertical axis now represents time, the appearance and growth rate of mass fragments with respect to each other may be observed.

A typical display for PFABDE is shown in Figure 20, subsection IV-4 (PFABDE Pyrolysis). The Z-axis display requires the use of a photomicrodensitometer for quantitative data reduction. Unfortunately, it was found, upon applying a uniform signal, that the oscilloscope trace was not uniform in brightness in either the vertical or horizontal axes, across the face of the tube. This method of data acquisition therefore was temporarily de-emphasized, especially in view of the success enjoyed by the cinematographic techniques employed in the dynamic FMTA studies.

(3) Time Resolution by Single or Dual Peak Display

The Bendix TOF mass spectrometer is equipped for monitoring the output at any mass number as a function of time. This operates essentially by amplifying only those signals appearing at appropriate time intervals after the electrical pulse that starts the ion beam down the flight tube. In practice, because of limitations of the readout equipment, it is difficult to obtain more than two traces, representing two different masses.

The dual peak time resolved mass spectrum technique employs a two-channel output from the mass spectrometer to the oscilloscope, as shown in Figure 17. The signal output from each channel then appears as a vertical line on the oscilloscope each 100 microseconds (the pulse rate of the mass spectrometer). The time resolved traces for m/e = 52 and 71 occurring during PBEP decomposition are shown in Figure 34, subsection IV-5 (PBEP PYROLYSIS).

c. Dynamic FMTA

For the Dynamic FMTA experiments, a Milliken DBM-5C high-speed framing camera was employed to photograph the spectrum oscilloscope trace at a speed of 200 frames per second or 1 frame each five milliseconds. In general, the heating rate was 100°C/second. With the small sample, the pyrolysis event usually was completed within two seconds. To synchronize the temperature trace oscilloscope with the spectrum oscilloscope, a flashlamp was triggered simultaneously with the beginning of current input to the ribbon. The flash overexposes the first few frames of the spectrum oscilloscope, thereby marking the beginning of the heating. The same trigger pulse that fires the flashlamp is also used to trigger the sweep of the temperature trace oscilloscope. Because the mass spectrograph operates continuously at 100 microsecond intervals, the experiment may be begun at any time without an error in time of greater than 100 microseconds. This presents no serious error in time or temperature for experiments lasting one second, covering 10,000 complete spectra. The mass spectra, from m/e = 12 to m/e = 250 are continuously displayed on another oscilloscope. This trace is photographed by a camera operating at 200 frames per second, so that

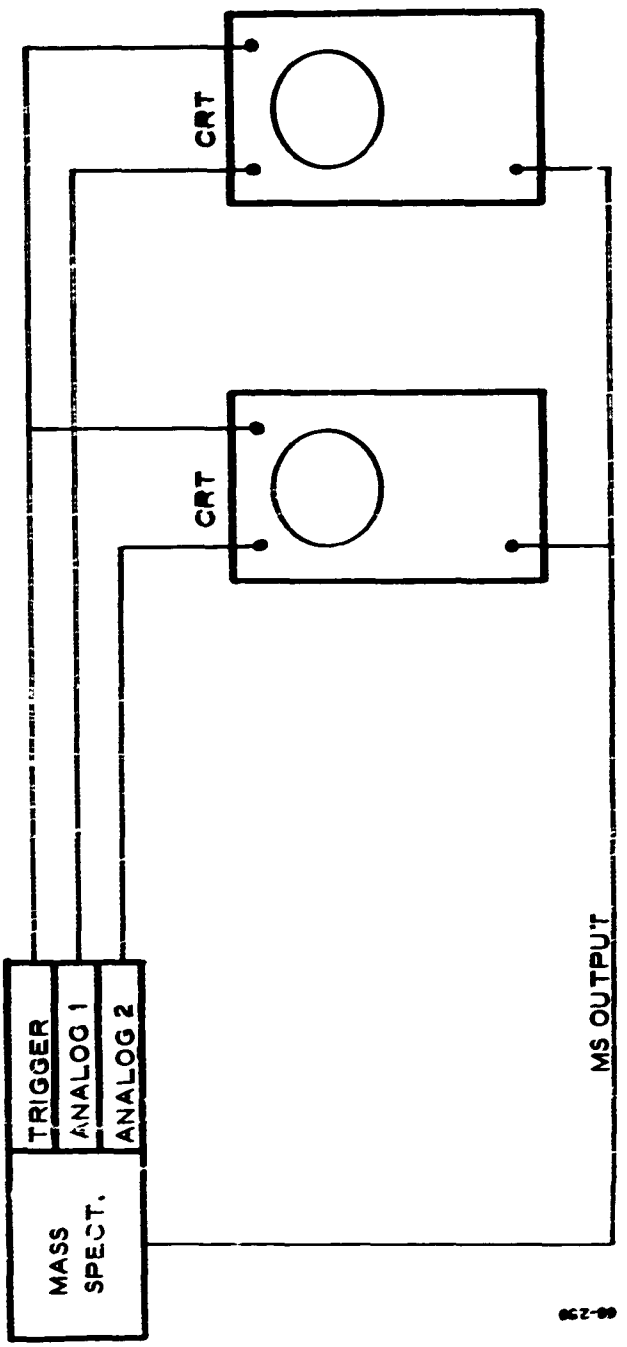

Figure 17 Oscilloscope Arrangement for Single Peak Data Display

data is recorded at five-millisecond intervals. This is sufficiently fast to permit accurately following the species formed in reactions induced by heating at rates from 100 to 200°C/second. In this heating rate range, the rate of temperature rise is 0.1 to 0.2°C/millisecond, corresponding to 0.01 to 0.02°C/complete mass spectrum trace or to 0.5 to 1.0°C/frame of film. Therefore, errors in temperature correlation, induced by one (or several) frame uncertainty for the start of the experiment would introduce an error no greater than that involved in the initial (zero time) sample temperature measurement.

(The reverse is blank)

SECTION IV

EXPERIMENTAL RESULTS AND INTERPRETATION

1. SUMMARY

(U) This section contains details of the experimental work -- from the taking of the data through the reduction of that data, to the deduction of reaction mechanisms and activation energies. INFO-635, PFABDE, PBEP, HP_2, and NC were studied by isothermal and dynamic FMTA. Reaction mechanisms were deduced for all but NC. Activation energies were determined for all but INFO-635.

(U) Correlations of mechanisms and activation energies were made and compared to those obtained by other workers. Comparison of the regions of the thermal decomposition curves studied by different techniques is discussed. The relationship of impact sensitivities of PFABDE and PBEP to their molecular structures, decomposition mechanisms, and activation energies is investigated.

2. DATA REDUCTION PROCEDURES

a. Reaction Mechanism and Mass Spectra

(U) Interpretation of mass spectra from the TOF mass spectrometer involves, to some extent, deduction of the reaction mechanism. The various individual mass spectrum lines and their corresponding intensities are meaningless without some idea of what caused them.

(U) In essence, the mass spectrum of a given compound is characteristic of its parent species, i.e., the parent can be expected to break up in a way characteristic of its internal bond strengths, the ionization potentials of the fragments, and the energy of the bombarding electron beam. Internal rearrangements may occur, or metastable ions may form, complicating the picture. However, above a certain electron beam energy, more than sufficient energy is available to fragment completely all of the primary ions and to ionize quantities of the secondary and tertiary fragments. Thus, each compound has its distinctive "cracking pattern." From these patterns, the tables of standard mass spectra are compiled.

(U) When working from the complete mass spectrum of a complex (or unknown) compound, it is necessary to identify the parent fragments from the complete spectrum by searching the standard tables, establishing tentative identities by shrewd guesses, subtracting the standard spectra from the experimental one, and determining how satisfactorily the initial assumptions explain the observed fit. This process is repeated until all species are identified. If there is foreknowledge of the probable molecular structure, it obviously shortens the process, because groups of atoms (or molecules) held to others by the weakest bonds can be deduced from thermodynamic considerations, and can be applied as the first guess.

(U) In studying pyrolysis species, it is important to identify the thermal fragments. Thermal fragmentation of the large polymer molecules produces the "parent" species that enter the electron beam to be ionized and "cracked." Thus, when the "parent" fragments have been deduced for a compound of known molecular configuration, their thermal decomposition mechanism becomes apparent.

(U) The above argument is strictly true only for time-integrated spectra of the pyrolyzing material. Time-resolved spectra offer additional helpful clues. The "100 percent peak" (the most intense line in the mass spectrum) of each parent thermal fragment will be the first to appear in the mass spectrum of the decomposing compound. Thus, the early time-mass spectrum will be relatively simple, affording a simple means for rapidly, and drastically, reducing the number of choices to make for "parents." Additional evolution of the mass spectra with time aids in the subsequent decisions between initial choices until the entire set of parent thermal fragments has been selected. At this point, comparison of the time of appearance and relative importances of the species (qualitatively, the size of the total area under the time-intensity curve) with the postulated molecular structure of the starting material reveals the thermal decomposition mechanism.

(U) Another outstanding feature that aids immeasurably is the isotope ratio of atoms such as chlorine. However, these are common to all methods of deriving data from the mass spectra, and the emphasis here is upon the unique advantages for interpretation afforded by time resolution of the mass spectra.

b. Derivation of Kinetic Rate Data

(U) To correlate the results of pyrolysis of PFABDE, PBEP, and other compounds with their impact sensitivities and thermal stabilities, it is necessary to derive quantitative relationships. These only can be derived if the experiment is capable of generating quantitative data. As currently established, quantitatively calibrating the Bendix Time-of-Flight mass spectrometer using classical techniques is a tedious process that must be repeated for each set of experiments. However, it was appreciated that the mass spectrometer is essentially a pressure-measuring device, and that the generation of pressure during a pyrolysis experiment can only be accomplished through decomposing a solid substance into gaseous species. The pressure signal generated in the mass spectrometer by a given gas therefore should be related to the rate of the decomposition reaction governed by the activation energy for decomposition and the temperature of the solid. Such was indeed found to be the case, and the techniques for application of the principles follow.

(1) Dynamic Flash MTA

(U) A mathematical technique has been developed that takes advantage of the unique differential data acquisition mode during linear programmed heating to derive reaction activation energies and, eventually, the absolute reaction rates.

(U) This method closely resembles the Differential Thermal Analysis (DTA) or Differential Scanning Calorimetry (DSC) techniques as regards linearly programmed sample heating rates and data evaluation, except that the data represent analytical time resolved mass spectra data instead of integrated caloric/thermal data, and that a considerably faster instrument response time is provided by using high-speed cinematography of the scope display instead of recorders (DTA).

(U) The films taken of the mass spectral traces are analyzed frame-by-frame for the order of appearance of species, and the parent species deduced from structural considerations and comparison with standard mass spectra (when available).

(U) It is expected that the key species in the initiation reaction(s) for thermal decomposition can be those attached to the polymer molecule with the weakest bonds, and hence appear first (at low temperatures) in the films of the mass spectra. Several of the key species are selected, and their spectral intensities are plotted as a function of time (and/or temperature) to facilitate deduction of the pyrolysis mechanism.

(U) To be able to extrapolate the data obtained at one temperature and reaction rate to another temperature, e.g., shelflife prediction, combustion rates, etc., it is necessary to derive the activation energies and preexponential factors for the reactions. Fortunately, for the determination of the activation energy (E), absolute reaction rate data are not required, but only the shape of the curve and the slope that can be derived therefrom. In the uncalibrated mass spectrometer, the line intensity, I, of a given species is related to its partial pressure, P, in the ion chamber through its ionization potential, its electron collision cross-section, the electron current, i.e., the number of electrons passing through the gas species, the electron accelerating potential (controls the electron kinetic energy available for removing an electron from the gas species), and the geometry of the mass spectrometer system. The partial pressure of a gas species in the mass spectrometer ion chamber is the difference between the rate of generation of the species (in this case by pyrolysis), and the rate at which the species is removed by the vacuum pumps, the cold traps, and to the rate of removal of ionized species by injection into the flight tube. Some of the ions are buried in the material of the ion collectors. The remainder are neutralized and removed by the vacuum pumps. All of the above phenomena involve proportionality factors that should be constants for any given gas species (ion or neutral) during any particular experiment.

(U) When the rate of reaction becomes rapid enough, the reaction energy is released at a rate faster than it can be conducted away through the solid, and auto-acceleration of the reaction occurs. The exact reaction rate at which auto-acceleration starts, therefore, is a function of the particle size, the thermal conductivity of the solid, the density of the solid, the specific heat of the solid, and the heat of reaction. In any given experiment, these quantities are all constant.

(U) The constant factors discussed above can be determined by application of a suitable computer program to results from a standard material possessing well-known thermal conductivity, specific heat, mode of decomposition, heat of reaction, density, and controlled (or measured) particle size. Development of the computer program for this purpose may involve a fairly large effort, so it is desirable to first determine the applicability of the method, as regards the validity of the mathematical treatment.

(U) If the rate of generation of a species can be represented by the Arrhenius rate expression as a first order reaction, then:

$$I \propto P \propto (1/x)(dx/dt) = k = A \exp. (-E/RT)$$

or: $$I = B \exp. (-E/RT)$$

wherein B contains the Arrhenius frequency factor, A, the mass spectrometer system constants, and the fraction, x, of a given species which remains unreacted at any given time. Consideration of x as constant over a small time or temperature interval introduces only a small error in calculating E, because it is the fraction reacted that is important in this case and not the absolute quantity. Taking the logarithm of the function yields:

$$2.303 \log. I = -E/RT + 2.303 \log. B$$

(U) A plot of log. I versus 1/T should yield a straight line with a slope of -E/(2.303 R). The intercept at log. I = 0 will yield a value of log. B that may be of value later to evaluate A, specific reaction rates, and mass spectrometer system constants.

(U) It is expected that the activation energy for the thermal decomposition reaction of a compound will reflect the activation energy of the primary decomposition species. Therefore, the Arrhenius plots of the first detected species are analyzed.

(U) To test validity of the foregoing treatment, it was necessary to study other compounds for which the activation energies already had been determined. The reference works selected concerned PFABDE and HP_2. The work on PFABDE performed at Dow Chemical Corporation (Ref. 7) used thermogravimetric (TGA) techniques. The TGA method uses data acquired after the reaction is in the autoacceleration phase, so that the Dow data correspond to the "high temperature" or "B" regime (see subsection IV-4 on PFABDE).

(C) Because the first product appearing in the decomposition spectrum of PFABDE is NF_2, that species is taken as representative of the initiation process. The "high temperature" regime yields an activation energy of 46 Kcal./mole for NF_2 comparing favorably to the value of 46 ± 5 Kcal./mole obtained by Dow.

(U) Work on HP_2 was performed at Thiokol's Reaction Motors Division (RMD) (Ref. 8), using time-to-acceleration techniques with a closed vessel. This technique yields the activation energy for a reaction that occurs

before autoacceleration -- corresponding to the "low temperature" regime. Figure 42 presents the Arrhenius plots of the HP_2 pyrolysis data using the LPC techniques. The "low temperature" regime yields a value of 23 Kcal./mole, comparing remarkably well with the value of 23.5 Kcal./mole obtained by RMD. Thus, not only the validity of the method is established, but also the fact that one experiment, using microgram quantities of material, yields data on two reaction regimes of interest.

(U) For complete definition of the reaction kinetics, the value of the reaction rate, reaction rate constant, or preexponential factor must be determined as well as the activation energy. The rate of disappearance of reactant, hence rate of appearance of products, during the first order reaction is given by:

$$dx/dt = kx$$

or: $$(1/x)(dx/dt) = k$$

which is mathematically identical to:

$$d(\ln x)/dt = K \quad \text{(where } \underline{\ln} \text{ refers to natural logarithms)}$$

on integration between limits:

$$\ln x_2 - \ln x_1 - k\,(t_2 - t_1)$$

(U) Because the ratio x_2/x_1 is the same if x is an absolute value or a fraction of the absolute value, the above rate expressions are likewise indifferent to the way in which x is expressed. This fact, together with the differential nature of the analytical technique, provides the key whereby the absolute reaction rates and preexponential factors may be derived from the data taken by the uncalibrated system. The total area enclosed by the intensity/time curve for a given mass species represents the total quantity of that species formed as the result of the reaction. Any portion of the total area, taken at a definite time, then represents a definite fraction of the quantity of that species formed. The total area, and suitable fractions thereof, taken at short time intervals during the initial stages of the reaction, then can be re-plotted as ln x versus time.

(U) The above arguments assume that no consecutive reactions are involved, which is a good assumption in these particular experiments, i.e., primary species evolved into a vacuum in close proximity to the ionizing electron beam. The mean free path of the primary species is much longer than the path to the electron beam.

(U) Because each time corresponds to a definite temperature, the slope of the plot, taken at several times, correspond to values of the absolute reaction rate constant, k, taken at several temperatures. The ln k then can be plotted against reciprocal absolute temperature in the conventional manner, and both the activation energy and the preexponential factor, A, determined routinely. While the theory is clear, a suitable simple kinetic system with which to test the theory has not been found yet.

(2) Isothermal Experiments

(U) As mentioned earlier, flash heating of a sample to an isothermal condition is essential to a complete understanding of the explosion criterion. Ubbelohde, Wenograd, and others (Refs. 9, 10) have demonstrated a relationship between explosive sensitivity and time-to-detonation of explosives. Wenograd's experiments most closely approximate the LPC experiments in that electrical flash heating of small samples was used to achieve a high heating rate. Therefore, Wenograd's relationship will be used at the start as the basis of comparison. Wenograd found that the time-to-explosion could be expressed by an Arrhenius-type equation:

$$t_E = A' \exp. (B'/RT_E)$$

where t_E was the time to explosion, T_E was the absolute temperature at which the explosion occurred, and A' and B' were arbitrary constants. He considered B' to be an "adiabatic" activation energy that could be used as a rough estimate of the true activation energy for explosion. His activation energy data did not agree with those of other workers who made low-temperature isothermal investigations. However, he found that when data were extrapolated by the use of the above equation, to t_E = 250 microseconds (the contact time during impact testing) that each organic nitrate/nitro explosive exhibited a characteristic temperature more representative of the impact sensitivity than the "activation energies." Thus, Wenograd's correlations must be included in any investigation into molecular structure/activation energy/explosive sensitivity relationships.

(U) The workers at RMD, whose experimental data was presented in the discussion of HP_2, correlated the time to autoacceleration to activation energy using a more rigorous mathematical treatment. By making the assumption that the concentration of reactant present is constant when autoacceleration begins at a given temperature, it is simple to transform the Arrhenius rate expression to:

$$1/t_i = k_o k = k_o A \exp. (-E/RT)$$

This would appear to be the reciprocal of Wenograd's equation, with:

$$1/t_i = t_E,\ k_o A = A',\ \text{and } -E = B'.$$

Note that in neither case is the value of the Arrhenius preexponential factor readily derivable from their experiment. However, with the value of the preexponential factor available from the linear programmed heating rate experiments using the LPC technique, and the value of the $k_o A$ available from LPC flash-heated isothermal experiments, it should be possible to produce a reasonable theoretical correlation between molecular structures, kinetic rate data, and explosive sensitivity.

(U) In essence, the isothermal technique uses a capacitor discharge in place of the battery used for linear programmed heating to achieve temperatures up to 500°C in less than 20 microseconds. (Details were given

in Section III.) The short duration of the isothermal heating technique makes it necessary to employ extremely rapid data gathering techniques. To date, the Z-axis modulation technique has proven the most successful, despite equipment deficiencies. Figure 20 shows a typical isothermal pyrolysis of PFABDE, displayed with the Z-axis modulation technique. The data are taken for 40 milliseconds, well within the time held at constant temperature as predicted by the computer.

(U) From the variation of intensity with time of the dots representing each key species, rates of isothermal decomposition can be obtained, as well as time to autoacceleration. The time to autoacceleration at several temperatures can be correlated with explosive sensitivity a la Wenograd, while identifying the species produced before and during autoacceleration, thereby providing clues to the molecular structure factors responsible for the sensitivity.

(U) As previously stated, this technique suffers from non-uniform brightness of the trace across the cathode ray tube (CRT). However, it may be possible to replace the present CRT with one which, if not uniform, would at least vary predictably so that calibration of the trace would be possible.

(U) In summary, the following combination of techniques have been evaluated for studying the phenomena as stated:

Phenomenon	Instrument Conditions	Data Acquisition
Thermal stability, shelflife	Moderately low linear heating rates	High-speed cinematograph of synchronized bridge imbalance/displays of mass spectra
Explosive monitoring	High heating rates to predetermined constant temperature	Z-axis modulation

3. INFO-635P RAPID PYROLYSIS

a. Results and Discussion

(U) The mass spectra resulting from a series of rapid pyrolyses at different temperatures are given in Table I, in addition to some high resolution data reported by Dow for a "slow" pyrolysis at 170°C (Ref. 11). The LPC spectra are time-integrated, i.e., they represent a superposition of spectral scans occurring every 100 microseconds during a 10-millisecond period initiated by triggering the capacitor discharge. The Pt ribbons were coated by the spray technique previously described, and the amount of sample was estimated by microscopic examination to be of the order of 10 micrograms.

TABLE I

MASS SPECTRA FROM INFO-635P ISOTHERMAL FMTA

Mass No.	Possible Positive Species	Relative Intensity[a, b] Filament 8 185°C (1.8 msec)	Filament 2 200°C (1.8 msec)	Filament 7 210°C (100 msec)	Filament 9 520°C (1.8 msec)	Dow Slow Pyrolysis 170°F (Ref. 11)
12	C			8	80	
13	CH				6	
14	N, CH_2	22	15	3	18	
15	NH, CH_3	11	8	2	42	
16	O, NH_2, CH_4	74	40	17	210	
17	OH, NH_3	180	210	56	10	
18	H_2O*, NH_4*	240	180	60	34	15
19	F		5	11		
20	HF*			2		13
25	C_2H				10	
26	C_2H_2, CN	13	5	4	60	
27	HCN, C_2H_3	26	24	30	82	
28	N_2*, CO*, CH_2N*, C_2H_4*	~ 0	~ 0	~14	~0	126
29	CH_3N, C_2H_5, CHO	36	18	42	20	
30	CH_4N*, NO	24	80	45	27	200
31	CF, CH_3NH_2, CH_3O	15	5	4		
32	O_2	~ 0	~ 0		~11	
33	NF*					85
34				<1		
35	Cl^{35}			1		
36	HCl^{35}	8		8		
37	Cl^{37}			1		
38	HCl^{37}, C_2N	7		3		
39	C_2HN	12	9	18	3	
40	C_2H_2N	21	8	6	6	
41	C_2H_3N, C_2HO	31	26	46	3	
42	C_2H_4N*, C_2H_2O	24	14	32	2	103
43	C_2H_5N, C_2H_3O, CHNO	50	40	54	190	
44	CO_2*, C_2H_6N*, C_2H_4O, N_2O, CH_2NO	16	120	54	22	230

TABLE I (Continued)

Mass No.	Possible Positive Species	Relative intensity (a, b) Filament 8 185°C (1.8 msec)	Filament 2 200°C (1.8 msec)	Filament 7 210°C (100 msec)	Filament 9 520°C (1.8 msec)	Dow Slow Pyrolysis 170°F (Ref. 11)
45	C_3H_7N, CNF, C_2H_5O	19	9	27	11	
46	NO_2, CHNF, C_2H_3F		7	4		
47	CH_2NF, C_2H_4F		3	1		
48	CH_3NF, C_2H_5F, $CHCl^{35}$			3		
50	CH_3Cl^{35}, CF_2			1	8	
51	$Cl^{35}O$	6		2		
52	NF_2			2		
53	$Cl^{37}O$, HNF_2	6		7		
54		7	5	8		
55	C_2HON	17	19	39	7	
56	C_2H_2ON	11	9	23		
57	C_2H_3ON, C_2NF	13	14	38	5	
58	C_2H_4ON, C_2HNF			11		
59	C_2H_2NF, $CHNO_2$, CH_3N_2O, C_2H_5NO	83	43	6		
60	C_2H_3NF, C_2H_6NO			12		
61				2		
62				< 1		
63				1		
64	CNF_2			6	5	
65				2	2	
66	N_2F_2		5	3	2	"some"
67	$Cl^{35}O_2^*$, C_3HON		8	10	2	130
68	C_3H_2ON		5	14	2	
69	$Cl^{37}O_2^*$, $C_3H_3ON^*$, CF_3		10	20	5	49
70	C_3H_4ON		9	34	2	
71	C_3H_5ON		6	20	2	
72	C_3H_6ON			8		
73	C_3H_7ON			8		
74	C_3H_8ON, C_2HNCl			1		

TABLE I (Continued)

Mass No.	Possible Positive Species	Relative Intensity(a, b) Filament 8 185°C (1.8 msec)	Filament 2 200°C (1.8 msec)	Filament 7 210°C (100 msec)	Filament 9 520°C (1.8 msec)	Dow Slow Pyrolysis 170°F (Ref. 11)
75	$C_2H_2NCl^{35}$*					37
76	$C_2H_3NCl^{35}$			1		
77	$C_2H_4NCl^{35}$			2		
78	$C(NF)_2$			1		
79	$HC(NF)_2$			5		
80	$CONF_2$*		3	2		10
81			5	14	18	
82	CCl_2		3	12	4	
83	$Cl^{35}O_3$, CNF_3		8	13	4	
84			6	10	4	
85	$Cl^{37}O_3$		5	9	2	
86				7		
87	$C_3H_5O_2N$*, $NFCOC_2H_3$			2		53
88	$NFCOC_2H_4$			1		
89				2		
91			<1	2		
92			<1			
93			<1	2		
94				1	2	
95			4	7	2	
96			6	11	2	
97			3	9		
98				6		
99	$Cl^{35}O_4$			3	12	
100	$HCl^{35}O_4$			2	3	
101	$Cl^{37}O_4$			1		
102	$HCl^{37}O_4$, F_2CNF_2			1		
103				1		
104				1		
105				2		

(This Page Unclassified)

TABLE I (Continued)

Mass No.	Possible Positive Species	Relative Intensity[a, b] Filament 8 185°C (1.8 msec)	Filament 2 200°C (1.8 msec)	Filament 7 210°C (100 msec)	Filament 9 520°C (1.8 msec)	Dow Slow Pyrolysis 170°F (Ref. 11)
106				1		
107				2		
109				4		
110				4		
111	$C(NF)_3$			3		
112				4		
113				2		
114				3		
115				1		
117				1		
119				1		
121				1		
122				1		
123	$C_6H_4N_2F$*			2		16
124				2		
125				2		
126				1		
128				1		
129				3		
135				1		
138				2		
156	$C_3H_6ON_3F_3$*					"some"
158	$C(NF_2)_3$*					"some"
196				1		
197				1		
198				2		
206				<1		
	Total ion intensity x 10^{-3}	6.04	13.3	65.5	10.8	

a) Relative to total ion intensity for particular run.
b) Mass range of 12-250 observed for No. 7, 14-100 for numbers 2 and 8, and 12-100 for No. 9.
* Species identified by Dow using high resolution apparatus, and slow heating (Ref. 11).

(U) The temperatures given in Table I are the averages over the length of the combined wire-ribbon filaments, calculated from the observed bridge imbalances after 250 microseconds. As discussed above, the temperatures are believed to be constant in time, but these average values are likely to be greater than the actual ribbon temperatures themselves because of excessive heating of the wire portions of the filament. Experiments are reported at essentially two temperatures (200 and 520°C) with the blanking circuit set to permit time-integrated spectra recorded for 1.8 milliseconds; one experiment was performed to provide a comparison between time-integrated spectra recorded for 1.8 and 100 milliseconds.

(C) The time-integrated spectra are extremely complex, making definitive conclusions on the basis of the few experiments quite risky. The following comments and conclusions are presented at this time.

(1) The present data are normalized by dividing the individual intensities by the sum of the intensities measured in a given experiment. This is judged less likely to introduce artifacts that may result from attaching too much significance to a particular peak, such as the 43 peak.

(2) For the most part, the differences in peak intensities between the 185 and 200°C experiments cannot be regarded as significant in view of the errors in detection and measurement. Some differences appear real, however, e.g., m/e 16, 30, 36, 40, 43, 44, but additional experimentation would be necessary to determine any causal relationship between these differences and the small temperature change.

(3) Relatively large amounts of fragments corresponding to the aliphatic amine and/or aliphatic ether portions of INFO are observed.

(4) Increasing the observation time from 1.8 to 100 milliseconds produces a several-fold increase in the total number of ions observed. On a relative basis, there is a particular increase in such species at F, some of the C_2H_xN and/or C_2H_xO, C_2H_xON, and numerous species above m/e 60. Simultaneously, relatively large decreases occur in m/e 15, 18, 30, and 44.

(5) Increasing the temperature from 200 to 520°C at 1.8 milliseconds yielded a particular increase in C, CH, CH_4, C_2H, m/e 43 (C_2H_5N, C_2H_3O, CHNO) and several others, while relative decreases occurred, for example, in m/e 18, 30, 44, and 19.

(6) The various Cl species are qualitatively, but not quantitatively, consistent with the fragmentation pattern of $HClO_4$ (Ref. 12).

(7) Similarly, the various N species below m/e 45 are qualitatively consistent with the fragmentation patterns of ethylene imine (Ref. 13) or ethylamine (Ref. 14). The existence of masses at 45 and 44 favors the amine and its radical ($-CH_2-CH_2-NH_2$), but the imine cannot be ruled out.

(8) Points 6 and 7 are in agreement with the concept that primary steps in the INFO-635P decomposition involve dissociation into $HClO_4$ and $(NF_2)_3$ $C-O-CH_2-CH_2-NH_2$ and breakage of the $-O-CH_2-$bond of the latter.

(9) Dow has postulated that an initial step of the decomposition may involve the formation of a solid residue that subsequently decomposes (Ref. 11). If this is consistent with the present observation of an increase in ethylamine fragments at low temperature and of $HClO_4$ and its fragments at high temperature it is not now apparent.

(10) Fragments containing Cl, NF, and F are conspicuous in their sparsity. The absence of NF itself in the rapid pyrolysis experiments, and the presence of H and various fragments (masses 45, 46, 48, 57, 58, 60, and 64) may indicate that breakage of the C-NF bond is relatively slow while F readily leaves the $C-NF_2$ groups. On the other hand, the mass spectrometric fragmentation pattern of $(NF_2)_3$ $COCH_3$ is reported to contain significant quantities of NF and NF_2 (Ref. 15).

(C) It would appear that the $-C(NF_2)_3$ and ClO_4 moieties are retained in reaction products above the m/e range observed, and the possibility exists of solid-solid or gas-solid reactions even within the very short times involved here. These results from very rapid pyrolysis are in contrast to those from the Dow slow-heating experiments (Para. 9, above).

(C) Several pyrolyses have been conducted with a ribbon filament upon the hydrochloride form (INFO-635C) of INFO-635P, the former being prepared by an ion exchange treatment of INFO-635P.* The resulting mass spectra contained little or no m/e = 35 (Cl) or 36 (HCl), and in view of the susceptibility of INFO-635C to hydrolysis and degradation, it appears probable that the samples no longer contained HCl at the time of pyrolysis. Although more elaborate handling procedures could be devised to minimize such prior decomposition, the problem has not been pursued.

b. Conclusions

(C) The most positive conclusion possible from the spectra reported herein is that they support the postulate of INFO-635P dissociating into

---

(U)* We are indebted to 3M for supplying us with information upon the preparation and stability of INFO-635C.

$HClO_4$ and $(NF_2)_3$ $-COCH_2-CH_2-NH_2$ with breakdown of the latter occurring at the $-O-CH_2-$bond.

(U) The present limited experiments indicate that the mechanism of thermal decomposition of INFO-635P may be entirely different at low (tens of degrees per minute) heating rates, and high (10^8 degrees per minute) heating rates.

4. PFABDE PYROLYSIS

(C) Both PFABDE and PBEP have been of interest as high energy oxidizer/binders for solid propellants. Both compounds are characterized by a high theoretical NF_2 content and relatively low stability. PFABDE has approximately three times the impact sensitivity of PBEP. To determine the possibility of chemically stabilizing these compounds, it is necessary to determine the factors responsible for their sensitivity.

(C) Comparisons between the decomposition mechanisms of PFABDE and PBEP are expected to emphasize differences between their structures. PBEP contains two vicinal NF_2 groups -- one on the backbone and one on the side-chains. PFABDE contains two tris (difluoramino) methoxy groups, both of which are on side-chains. Therefore, it appears reasonable to expect different mechanisms for the decomposition initiating reactions.

a. Isothermal Pyrolysis Results and Discussion

(U) Numerous pyrolyses have been conducted upon PFABDE, using both time-integrated and time-resolved recording of the spectra obtained at 10 KHZ frequency (100 microseconds).

(U) Figure 18 is a line drawing typical of the time-integrated spectra of the low mass range obtained during rapid pyrolysis of the PFABDE. Results are shown for a 1.8 milliseconds observation (18 scans) of PFABDE gaseous products at a pyrolysis temperature of 260°C. Tentative identification of the species from these and time-resolved experiments are shown in Table II.

(U) A pyrolysis run was completed with PFABDE at 200°C using time-integration and monitoring the high mass range. The spectrum obtained is reproduced in Figure 19. The observed m/e peaks, and their tentative identification are presented in Table III.

(C) Other m/e peaks were observed at low intensity. This pattern suggests that one of the pyrolysis routes involves elimination of the tris-(difluoramino) methoxy group, breakdown of the latter to generate $.NF_2$ and .F radicals and fast reaction of these fluorine species with the polymeric C_4 units.

(U) The Z-axis multiple peak technique (Ref. 2) was used for obtaining qualitative time-resolved mass spectra during pyrolysis, i.e., for separately recording the spectral intensities every 100 microseconds over a relatively broad mass range.

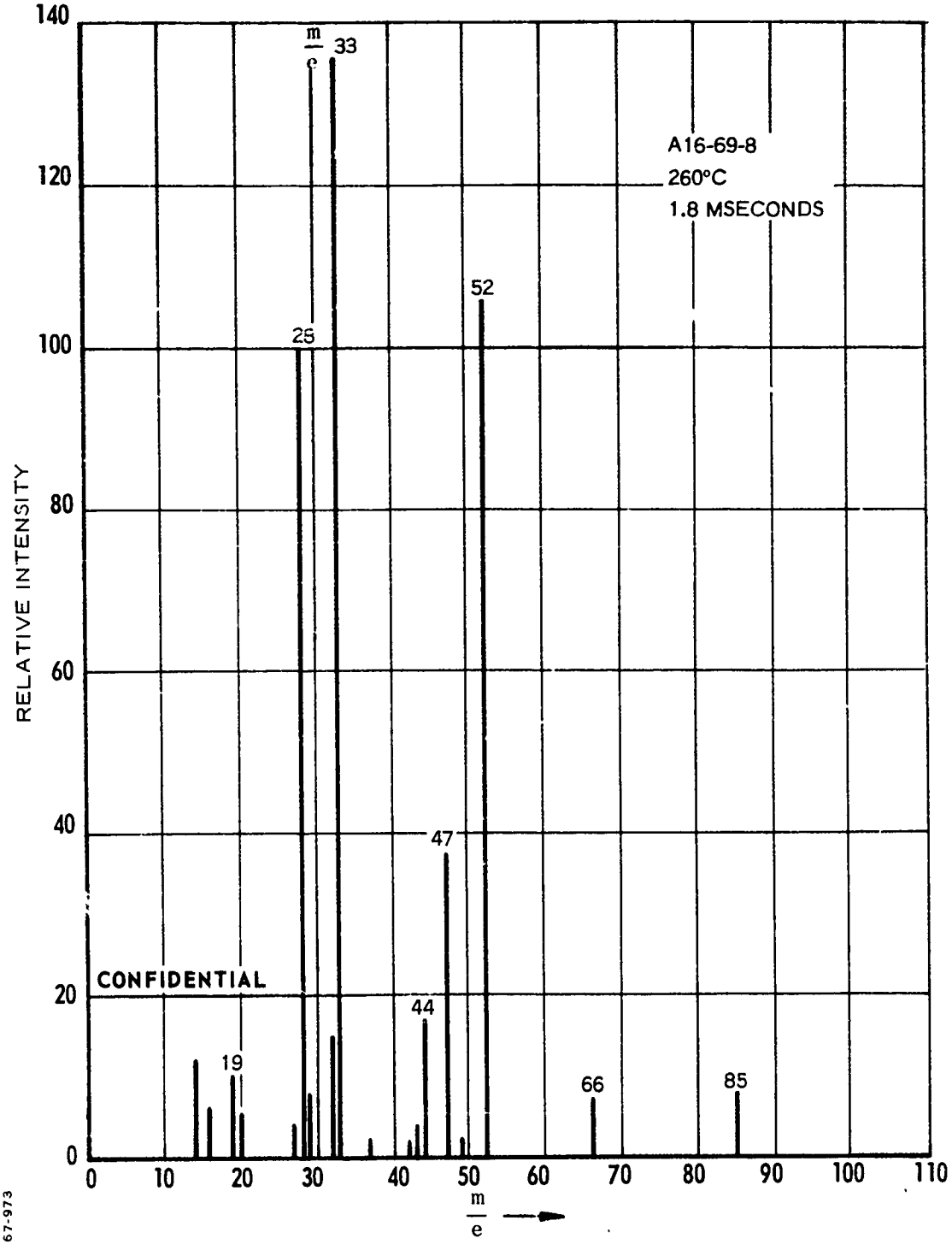

Figure 18 Line Drawing of Time-Integrated Spectra from PFABDE Isothermal FMTA

TABLE II

TENTATIVE MASS SPECTRA PEAK ASSIGNMENT FOR PFABDE ISOTHERMAL FMTA

m/e	Possible Positive Species	m/e	Possible Positive Species
14	N, CH_2	43	HNCO*, C_2H_3O(i/5)
15	NH, CH_3	44	CO_2, C_2H_4O
16	O, NH_2	47	N_2F*, COF*
17	OH, NH_3	49	
18	H_2O	50	
19	F	52	NF_2*
20	HF*	55	C_2HON, C_3H_3O
27	C_2H_3, HCN	61	CONF*
28	CO*, N_2* (1/7)	66	COF_2*, $N_2F_2H_2CNF_2$
29	HCO, C_2H_5	69	CF_3
30	H_2CO, NO	80	$CONF_2$
31	CF	85	N_2F_3*
32	O_2	96	
33	NF*	103	$C_4O_2H_4F$, $C_3O_2H_2NF$
35	H_2NF	120	$C_4OH_4NF_2$, $C_3O_2NF_2$
37		156	$C_3O_2H_3N_2F_3$ [OCH CH_2O C(NF)(NF_2)?]
41	C_2HO, C_3H_5	165	CON_3F_5 [OC (NF)(NF_2)$_2$?]
42	NCO*, C_2H_2O* (1/6)		

* Reported by Dow in high resolution experiments of slow pyrolyses at 135°C. Numbers in parenthesis represent relative intensities of two species at same m/e. (Private communication, J. Flynn and T. Dergazarian, Dow Chemical Company)

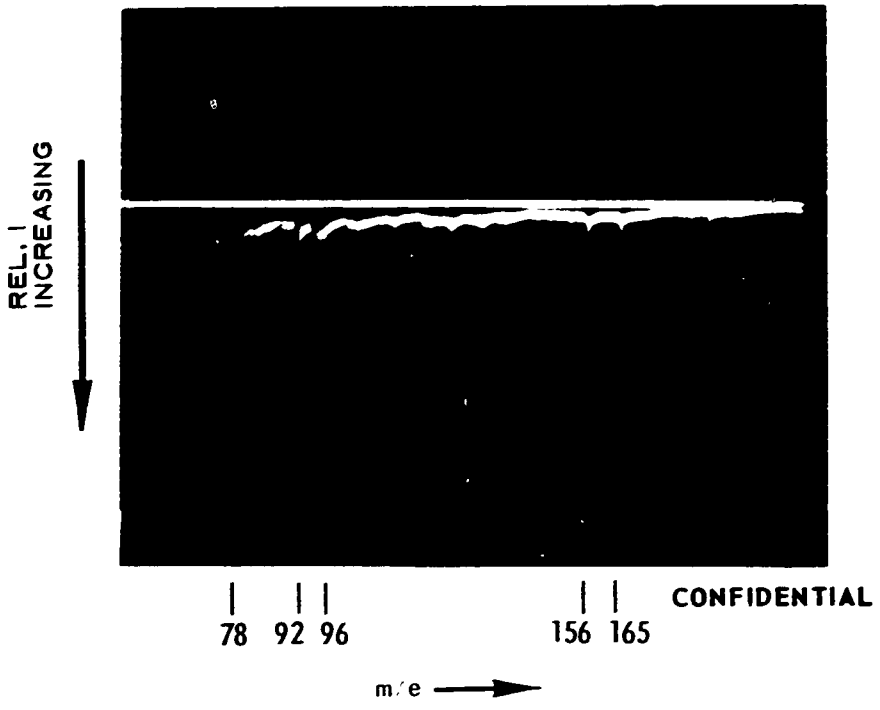

Temperature = 200°C

Figure 19 High Mass Spectrum of PFABDE Isothermal FMTA

TABLE III

HIGH MASS SPECIES FROM PFABDE
ISOTHERMAL FMTA

m/e Value	Intensity	Species	Likely Origin*
78	Strong	$CN_2F_2^+$	$-O-CX_3$
92	Medium	Not Identified	
96	Medium	Not Identified	
103	Weak	$C_4O_2H_4F^+$, $C_4H_6ONF^+$	$-\overset{\overset{F}{\vert}}{C}-\overset{\overset{F}{\vert}}{C}-O$
120	Very Weak	$C_4H_4ONF_2^+$	
156	Weak	$(C_4H_6ON_2F_2 \cdot HF^+)$	
165	Weak	$CON_3F_3^+$	$-O-CX_3$

*Refers to original structural group present in species.

(U) Figure 20 reproduces actual oscilloscope tracings obtained during two successive pyrolyses upon a single PFABDE sample at temperatures of 230 and 260°C. Separate scans are made over the mass range (~10 to 100) at 100 microsecond intervals. In this representation, the concentration of any species is indicated by the brightness of the dot (Z-axis). Experiments with a standard signal input and with constant background (air) signal have demonstrated significant departures from linearity of the light spots over the face of the oscilloscope screen. Consequently, interpretation of any small changes in dot brightness with time or from species to species must be made with caution. With this reservation in mind, representative data are presented graphically in Figures 21 and 22 for PFABDE (Intensities are designated as: Weak, Moderate, Strong, Very Strong).

(U) Structural assignments to the observed m/e values are tentative, particularly, of course, for the quite high m/e species.

(C) The following comments are presented in summation of Figures 18 through 22, plus the results of other similar experiments:

- Numerous species are produced even within the first 100 microseconds of pyrolysis, demonstrating the presence of extremely rapid and probably complex processes.
- The most intense peaks observed with PFABDE include 33 (NF), 52 (NF_2), 47 (N_2F, COF ?). Less intense peaks include 19 (F), 20 (HF), 66 (COF_2, H_2CBF_2, N_2F_2 ?), 165, 156, etc.
- The largest species observed so far with PFABDE are 165 and 156. These undoubtedly contain within themselves the potential for producing -- qualitatively -- many of the lower species observed as the result of electron bombardment. Fragmentation patterns of model compounds in conjunction with computerized data reduction will be of great value in interpreting such data. Primary decomposition steps may involve loss of the tris (NF_2) methoxy group as well as unimolecular breakage of the C-N and N-F bonds, giving rise to free radical chains.

b. Dynamic FMTA Results and Discussions

(U) Dynamic FMTA were also performed with PFABDE. Figures 23 and 24 show the data obtained from the 16 mm film at selected intervals (as described in a previous section). The relative growth and disappearance of all species may be observed easily from these figures.

(1) Mass Spectrum Assignments

(U) The assignments of ionized species to the observed m/e's, as presented in Table IV, were made on the basis of previous experience and by comparison with literature.

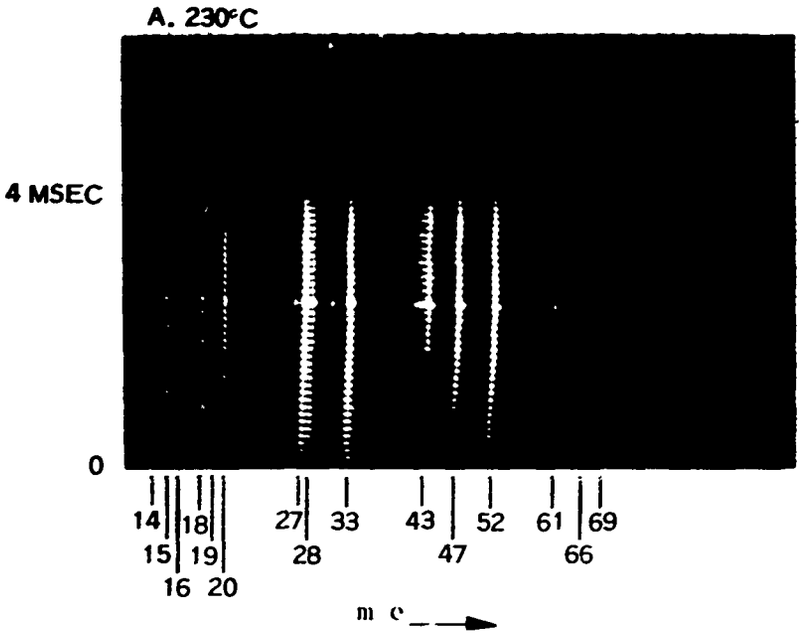

CONFIDENTIAL

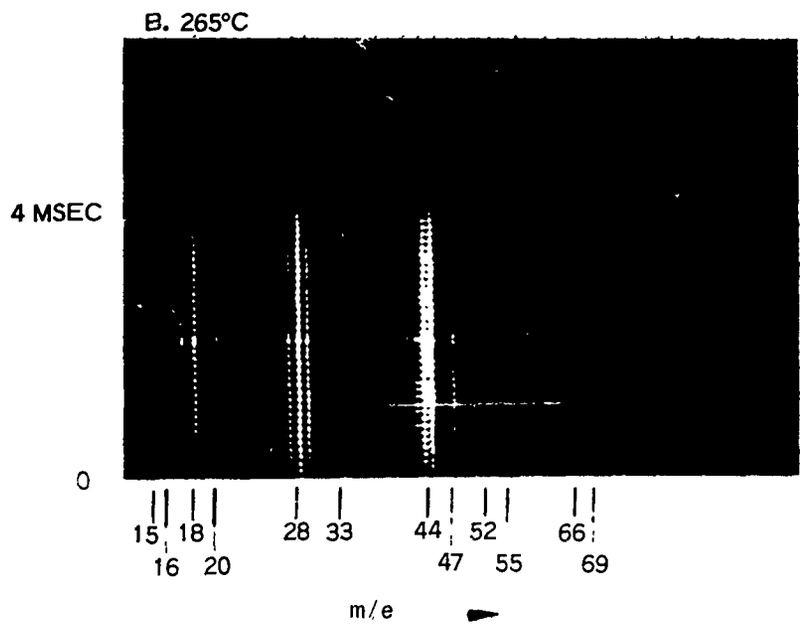

CONFIDENTIAL

Figure 20 Z-Axis Mass Spectra of PFABDE Pyrolysis

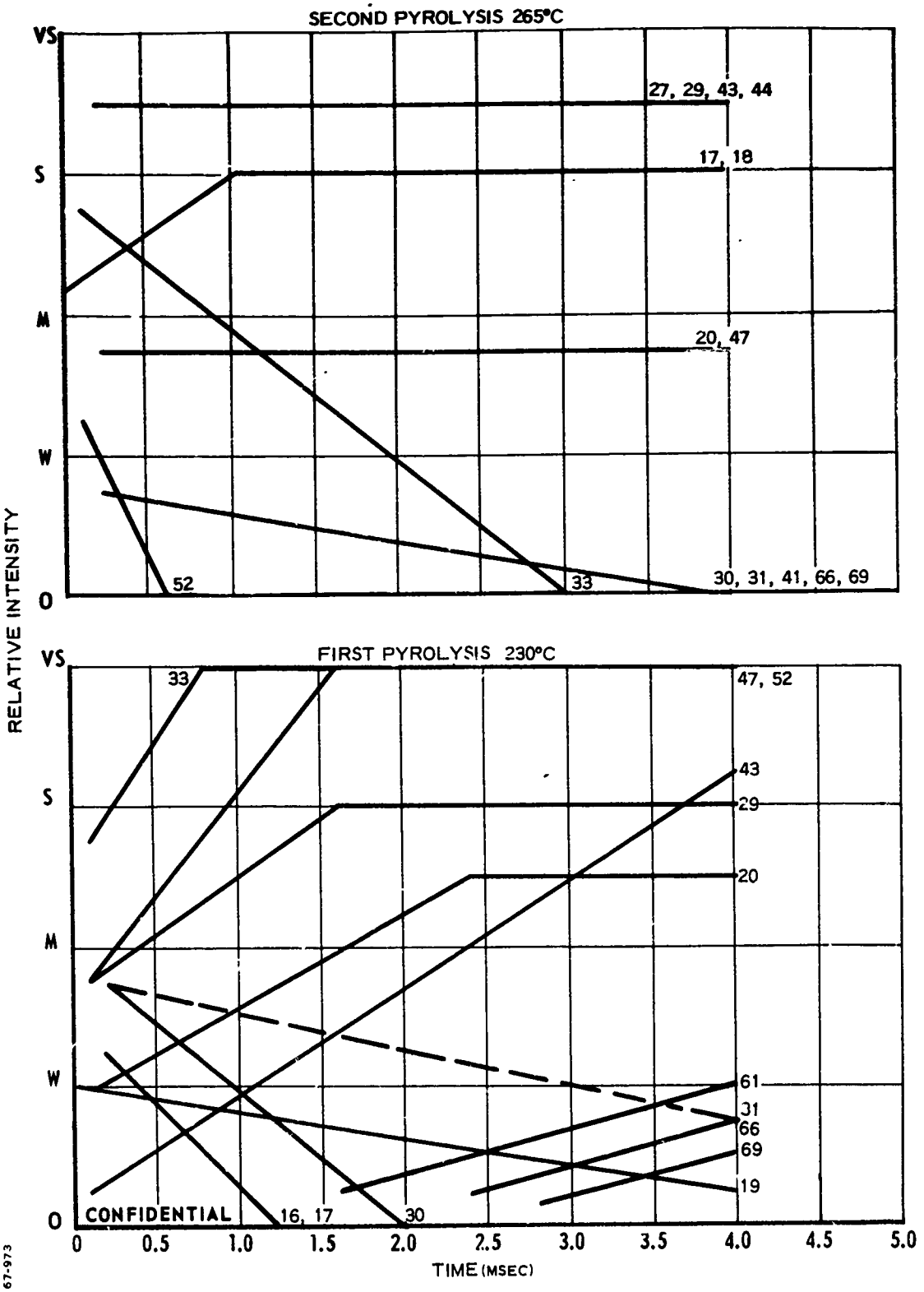

Figure 21 Time-Resolved PFABDE Isothermal FMTA Spectra (A16 - 61 - 9), Z-Axis Multiple Peak from m/e = 12 to m/e = 100

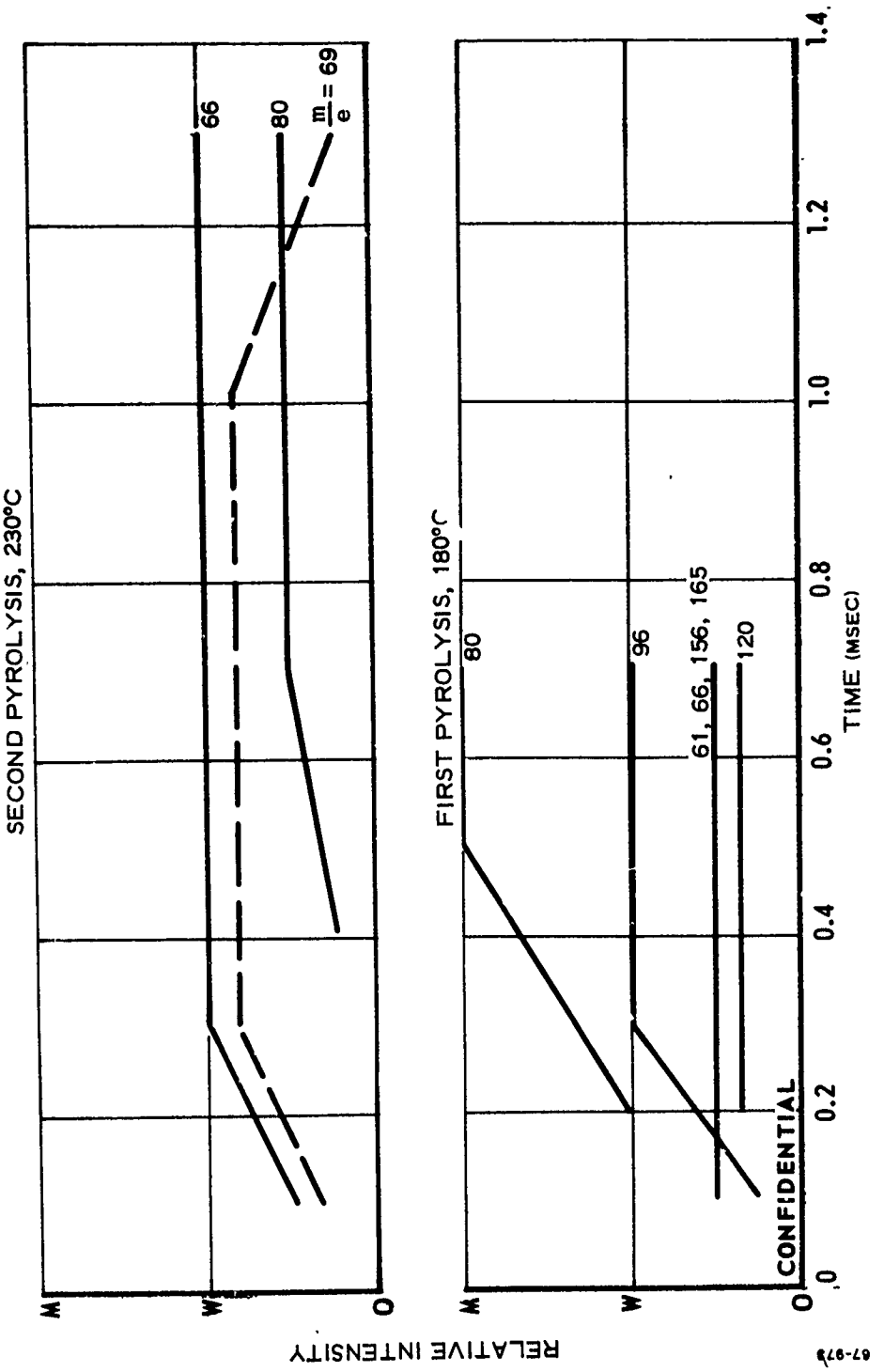

Figure 22 Time-Resolved PFABDE Isothermal FMTA Spectra (A16 - 62 - A), Z-Axis Multiple Peak from m/e = 40 to m/e = 200

TABLE IV

PFABDE PYROLYSIS FRAGMENT HISTORIES FROM DYNAMIC FMTA

Time (msec) Initial	Max.	m/e	Intensity	Ion Fragment
855	1050	52, 33	120	NF_2, NF
	1050, 1250	47	34, 36	N_2F, COF
	--	45	1	CNF
	1350	44	5	CO_2
	1020	43	6	C_2H_3O
870	1020	61	9	OCNF
	1330	18	8	H_2O
915	1050, 1250	66	7, 7	N_2F_2, COF_2
	1020	80	6	$OCNF_2$
	1020, 1230	20	8, 13	HF
	1020	42	4	NCO, C_2H_2O
930	--	17, 19, 31, 71, 78	1	--
	1020	29	3	HCO
	1075	69	3	CF_3
935	--	15, 57, 64	-	
940	--	30	-	H_2CO
	1015, 1280	59	2, 2	FNCN
950	--	40	-	C_2O
	1230	41	2	C_2HO
955	1250	55	2	C_3H_3O
1010	1030	65, 73	1	--
	1050, 1150	54, 95, 98	1, 1, 1	(Peak Activity)

(C) Table IV also shows that ion fragments with m/e = 52, 33, 28, 47, 45, 44, and 43 are first to appear. The product species represented by m/e = 52, 33, 28, and 47 are dominant, whereas product species represented by m/e = 44 and 43 are minor. The species at m/e = 45 never appears as more than a trace; m/e 52 and 33 can be attributed to the positive ions, NF_2^+ and NF^+, presumably with NF_2^+ as the parent and NF^+ the daughter produced by splitting off an F atom in the ionization chamber of the mass spectrometer. The absence of F^+ or F_2^+ ions at this stage and the low level of F^+ throughout, strongly suggests that NF_2 and NF may be product species produced simultaneously, but by different thermal mechanisms, so that the contributions to the m/e = 33 (NF^+) peak could be due to "parent" NF as well as "daughter" NF^+ from NF_2^+.

(C) The formation of some N_2F_4 also is a possibility, with resultant cracking to yield $N_2F_3^+$, $N_2F_2^+$, NF_2^+, F^+ and N^+. Again, the relatively low level of F^+ at m/e = 19 argues that this is not a high probability process.

(C) The behavior of m/e = 43, Figure 25, suggests that several reactions, occurring sequentially, contribute during the course of the experiment. In the early stages, only m/e = 43 is evident, but is later joined by ions with m/e = 41, and 40 (Figures 23 and 24). This cracking pattern is highly suggestive of a hydrocarbon fragment and the most reasonable assignment yields $C_2H_3O^+$ for m/e = 43 as the parent.

(C) The ion at m/e = 44 would seem to be due to CO_2^+, rather than to a larger hydrocarbon fragment such as $C_2H_4O^+$, since the behavior of the m/e = 44 trace does not coincide with the behavior of the m/e = 43 as do the ions with m/e = 42, 41, and 40.

(C) The fragment at m/e = 47 contributes a major share to the mass spectra, and shows a distinctive double peak in the time-intensity curve (Figure 25), as do m/e = 52 (NF_2), 33 (NF), and 20 (HF). This peak could be due to N_2F^+ as a fragment of the parent N_2F_4 ion, but the absence of the $N_2F_3^+$ peak indicates that this can only be a minor contribution. The alternatives are H_2CNF and COF.

(C) It is doubtful if H_2CNF^+ could be present in the large amounts observed for m/e = 47 without producing sizeable peaks at m/e = 46 and 45. Since no m/e = 46 appears and m/e = 45 is very weak, the m/e = 47 peak must be attributed to COF^+ which could be a daughter of COF_2^+, $FNCOF^+$, $FNC(F)O^+$, or $OC(F)NF_2$. Because most of these parent compounds should be very unstable, they may be fragmented thermally, or by electron impact in the ionization chamber of the mass spectrometer.

(C) The other mass assignments were made routinely by considering them as possible parents or daughters of the ion species already assigned. Some assignments were made on the basis of an alternative but minor decomposition mechanism whereby the tris (di-fluoramino) methoxy group first loses oxygen. Many of the products then are similar to those in the cracking pattern of perfluoroguanidine.

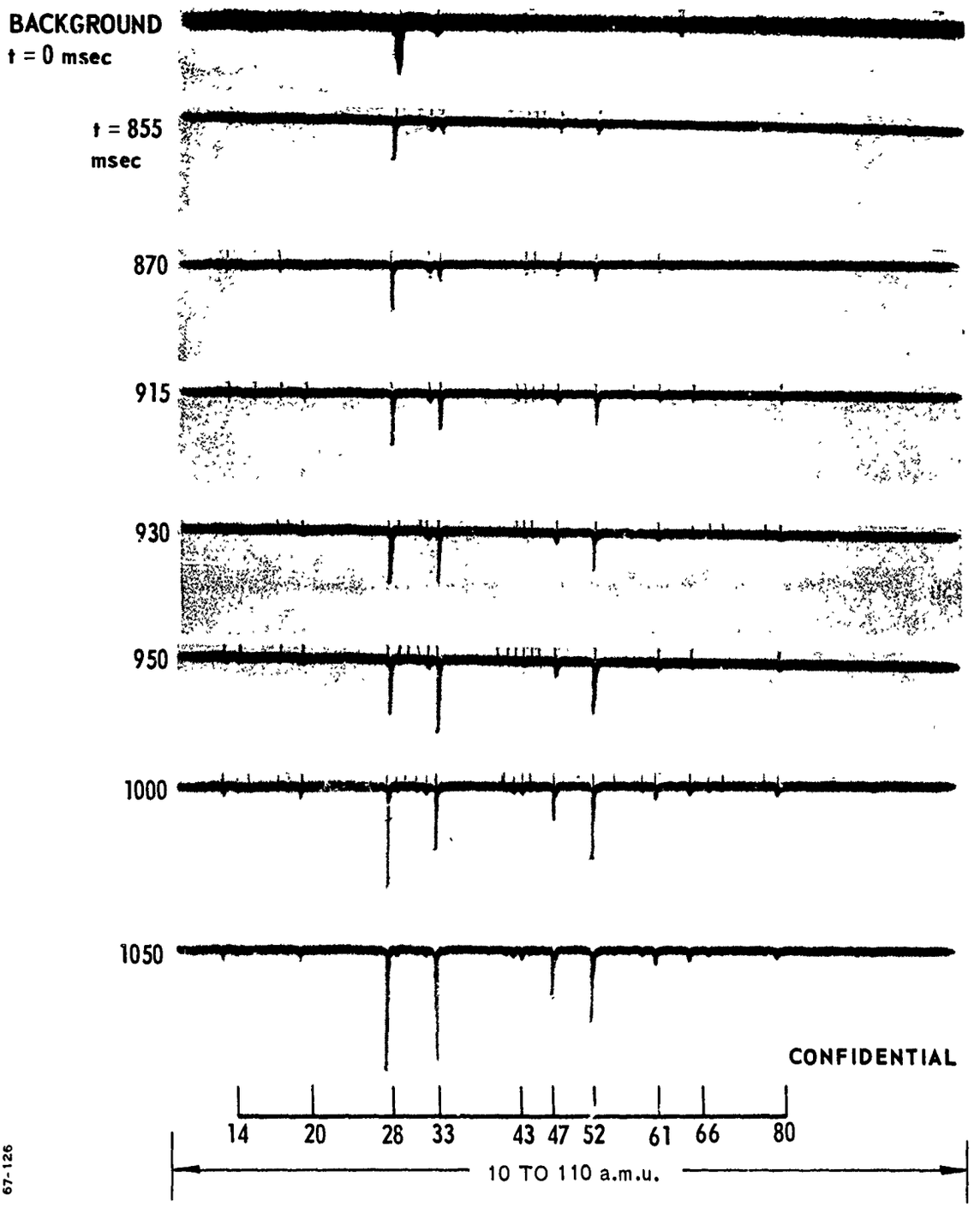

Figure 23 PFABDE Dynamic FMTA, 855 to 1,050 Milliseconds

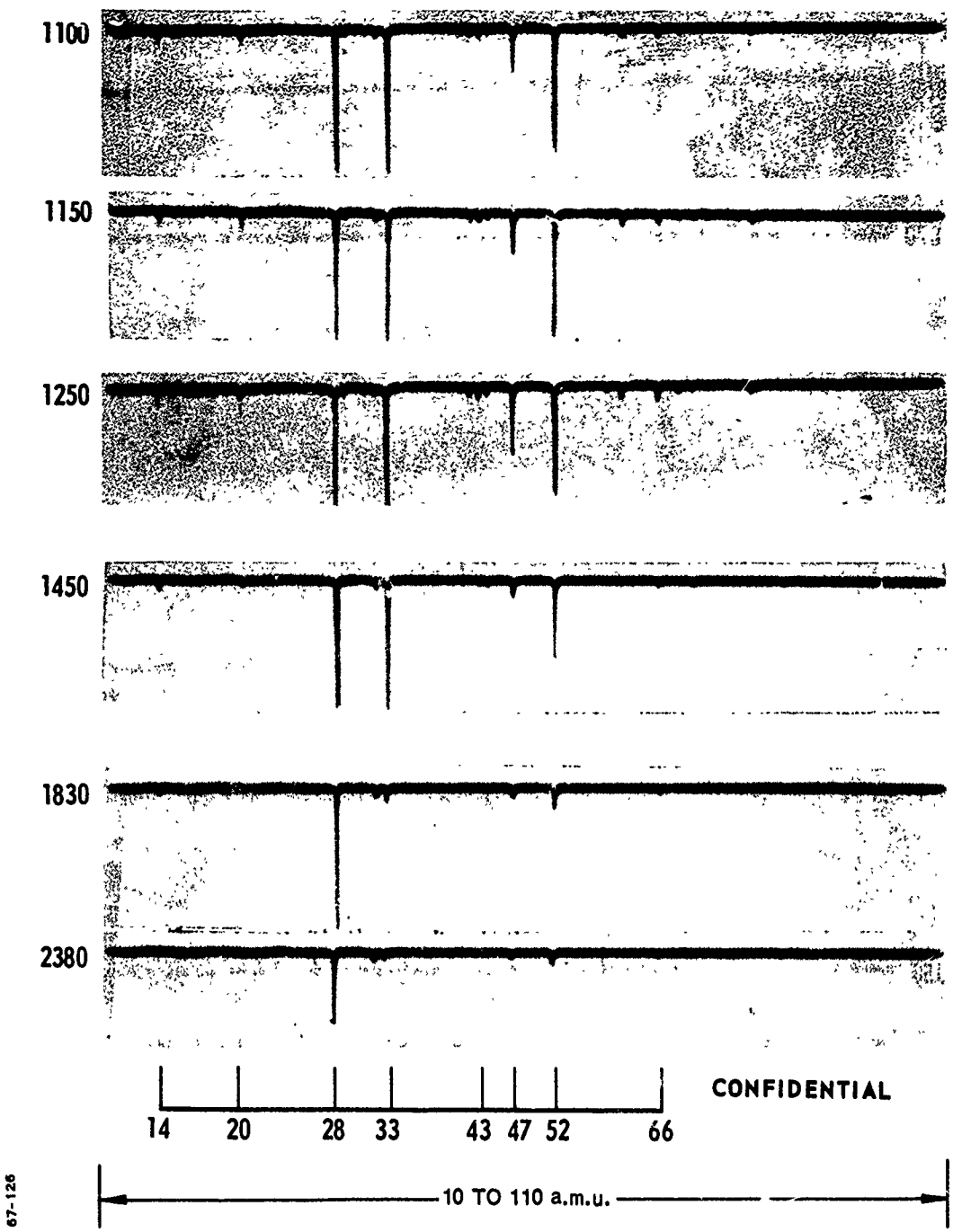

Figure 24 PFABDE Dynamic FMTA, 1,100 to 2,400 Milliseconds

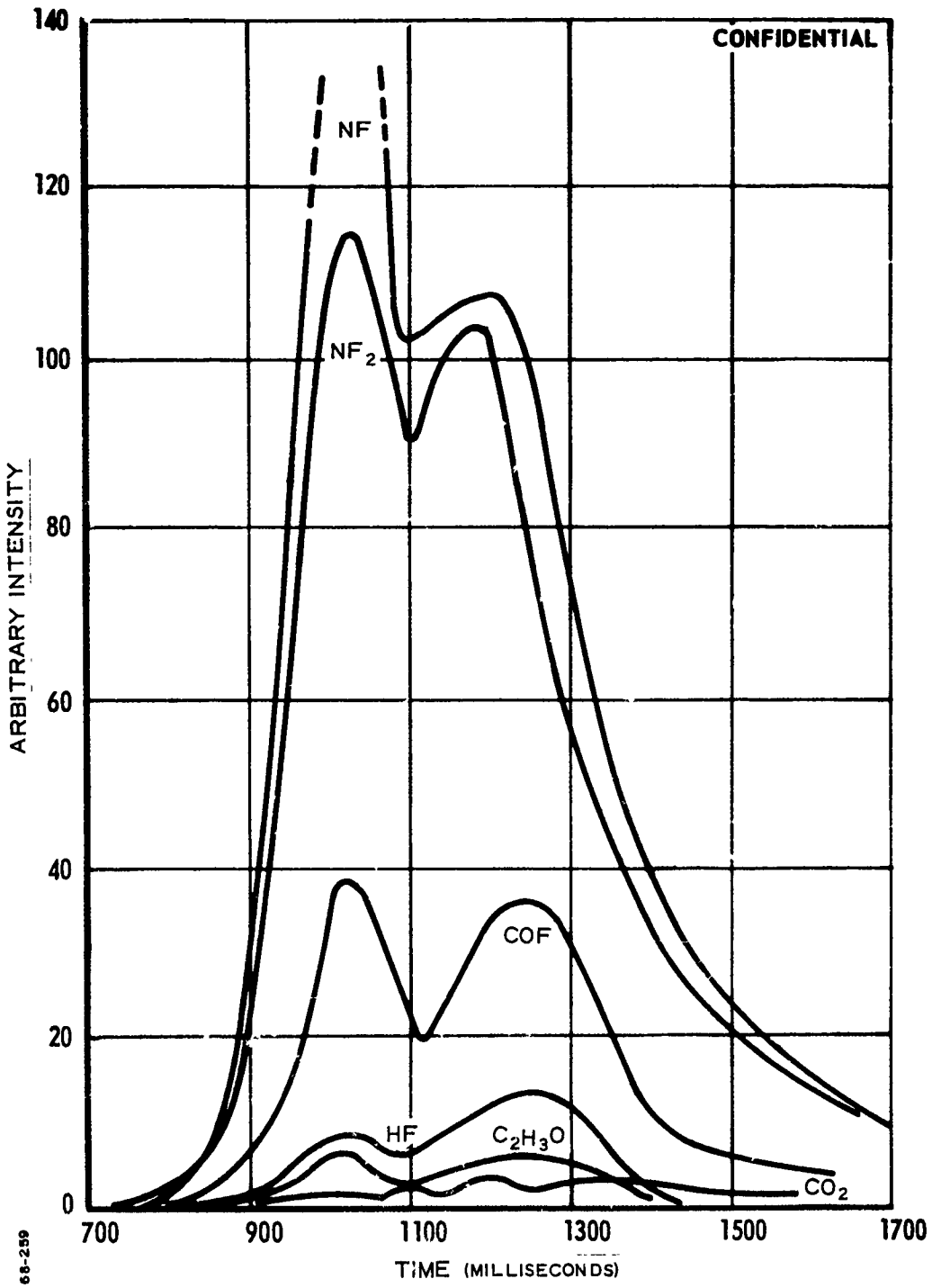

Figure 25 PFABDE Species Intensity History, Dynamic FMTA

(2) PFABDE Thermal Decomposition Mechanism

(C) A tentative mechanism for the production of the early-appearing species in the thermal decomposition of PFABDE may be inferred from the order of species appearances and their relative quantities as shown in Table IV and Figures 23, 24, and 25. This mechanism, presented in Figure 26, involves thermal degradation initiated at the tris-NF_2 groups down the whole length of the polymer, simultaneous with degradation down the chain proceeding from the ends. The complete loss of one tris NF_2-methoxy group from each pair in the structural unit, followed by temporary stabilization of the resulting diradical through cyclization provides a reasonable explanation for the binodal curves portraying the history of NF^+ (m/e = 33), HF^+ (m/e = 20) and FCO (m/e = 47). Details of the evidence and reasoning leading to the mechanisms are presented in the following paragraphs.

(C) The shape of the NF^+ (m/e = 33) production curve shows the double peak also found by workers at Dow. They concluded that N_2F_4 was the initial thermal decomposition product whereas comparison of LPC data with Schoenfelder's N_2F_4 cracking patterns (Ref. 16) demonstrates the absence of all but low levels of N_2F_4. However, LPC's heating rate was 110°C/sec compared with Dow's 2°C/min -- a factor of 3,300 times as fast. The Dow data also show that, under the assumed conditions, decomposition began at 180°C -- a temperature much higher than the 120°C observed under LPC conditions (Figure 27).

(C) The production of the ions at m/e = 47 and 45 concurrent with the production of NF_2^+ and NF^+ indicate that loss of a second NF_2 group from either tris-carbon results in cleavage of the C-O bond at the carbon nearest the PFABDE backbone, as shown by intermediate III in Figure 26. At the time of the split, one F-atom from the remaining NF_2 group can migrate to the central carbon atom to form the radical OC(F)NF that then appears to decompose either spontaneously or under the influence of the mass spectrometer electron beam. This decomposition appears to proceed primarily to yield NF^+ and FCO^+ (m/e = 47). The complex may also split to yield CNF^+ (m/e = 45) by the minor route indicated. The NF_2^+/FCO^+ ratio (Table V) agrees well with this mechanism.

(U) A cyclization of the type indicated by Figure 26, would be expected to proceed so as to neutralize the free valencies brought about by the preceding steps. Later decomposition at higher temperature then would be expected to reproduce the shape of the curves recorded in Figure 25.

(C) The production of HF (m/e = 20) reaches its maxima at the same time as the production of NF_2 (m/e = 52) and NF (m/e = 33). However, HF does not begin to appear in the mass spectra until 60 milliseconds after (approximately 66°C above) the appearance of NF_2 and NF. The relative maxima for the HF curve are also the reverse of those due to NF_2 and NF, i.e., more HF is generated at higher than at the lower temperatures. These data indicate that an alternative mechanism possessing a higher activation energy parallels the early mechanism that was proposed. However, the proposed mechanism adequately covers the species observed to appear at a much earlier time.

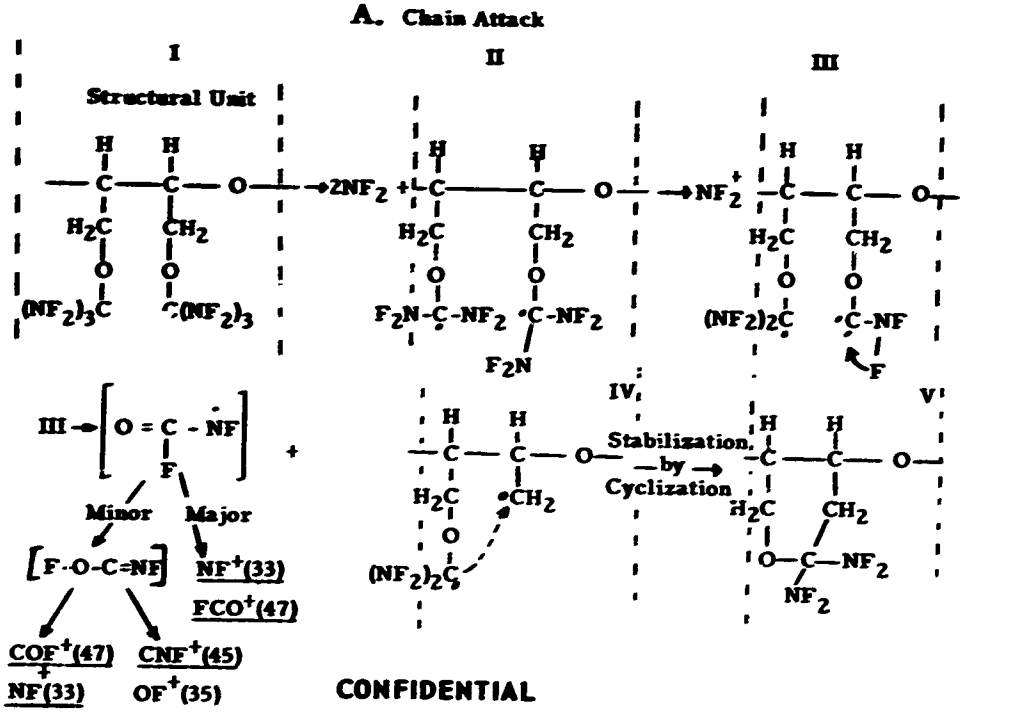

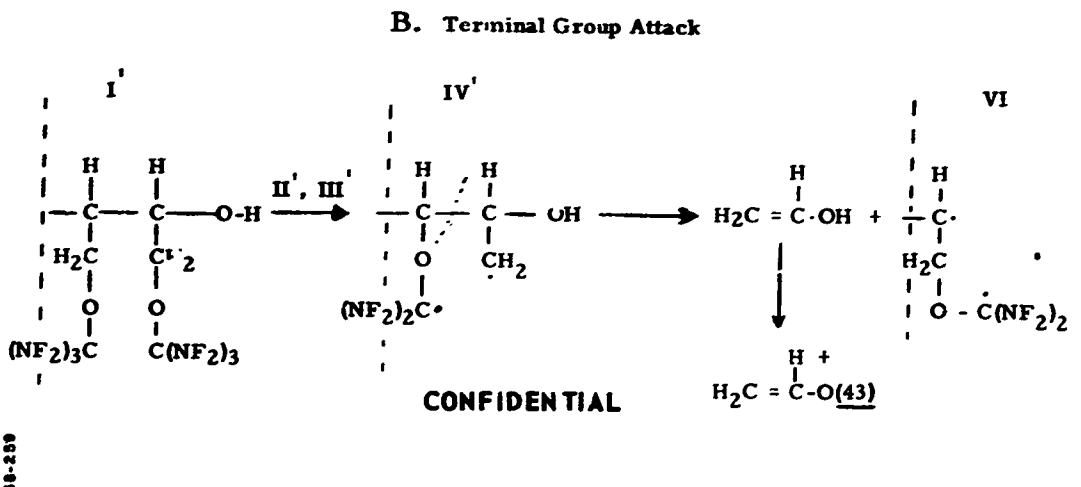

Figure 26 PFABDE Decomposition Mechanism, Dynamic FMTA

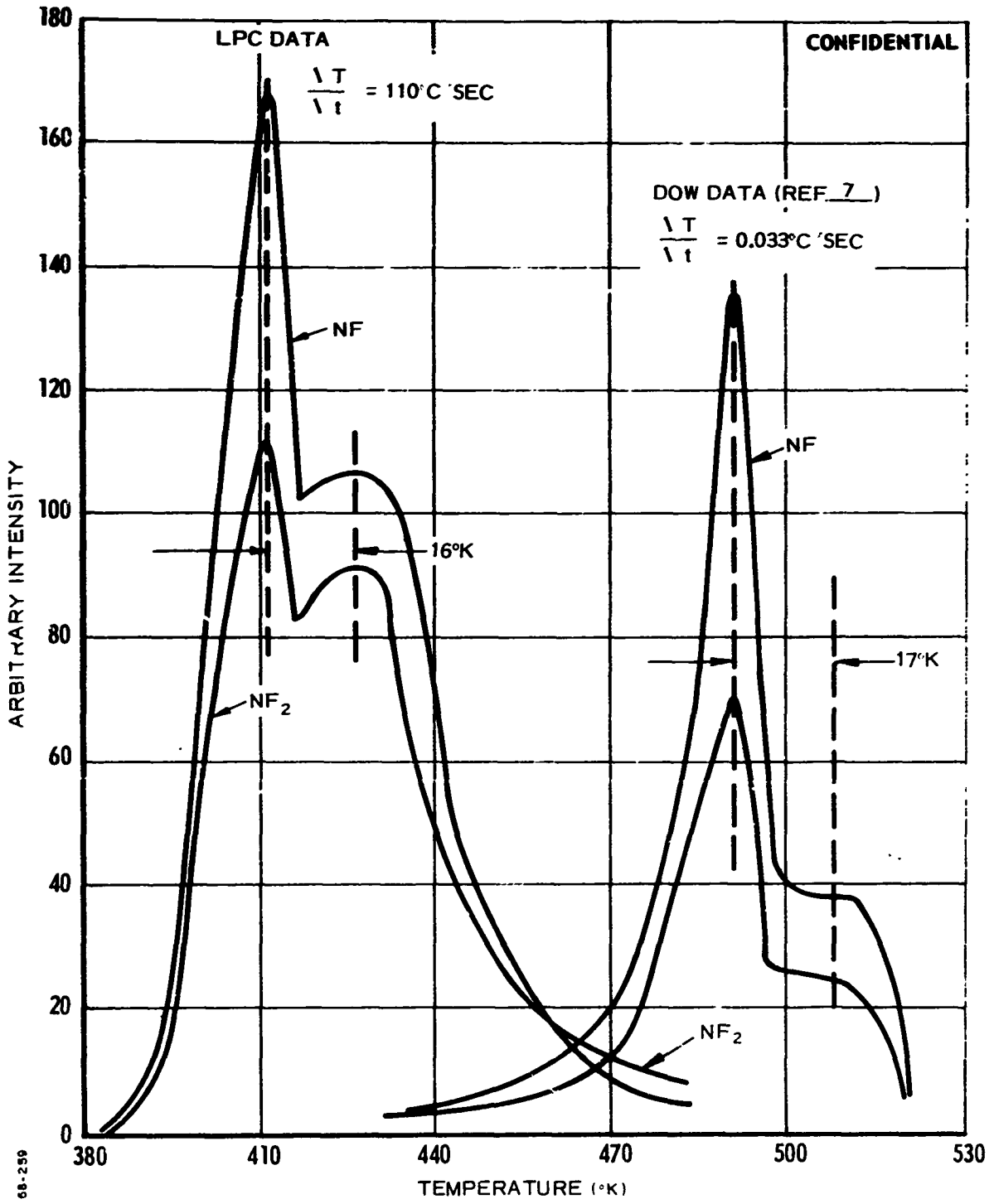

Figure 27 Comparison of Dow and LPC Data on PFABDE MTA Pyrolyses

TABLE V

CORRELATION OF MECHANISM WITH EXPERIMENT, PFABDE DYNAMIC FMTA

Ratio	Calculated	Experimental
NF_2^+/FCO^+	≈3	3.5
$NF_2^+/C_2H_3O^+$	15-20*	~20

*Calculated on the basis of two terminal groups per polymer chain and polymer weights in the range of 4000 to 6500 g/mol. (10-15 monomer units/ polymer molecule).

(C) The production of $C_2H_3O^+$ (m/e = 43) at an early stage would appear to require the breaking of the PFABDE backbone. If such breakage occurred readily, much larger fragments and single peak curves would be expected. However, the prompt appearance of m/e = 43 and its complex curve, Figure 25, again indicate that more than one process is occurring.

(C) A prompt source of $C_2H_3O^+$ can be found in the thermal degradation of the polymer end-groups, as shown in Figure 26. Such a scheme not only provides immediate production of $C_2H_3O^+$, but assures its continual appearance throughout the pyrolysis. This mechanism also provides a continuous low-level source of NF_2 from the end diradical, which cannot be stabilized by cyclization.

(C) The behavior of CO_2^+ (m/e = 44) also is anomalous. Its early appearance and relatively late growth (ca. 500 milliseconds) would appear to identify it as a reaction product of fragments, and also of a species initially present. It is possible that initiators used for the polymerization of the PFABDE would add to the growing polymer, and serve as terminator, instead of the OH represented in I, Figure 26. Rearrangements of such groups and release during pyrolysis could account for the early appearance of CO_2^+, whereas larger scale rearrangements or abstraction reactions could account for the later rise to a higher yield.

(U) The complexity of the PFABDE macromolecule is such that all atomic species are in close proximity to all other type species at some point. Thus, more than one side-chain or structural unit may be involved in the decomposition scheme. However, the major portion of the mechanism is satisfactorily explained by the present assumptions.

c. Kinetic Data

(U) The results of the Arrhenius treatment for the initial decomposition products of PFABDE are shown in Figure 28 and in Table VI.

(U) There are two distinct regimes -- the "low temperature" regime is labelled "A", and the high temperature regime is labelled "B" to facilitate comparison with the previously obtained Intensity versus Time traces. Both "A" and "B" are taken from the data obtained from the first peak in the decomposition.

(C) The graphical analysis yields apparent activation energies of 77 Kcal/mole for the low temperature regime and 46 Kcal/mole for the high temperature regime of NF_2 production. Comparison of all five species shows a marked similarity in the activation energies in both regimes, with the exception of $C_2H_3O^+$. In fact, the NF curve lies so close to the NF_2 curves that it can be considered coincident. Thus, the NF seen in these regimes probably is due solely to mass spectral cracking of the NF_2. At still higher temperatures (later times) where the second maximum of NF occurs, a different source of NF is required.

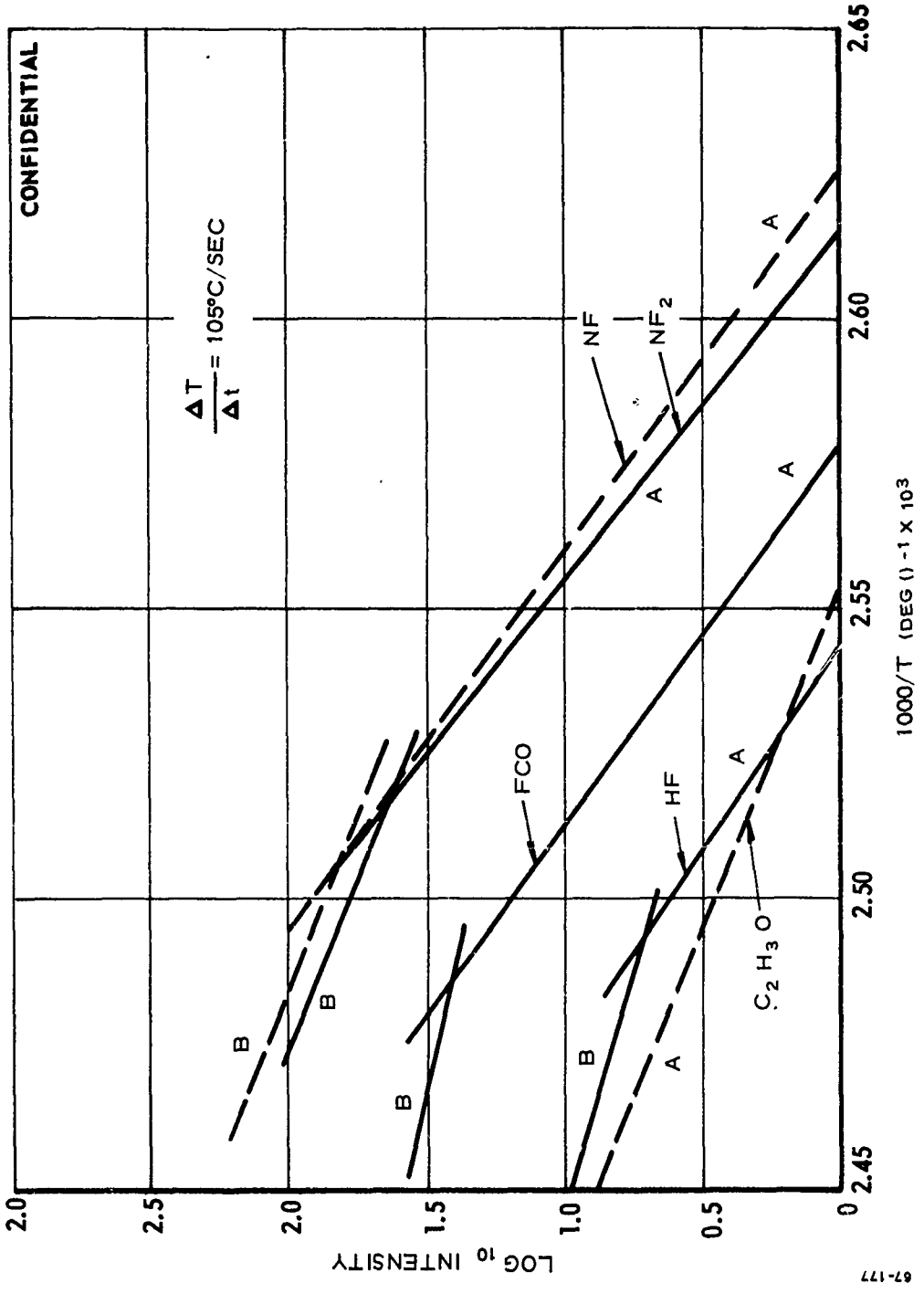

Figure 28 Arrhenius Plot for Initial PFABDE Pyrolysis Species, Dynamic FMTA

TABLE VI

ACTIVATION ENERGIES OF PFABDE PYROLYSIS SPECIES FROM DYNAMIC FMTA

	Activation Energies, Kcal/mole		
	LPC		Dow
Species	A	B	B
NF_2	77	46	
NF	71	38	41.6
HF	67	28	
C_2H_3O	40		
FCO	70	23	

N. B. The letters A and B refer to the corresponding portions of the Arrhenius plots, Figure 28. In general, the A portion occurs at early times (lower temperatures) and the B portion at later times (higher temperatures).

(C) The lower activation energy (40 Kcal/mole) for the $C_2H_3O^+$ production would appear to indicate that this may be the decomposition-initiating reaction. However, 40 Kcal/mole is still high enough so that appreciable thermal decomposition by this means would not be anticipated at room temperature. There is some indication that low levels of products are being formed that were detected but were not measurable by the present experimental arrangement. Higher amplification of the product ion signals would resolve this question. Comparison of the activation energy for NF production with that obtained by Dow (see subsection IV-2) tends to confirm the validity of the present treatment. It is of interest to apply the same treatment to the Dow MTA data, to complete the picture. (Dow did not attempt to extract activation energies from MTA data.)

(C) The result of this treatment is shown in Figure 29. A value of 41.6 Kcal/mole is obtained from the B region of the MTA data. This also tends to confirm the previous argument as to the decomposition region being investigated by DTA, TGA, and Taliani methods.

d. Conclusions

(C) Several important conclusions can be drawn from the work on PFABDE without a comparison to PBEP. (This comparison will be made at the end of the section on PBEP.) These conclusions include the following:

- The time-integrated spectra for the Isothermal FMTA showed that a high threshold value for the decomposition temperature existed that did not seem reasonable by comparison with reported thermal data for the compounds being studied.

- As found in subsequent work, different heating rates gave rise to different mass spectral patterns. This suggests that different mechanisms are responsible for the thermal decomposition of PFABDE during the isothermal and the dynamic experiments. It implies a heating rate dependence of the mechanism.

- During isothermal decomposition, the PFABDE molecule first eliminates the tris (difluoramino) methoxy group that further decomposes to generate $\cdot NF_2$ and $\cdot F$ radicals.

- During dynamic FMTA, the PFABDE molecule first eliminates $\cdot NF_2$ radicals, and appears to stabilize temporarily, presumably through cyclization. Subsequent decomposition results in excision of the tris-methoxy residue and of the $\cdot NF$ radicals. The $\cdot F$ radical never becomes an important product.

- The initial high activation energy for the decomposition (77 Kcal/mole) can result in extremely fast self-acceleration of the decomposition reaction once the

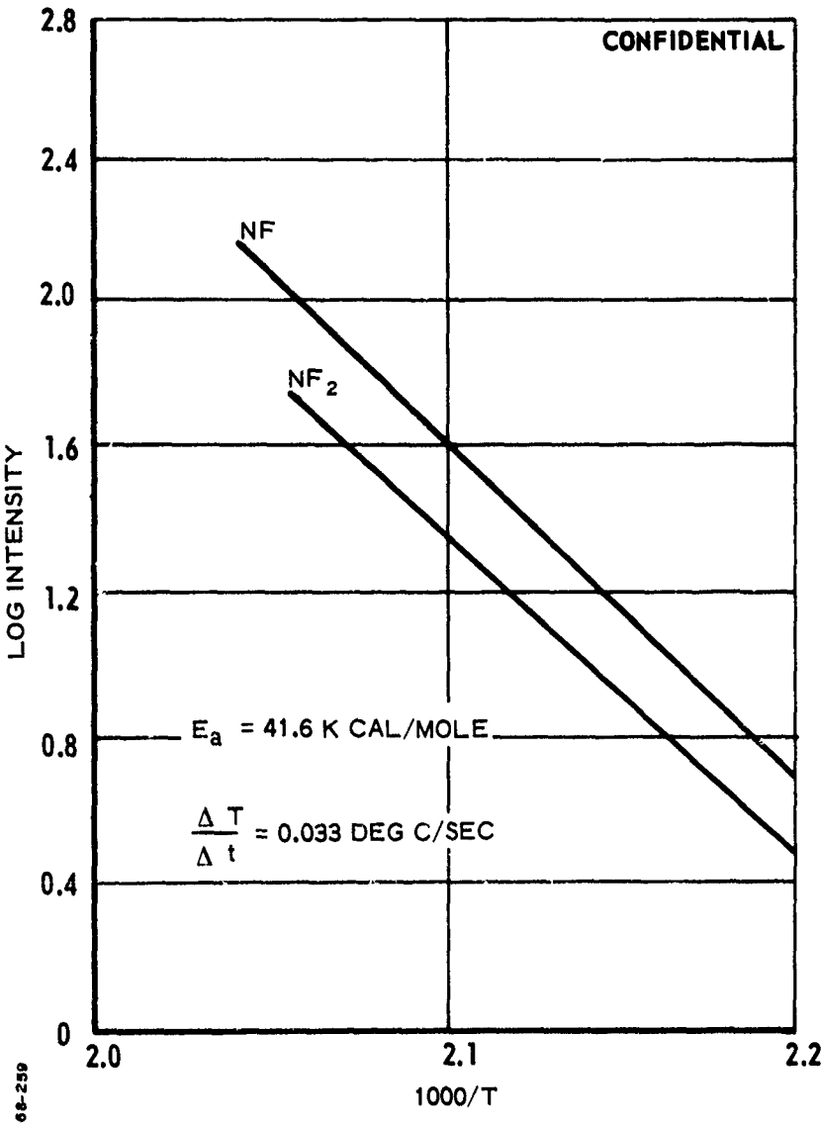

Figure 29 Arrhenius Plot of Dow PFABDE MTA Data

control temperature is attained. This could be a clue to the extreme impact sensitivity of PFABDE.

5. PBEP PYROLYSIS

a. Isothermal FMTA Results and Discussion

(U) Numerous pyrolyses have been conducted upon PBEP using both time-integrated and time-resolved recording of the spectra obtained at 10 KHZ frequency (100 microseconds).

(U) Figure 30 is a line drawing typical of time-integrated spectra obtained during rapid pyrolyses of PBEP. Figure 30 results from 100 millisecond observations (1000 scans) of PBEP gaseous products at pyrolysis temperatures of 165 and 200°C. Tentative identification of the species from these and time-resolved experiments are shown in Table VII.

(U) The Z-axis multiple peak technique also was used for obtaining qualitative time-resolved mass spectra of PBEP during pyrolysis. Figures 31 and 32 were constructed from the Z-axis modulated photograph from the apparent brightnesses of the spots, i.e., with no attempt at correction for the variable brightness across the screen. (Intensities are designated as: Weak, Moderate, Strong, Very Strong).

(U) Detailed interpretation of this data certainly is premature. Structural assignments to the observed m/e values are tentative, particularly, of course, for the quite high m/e species.

(C) The following comments are presented in summation of Figures 30 through 32 plus the results of other similar experiments:

- Numerous species are produced even within the first 100 microseconds of pyrolysis, demonstrating the presence of extremely rapid and probably complex processes.

- The most intense peaks observed with PBEP include 45 (CNF), 20 (HF), 71 (NF_3), 33 (NF), 47 (H_2CNF, COF, N_2F ?), 52 (NF_2). Notable differences from PFABDE are the strong 20 (HF) and 71 (NF_3), the weak 19 (F) and comparatively weak 52 (NF_2) with PBEP. In fact, in some time-resolved experiments with PBEP the 52 (NF_2) peak has not appeared until relatively late.

- The largest species observed so far with PBEP are 143 and 131. These undoubtedly contain within themselves the potential for producing -- qualitatively -- many of the lower species observed as the result of

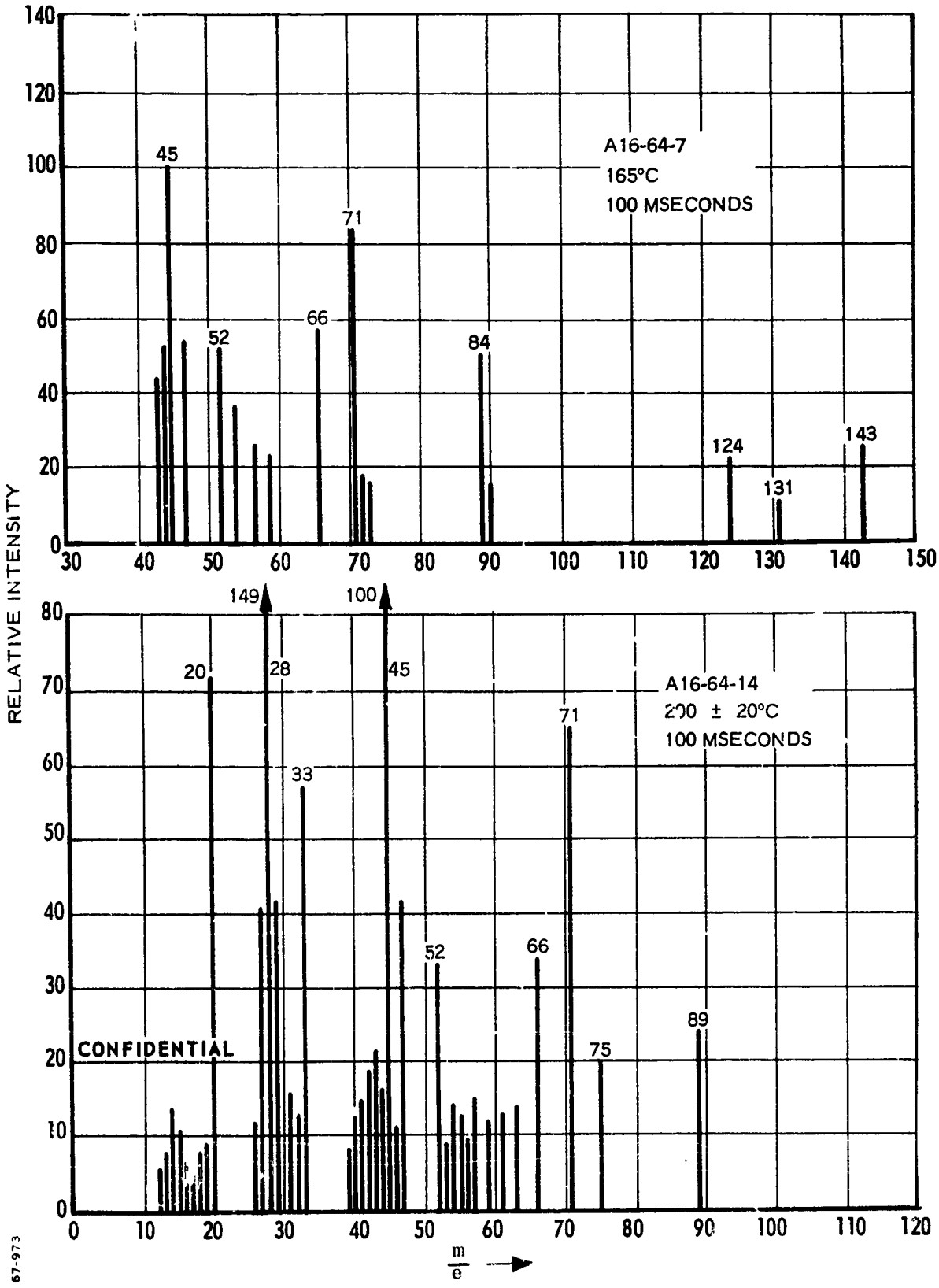

Figure 30 Line Drawing of PBEP Pyrolysis Time-Integrated Spectrum, Isothermal FMTA

TABLE VII

TENTATIVE MASS SPECTRA PEAK ASSIGNMENT FOR PBEP ISOTHERMAL FMTA

m/e	Possible Positive Species	m/e	Possible Positive Species
12	C	44	CO_2, C_2H_4O
13	CH	45	CNF
14	N, CH_2	46	HCNF
15	NH, CH_3	47	H_2CNF, N_2F, COF
16	O, NH_2	52	NF_2
17	OH, NH_3	53	HNF_2
18	H_2O	54	C_3H_2O
19	F	55	C_3H_3O
20	HF	56	C_3H_4O
27	HCN, C_2H_3	57	C_2NF
28	CO, N_2	59	H_2C_2NF
29	CHO, C_2H_5	61	H_4C_2NF
30	H_2CO, NO	66	H_2CNF_2, COF_2, N_2F_2
31	CF	71	NF_3
32	O_2	75	C_2H_2O NF
33	NF	89	C_3H_4O NF, $C_4H_9O_2$
39	C_2HN	90	C_3H_5ONF, $C_4H_{10}O_2$
40	C_2O, C_2H_2N	124	$C_3H_3N_2F_3$
41	C_2HO	131	$C_2H_3N_2F_4$
42	C_2H_2O	143	$C_3H_3N_2F_4$
43	C_2H_3O, C_2F		

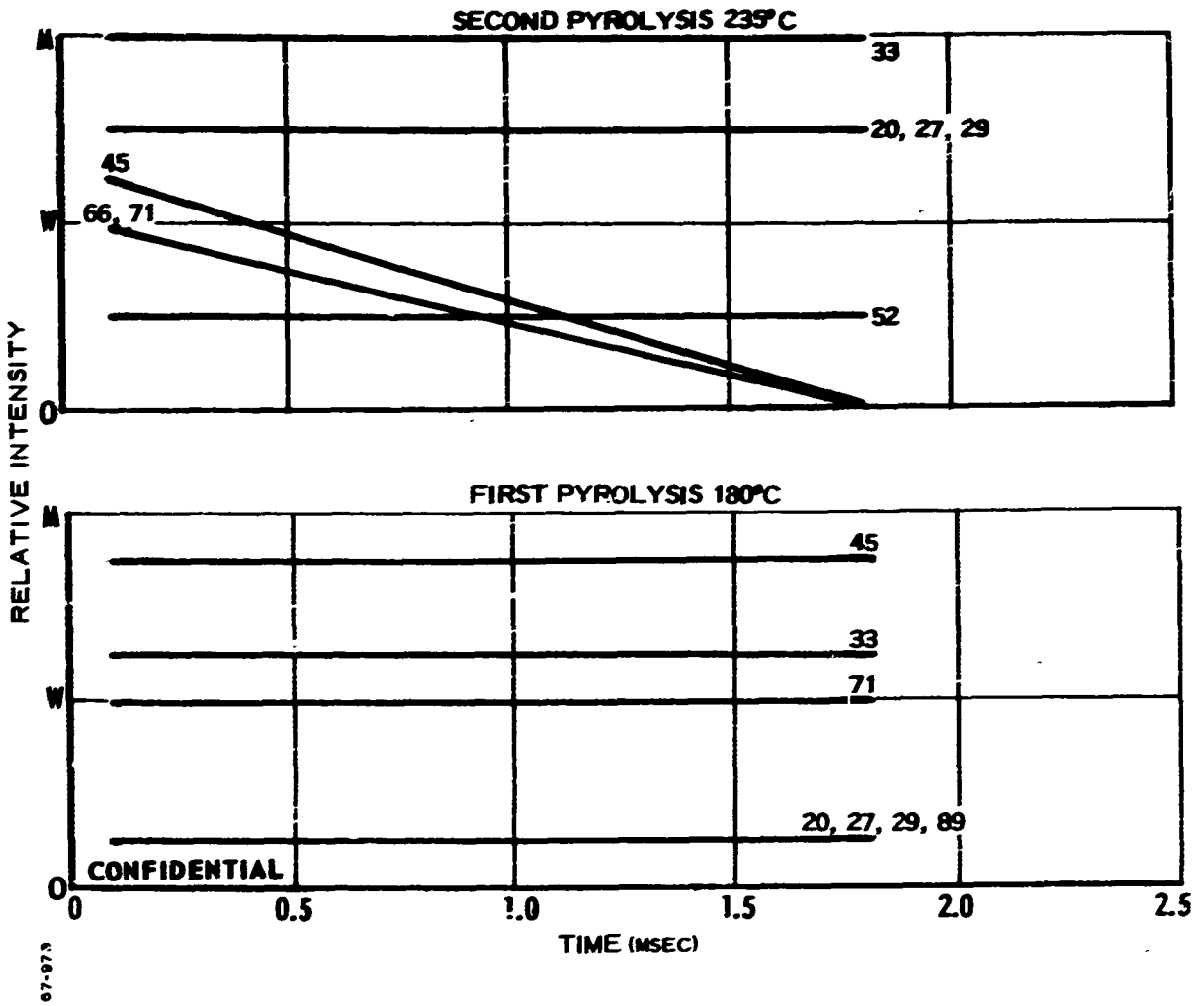

Figure 31 Time-Resolved PBEP Isothermal FMTA Spectra (A16 - 64 - 13), Z-Axis Multiple Peak from m/e = 12 to m/e = 100

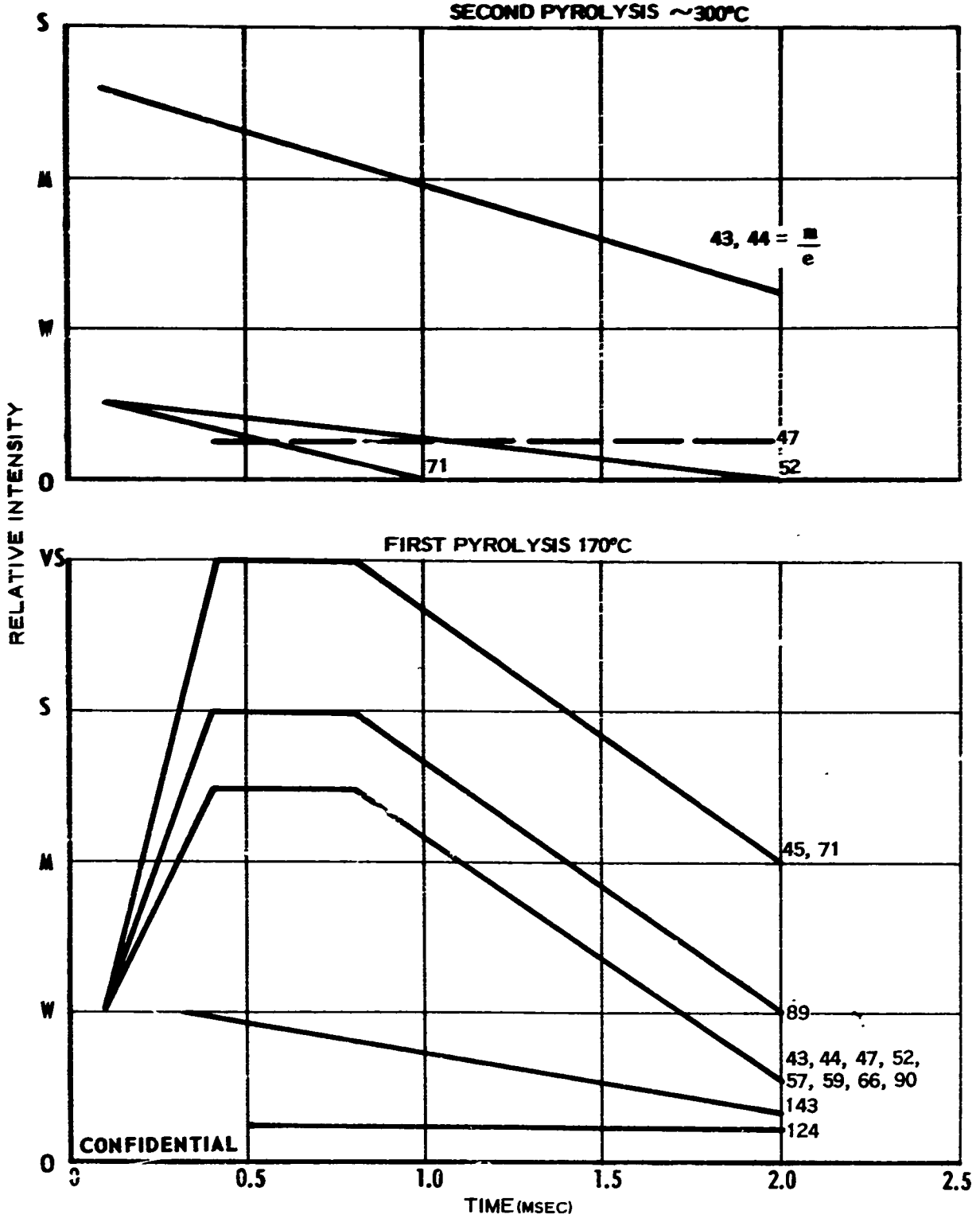

Figure 32 Time-Resolved PBEP Isothermal FMTA Spectra (A16 - 64 - 5), Z-Axis Multiple Peak from m/e = 40 to m/e = 200

electron bombardment. Again fragmentation patterns of model compounds in conjunction with computerized data reduction would be of great value in interpreting such data. In addition, present capabilities now include the simultaneous and quantitative monitoring of peak heights for two species during pyrolysis. Aside from its quantitative kinetic value, such monitoring would aid in determining, for example, whether NF_2 is solely a fragmentation (electron bombardment) product of a species or results from direct C-N bond breakage.

(C) The data, still considered preliminary, suggest that an initial step in the isothermal PBEP pyrolysis involves the elimination of NF_3 and HF, perhaps by a mechanism as shown in Figure 33.

(C) A first run was completed applying the dual peak time-resolution technique for monitoring relative rates of NF_3^+ and NF_2^+ generation upon PBEP pyrolysis at 230°C. The time dependent intensities for these two mass peaks (NF_3^+, m/e 71; NF_2^+, m/e 52) are shown in Figure 34. In both traces, the initial high maximum is caused by electronic noise; the subsequent lines (100 microsecond time intervals) represent sweeps of the particular mass peaks. The data indicate that NF_3^+ and NF_2^+ are formed and/or decay at closely identical rates. It is noted that this technique has not yet been calibrated to provide information on relative quantities. This latter information would be available from the time-integrated spectra. Because of the greater immediate applicability of the Dynamic FMTA (described in the following paragraphs), this method was temporarily discontinued. However, it has great potential for routine determinations, where the major species affecting stability have been predetermined.

b. Dynamic FMTA Results and Discussion

(U) The pyrolysis of PBEP resulted in much more complex mass spectra than that of PFABDE. This probably is because of the high impurity level (20 to 25 percent) in the PBEP. The following discussion applies only to the impure PBEP available for use in this program. Future improvements in the quality of PBEP may result in different mechanisms.

(1) PBEP Polymer Structure

(C) The exact molecular structure of PBEP polymer has not yet been established, so the following arguments are based upon the simplest model that would fit all the experimental data. The mass spectra, as shown in Figures 35, 36, and 37, indicate the presence of hydrocarbon species, as well as large oxygen-containing compounds. This confirms the structure deduced from chemical analysis of the sample, Shell Lot No. 9557-90 (Table VIII). The F/N ratio of 1.89 shows that all fluorine cannot be present as NF_2. It is reasonable to assume that some fluorine is present as NF, because the assumption of F bonded directly to C implies a nitrile (C≡N) bond for nitrogen balance, and then the sites available for hydrogen become far too few to account for the amount of hydrogen found. With the above F/N ratio and assumption, the ratio NF_2/NF can be calculated to be approximately 8.

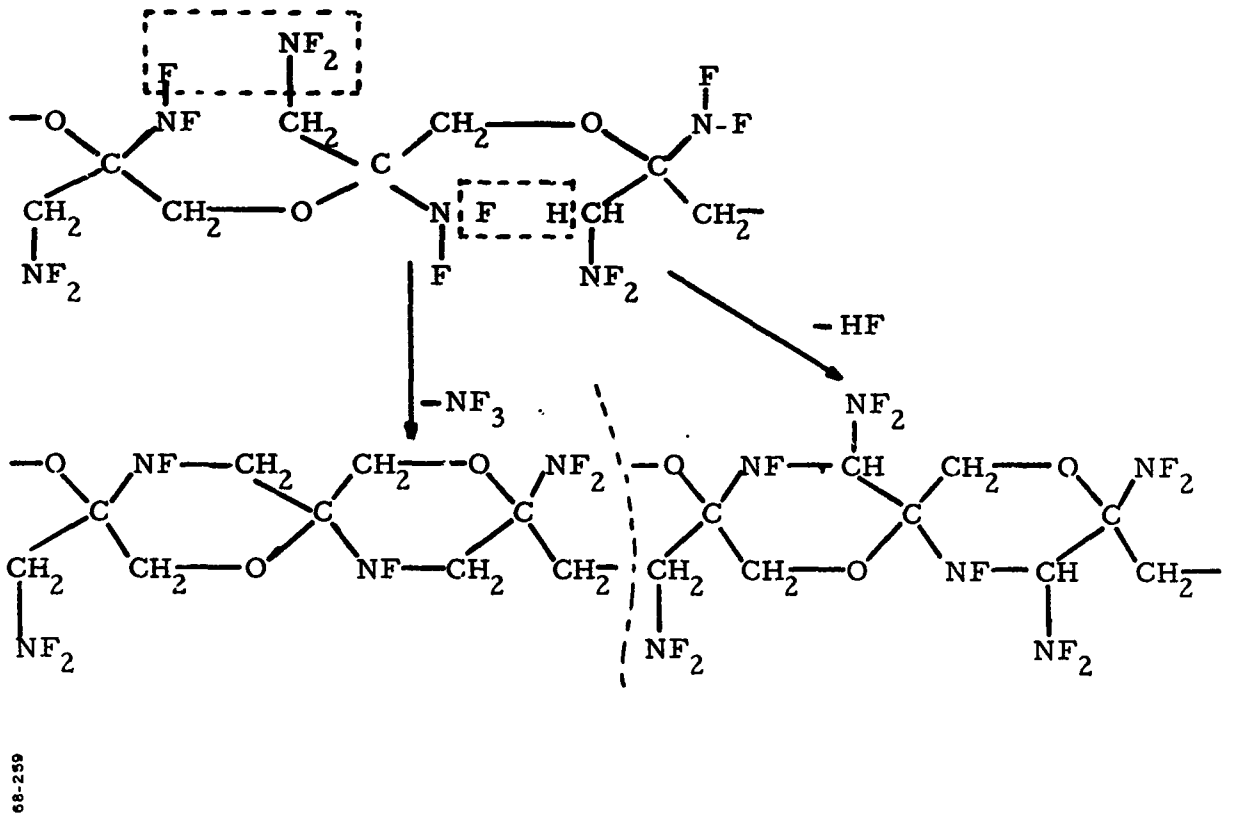

68-259

Figure 33 Isothermal FMTA Decomposition Mechanism for PBEP

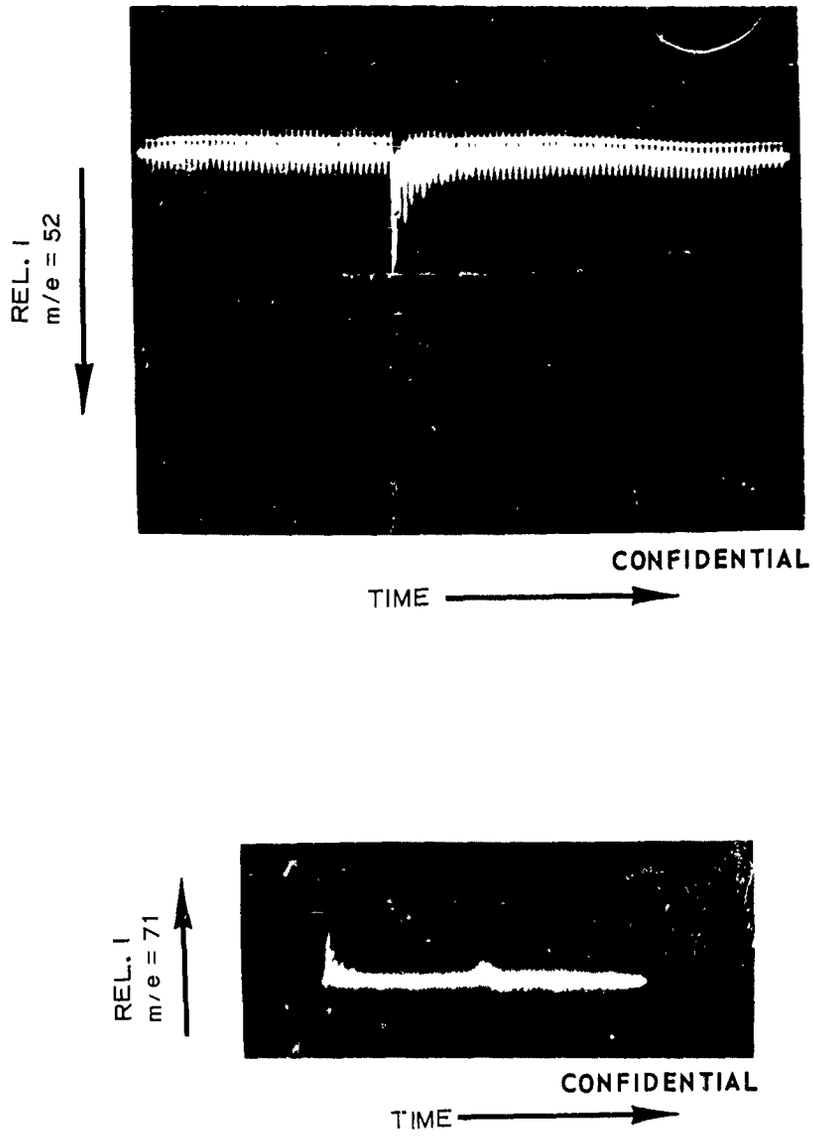

Figure 34 Dual Peak Time-Resolved Spectra of PBEP

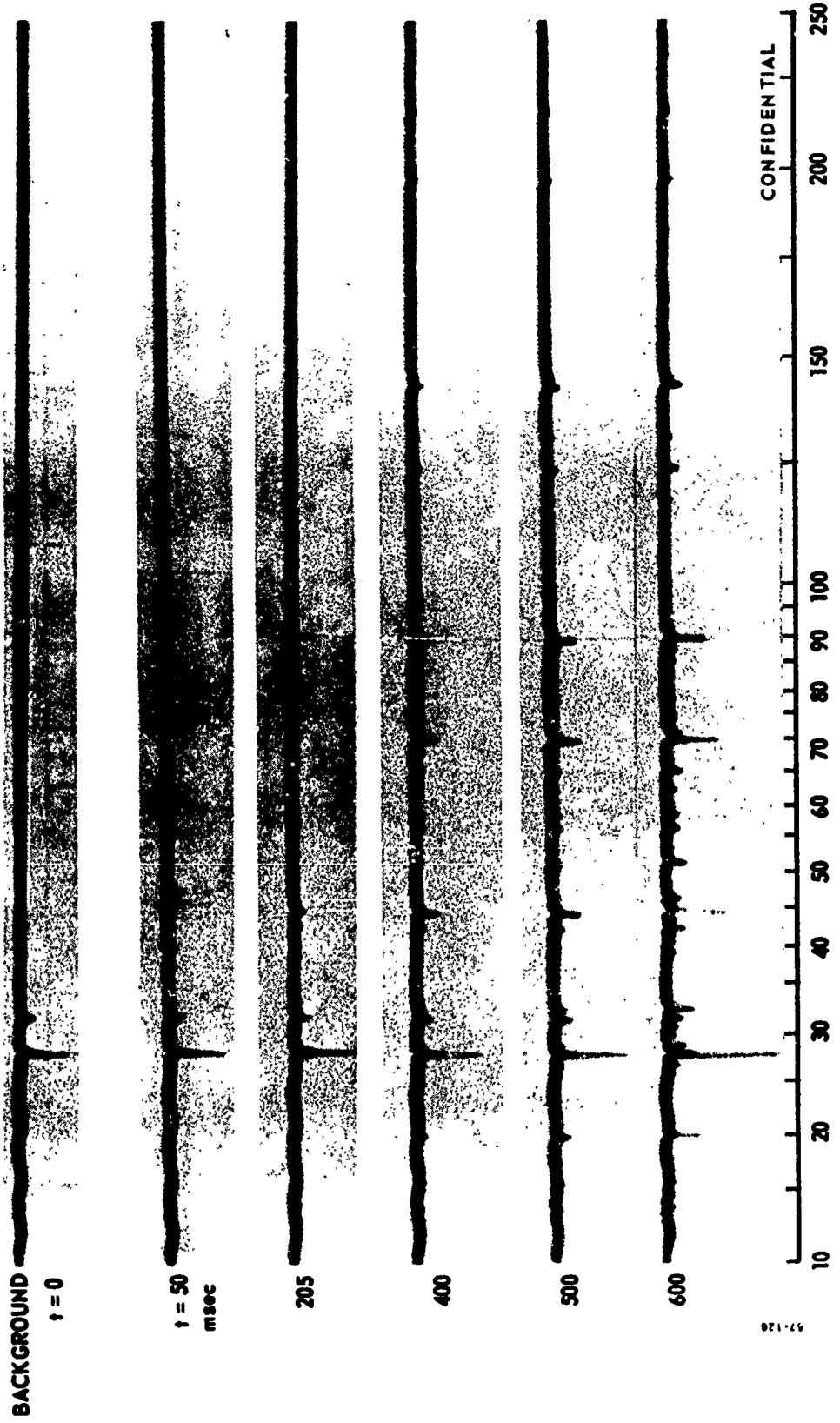

Figure 35 PBEP Dynamic FMTA, 0 to 600 msec, $\Delta T/\Delta t = 118^{\circ}C/sec$, Sample 9557-90

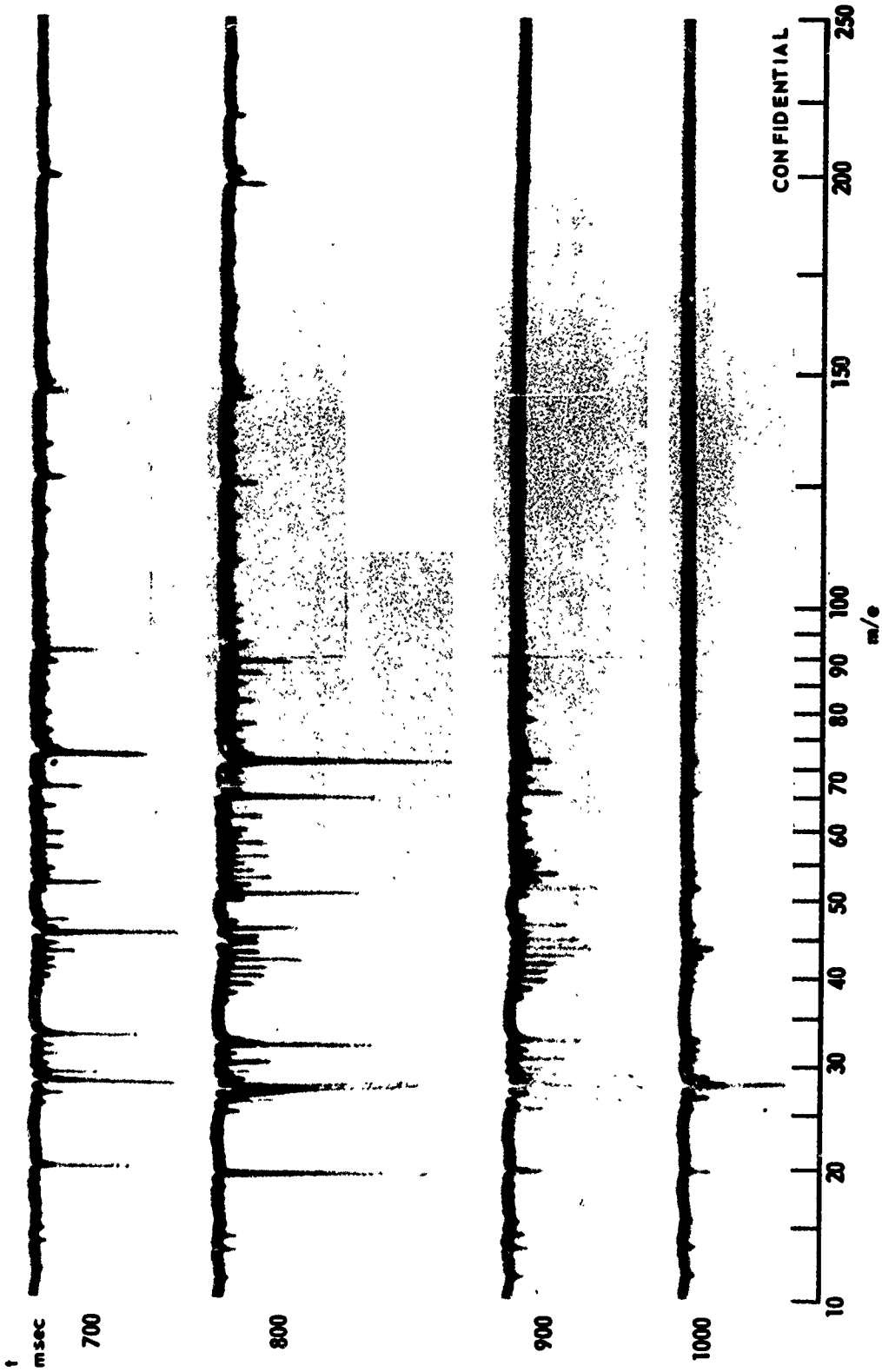

Figure 36 PBEP Dynamic FMTA, 700 to 1,000 msec, $\Delta T/\Delta t = 118^{\circ}C/sec$, Sample 9557-90

7274

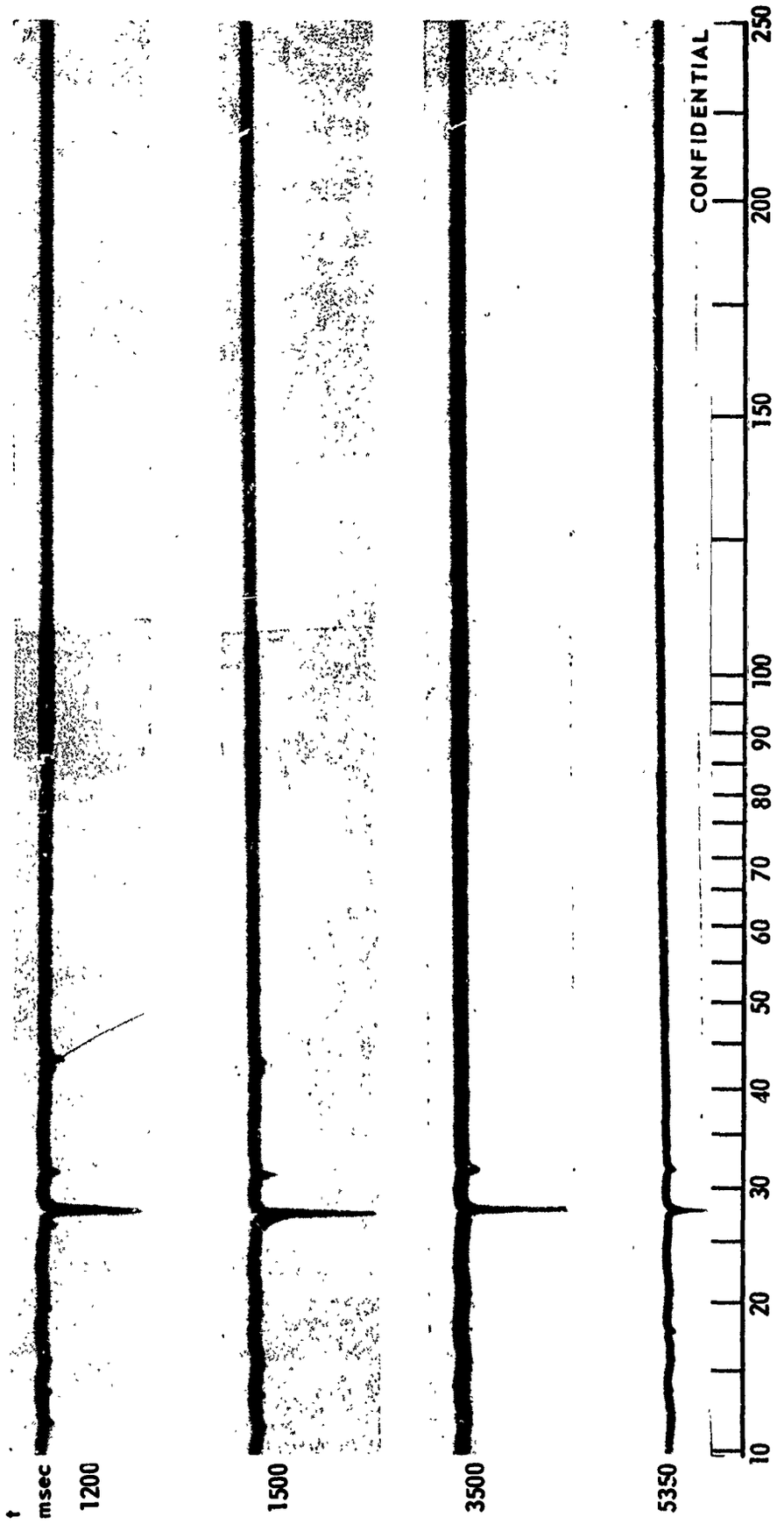

Figure 37 PBEP Dynamic FMTA, 1,200 to 5,400 msec, $\Delta T/\Delta t = 118^{\circ}C/sec$, Sample 9557-90

7261

TABLE VIII

PBEP Analysis, Shell Lot 9557-90

Species	Weight %
C	26.1
H	3.0
N	15.9
F	40.8
O	14.2 (by difference)

Average molecular weight = 3680
OH equivalents/100 g = 0.085 (TDI)

(C) Through the use of the atomic weights of the elements and the average molecular weight, the polymer composition can be calculated to be approximately $C_{80}H_{110}N_{42}F_{79}O_{33}$. Use of the NF_2/NF ratio shows that there will be thirty-seven NF_2 groups and five NF groups per polymer chain. The OH functionality demands three OH per chain.

(C) A simple series of calculations will show that these conditions can be met by an average polymer chain length of 25 units, terminated at one end by methyl-glycol ether and at the other end by glycerol. The polymer chain will be only 78 percent reacted with N_2F_4 to form PBEP. The remainder will be unreacted. The results of these structure calculations are presented in Table IX.

(2) Mass Spectrum Assignments

(C) The mass spectra of PBEP was much more complex than that of PFABDE, although the hypothetical monomer unit of PBEP is considerably simpler. The only reasonable interpretation of the spectra indicated considerable quantities of large molecular weight fragments containing hydrogen and oxygen. This view was reinforced by the lot analysis (previous section) showing that more than 20 percent of the average PBEP polymer molecule did not correspond to the hypothetical PBEP monomer.

(C) Table X contains the order of appearance of the ion fragments from the pyrolysis of PBEP in the mass spectrometer, and Figures 38 and 39 present histories of selected m/e peaks. The first species to appear were at m/e of 40, 43, 45, and 46. Their subsequent behavior led to the assumption that these were the major ion fragments resulting from separate thermally detached species. Comparison of standard API spectra (Ref. 14) to the corresponding structure, indicated that these fragments were caused by the species $C_3H_4^+$(40), $C_2H_3O^+$(43), C_2H_5O (45)(from the methyl ether of ethylene glycol) and $HCNF^+$(46).

(C) All of the activity at m/e = 71 and 33 cannot be because of NF_3 or NF_2 cracking alone, as shown in Table XI. Again, the m/e = 33 probably is due to NF removed from the polymer as the NF entity. This probably results from the partial dehydrofluorination of adjacent CH_2 and NF_2 groups. The large quantities of HF (m/e = 20) produced tend to confirm this hypothesis. The peak at m/e = 71 cannot all be due to NF_3, since this would yield more NF_2 than was observed. The only reasonable thermal fragments that could yield the m/e = 71 peak, other than NF_3, would be $C_3H_3O_2$ and C_3H_2NF. Both these fragments can result from the fragmentation of the already partially decomposed polymer molecule.

(C) The assignment of $C_2H_5O^+$ (from end groups) to m/e = 45 initially fits all the data. However, it cannot account for the great quantity of species observed subsequently, as the ratio of end groups to chain links is approximately 2:25.

(C) The only other choices available are CNF^+ and $H_2C_2F^+$. It appears improbable that if the m/e = 46 peak is due to $HCNF^+$ that the daughter CNF^+ would become much stronger at a later time. However,

TABLE IX

POSSIBLE MONOMERIC UNITS PRESENT IN IMPURE PBEP SAMPLE 9557-90

Number of Groups	Type of Group	Position of Group
16	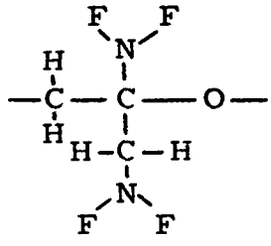	Chain
5	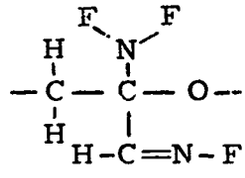	Chain
4	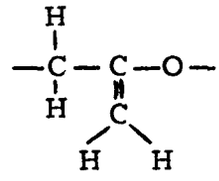	Chain
1	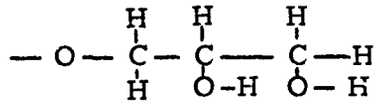	Terminal
1	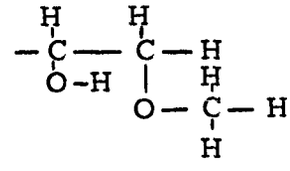	Terminal

TABLE X

PBEP PYROLYSIS FRAGMENT HISTORIES
SAMPLE 9557-90 DYNAMIC FMTA

Time of Appearance (msec) Initial	Maximum	m/e	Probable Species	Maximum Intensity
50	(800?)	28	N_2^+, CO^+, $C_2H_4^+$	O.S.
	870	40	$C_3H_4^+$, C_2O^+	38
	870	43	$C_2H_3O^+$	62
	800	45	$C_2H_5O^+$, $C_2H_2F^+$, CNF^+	O.S.
	800	46	$HCNF^+$	25
150	870	14	N^+, CH_2^+	18
	870	53		28
	805	57	C_2NF^+	36
	800	59	$H_2C_2NF^+$, CN_2F^+	30
	825	71	NF_3^+, $C_3H_3O_2^+$, $C_3H_2NF^+$, $C_2N_2F^+$	144
	805	75		17
	770	76		8
	725	90	$C_3H_6O_3^+$, $(CNF)_2^+$	48
310	870	20	HF^+	175
	(800?)	29	CHO^+, $C_2H_5^+$	O.S.
	(?)	32	O_2^+	5*
	860	33	NF^+	215
	870	39		18
	870	41		38
	860	52	NF_2^+	116
	810	63		32
	810	66	COF_2^+, $N_2F_2^+$	110
	810	72		20
	800	125		23
500	870	30	CH_2O^+, NO^+	30
		31	CH_2OH^+, CF^+	
	870	42		42
	900	44	CO_2^+	56
	870	47	COF^+, H_2CNF^+	62
	810	78		26
	810	146		13
		182		
550	870	15	CH_3^+, NH^+	16
	905	16	O^+	8
		17	OH^+	
		18	H_2O^+	
	810	36		17
	805	202		13

TABLE X (Continued)

Time of Appearance (msec) Initial	Maximum	m/e	Probable Species	Maximum Intensity
700	900	1	$\underline{C}^+$	10
	870	19	$\underline{F}^+$	trace
	870	38	$\underline{F_2}^+$	9

Other species appearing at this time, having a peak height greater than 10, and reaching a maximum between 800 and 875 millisecond are m/e: 48, 49, 54, 55, 56, 58, 60, 69, 70, 73, 74, 77, 81, 82, 83, 84, 85, 89, 91, 95, 100, 109, 123, 136, 148 and 220.

There are other species occurring at other times that have not been included because their identification has not yet been established.

---

*O_2 rose to a constant value above background
O.S. = trace went Off Scale
Underlined species are the assumed major contributors

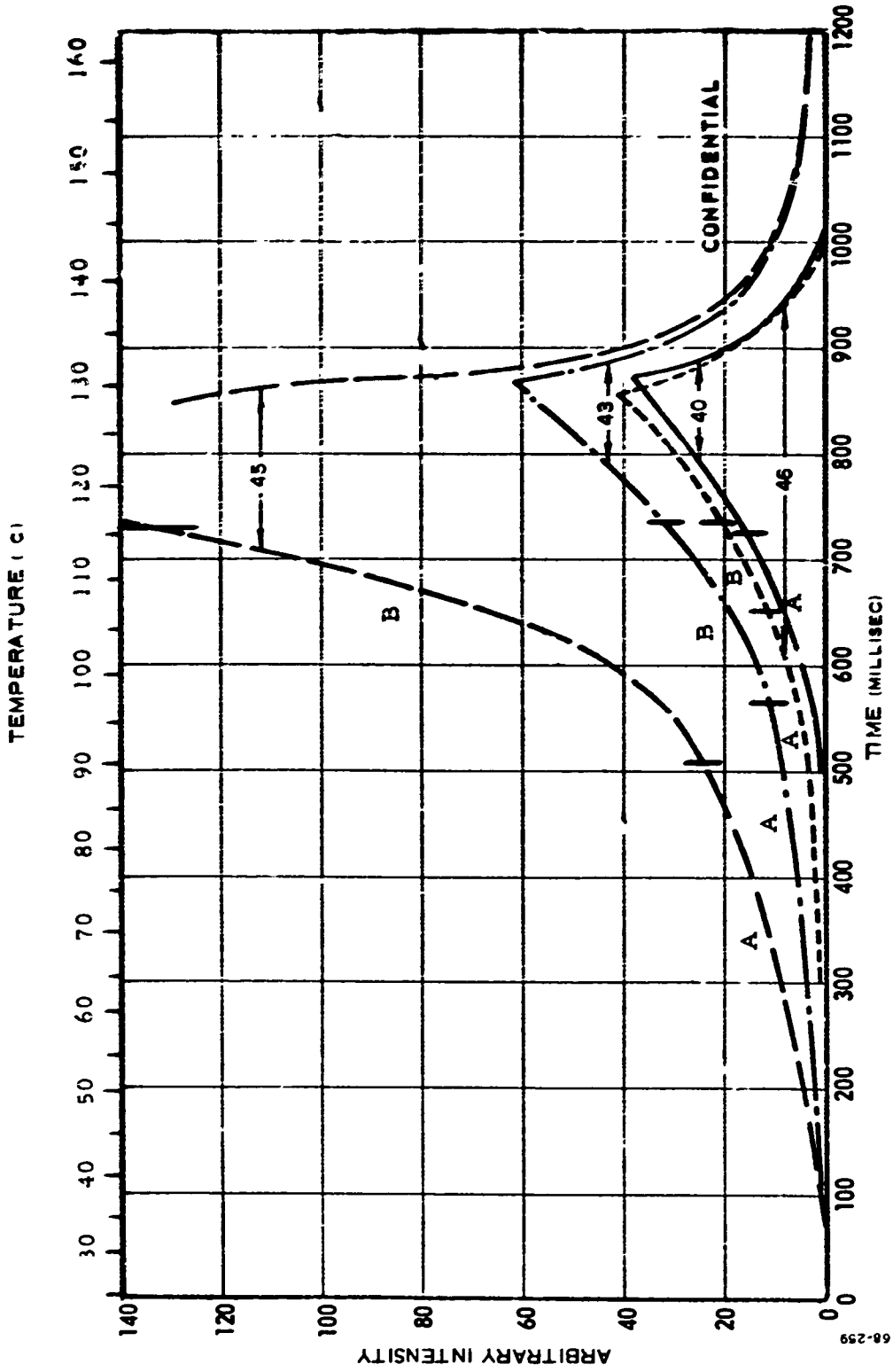

Figure 38 PBEP Pyrolysis Fragment History, Initial Species, Dynamic FMTA

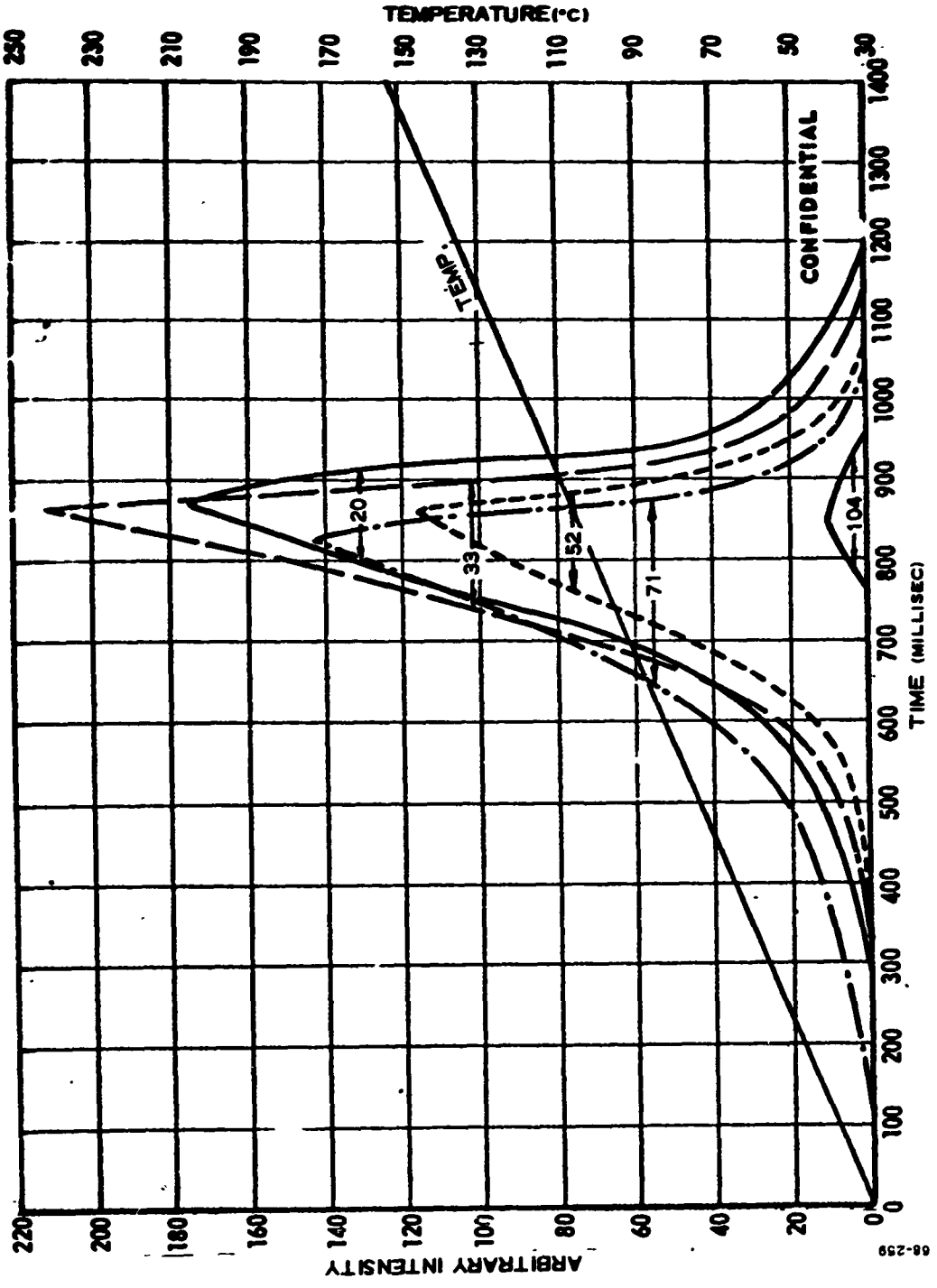

Figure 39 PBEP Pyrolysis Fragment History, Later Species, Dynamic FMTA

TABLE XI

ABUNDANCE OF N — F FRAGMENTS
FROM DYNAMIC FMTA OF
SAMPLE 9557-90

m/e	Observed I	I From Cracking: N_2F_4 (16)	NF_3 (14)
104	10	3.2	0
71	144	0	56
52	116	100	100
33	215	43	22

there could be again, as in the case of NF, a mode of formation of CNF^+ independent of the formation of $HCNF^+$. The species $H_2C_2F^+$ would require a rearrangement reaction not improbable in the time available. This point remains to be resolved.

(3) PBEP Pyrolysis Mechanism

(C) The thermal decomposition of PBEP in these experiments was characterized by the initial appearance of a few fragments at close to room temperature, followed by a sudden acceleration of the decomposition, and therefore rapid appearance of many fragments at approximately 75^0C. The expected fragments due to HF and NF_2 were not the first to appear, leading to the postulate that the unfluoraminated (impurity) fractions of the polymer were responsible for the early fragmentation. The initiation mechanism is shown in Figure 40. It is probable that the production of the free valencies by the loss of the initial fragments then leads to unzipping of the polymer chain. The small units (dimers at least) then are thermally split and/or split by the electron beam in the mass spectrograph. This sequence that also can explain the late appearance of HF, NF_3, and NF_2 is shown in Figure 41. The reasoning leading to these conclusions is summarized in the following paragraphs.

(C) Early production of HCNF, without concurrent production of HF, F, NF, or NF_2, can best be explained by the mechanism shown in I, Figure 40, in which the "impurity" group, HCNF, is detached from the polymer chain. Because the HCNF group is only one-eighth as abundant as NF_2 groups, some other mechanism may be responsible for the later production of HCNF. This mechanism, shown in Figure 41, also leads to the later production of HF and NF species.

(C) The HC=NF may have been formed from the normal H_2CNF_2 side-chain by the loss of HF during processing or storage. It is quite possible that these defect structures are concentrated in a definite molecular weight fraction of the finished bulk polymer, so that fractionation would result in fewer defects and hence more stable PBEP.

(C) Glycerol is the most probable terminal group for the PBEP polymer, as it is used in the initial preparation of the polymer from epichlorohydrin. However, in the process of dehydrochlorination, some of the end groups react and rearrange to form the methyl ether of ethylene glycol (Ref. 17). The presence of the ether linkage is shown by the mass peak m/e = 45, the characteristic 100 percent mass spectral peak for methyl ethers. The other features of the mass spectra also show that the parent fragment is the methyl ether of ethylene glycol. The reaction shown in II and III, Figure 40, shows how the glycerol and methyl-glycol ether can produce the observed mass spectral features. Once these groups are lost from a polymer chain, the resulting free valencies on the polymer backbone result in the rapid cleavages and rearrangements shown in Figure 41. The abundance of high m/e peaks can only be explained on the basis of high molecular weight species entering the electron beam of the mass spectrometer. It is not known if larger species than dimers are responsible because the mass range above 250 was not scanned. However, a dimer is the smallest unit that can satisfactorily account for all the species present.

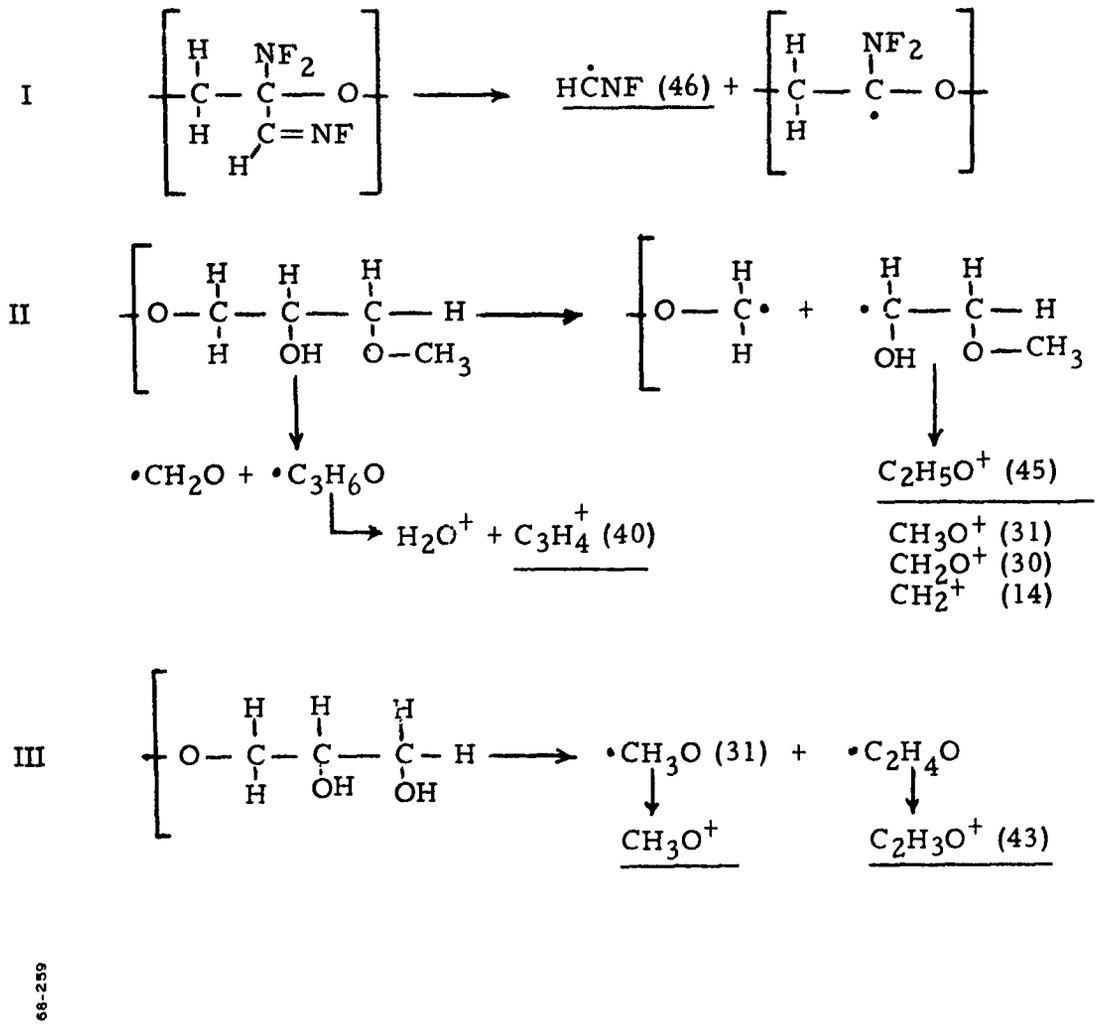

Figure 40 Initiation Mechanism, PBEP Dynamic FMTA, Sample 9557-90

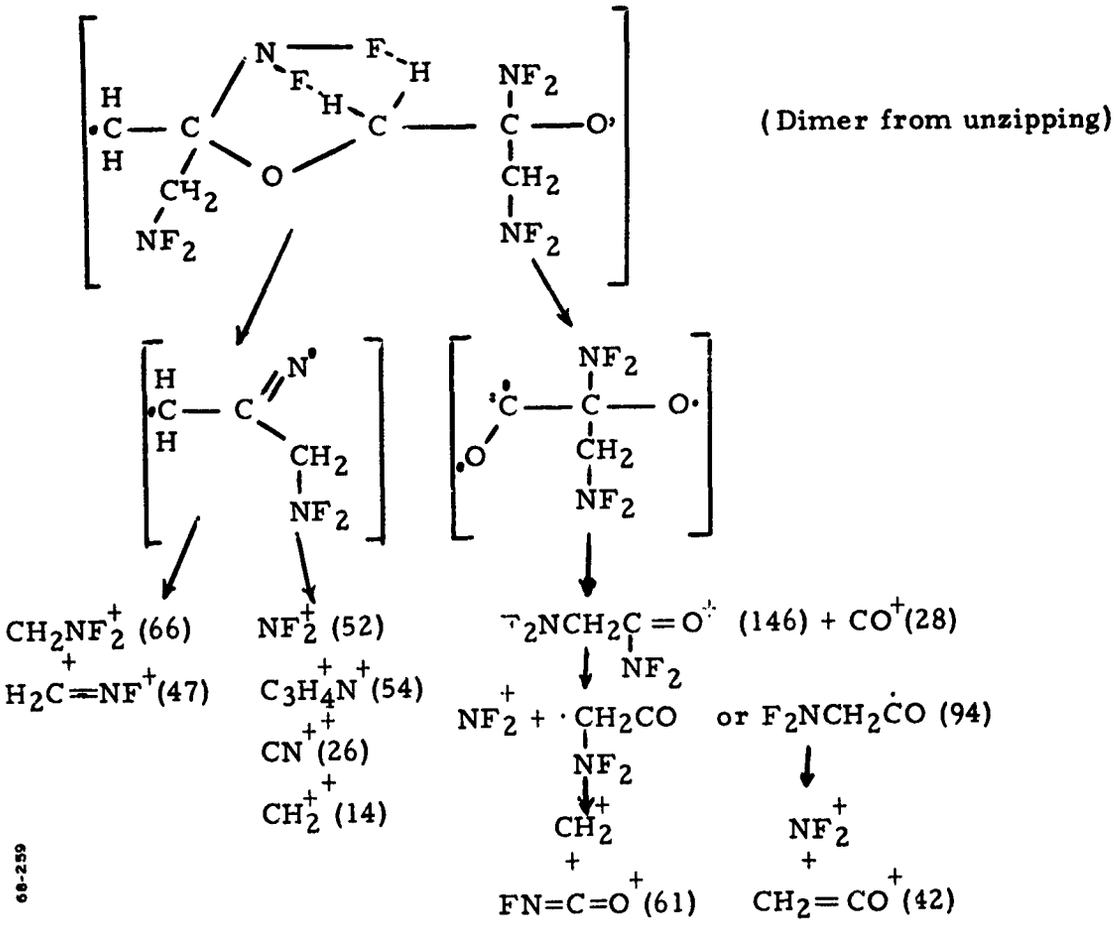

Figure 41 Later PBEP Decomposition Mechanism, Dynamic FMTA, Sample 9557-90

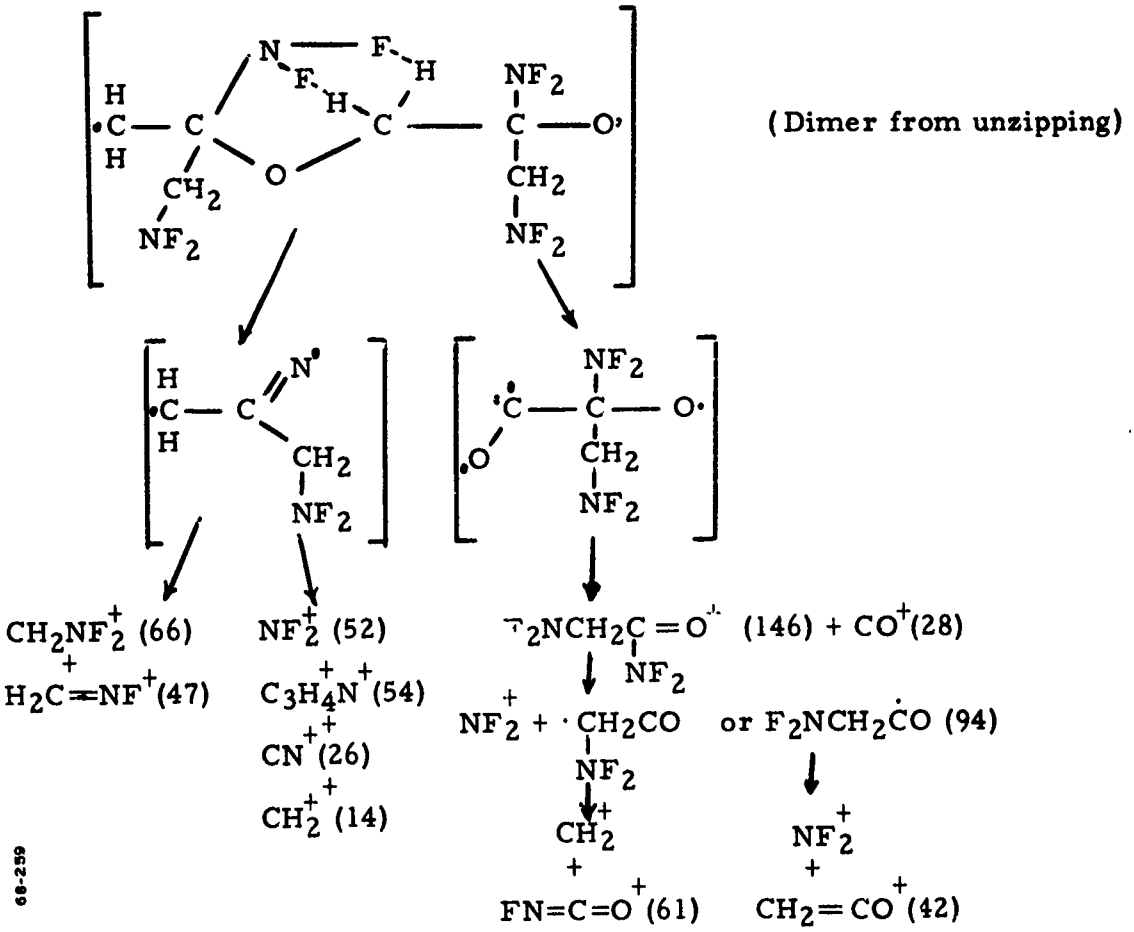

Figure 41 Later PBEP Decomposition Mechanism, Dynamic FMTA, Sample 9557-90

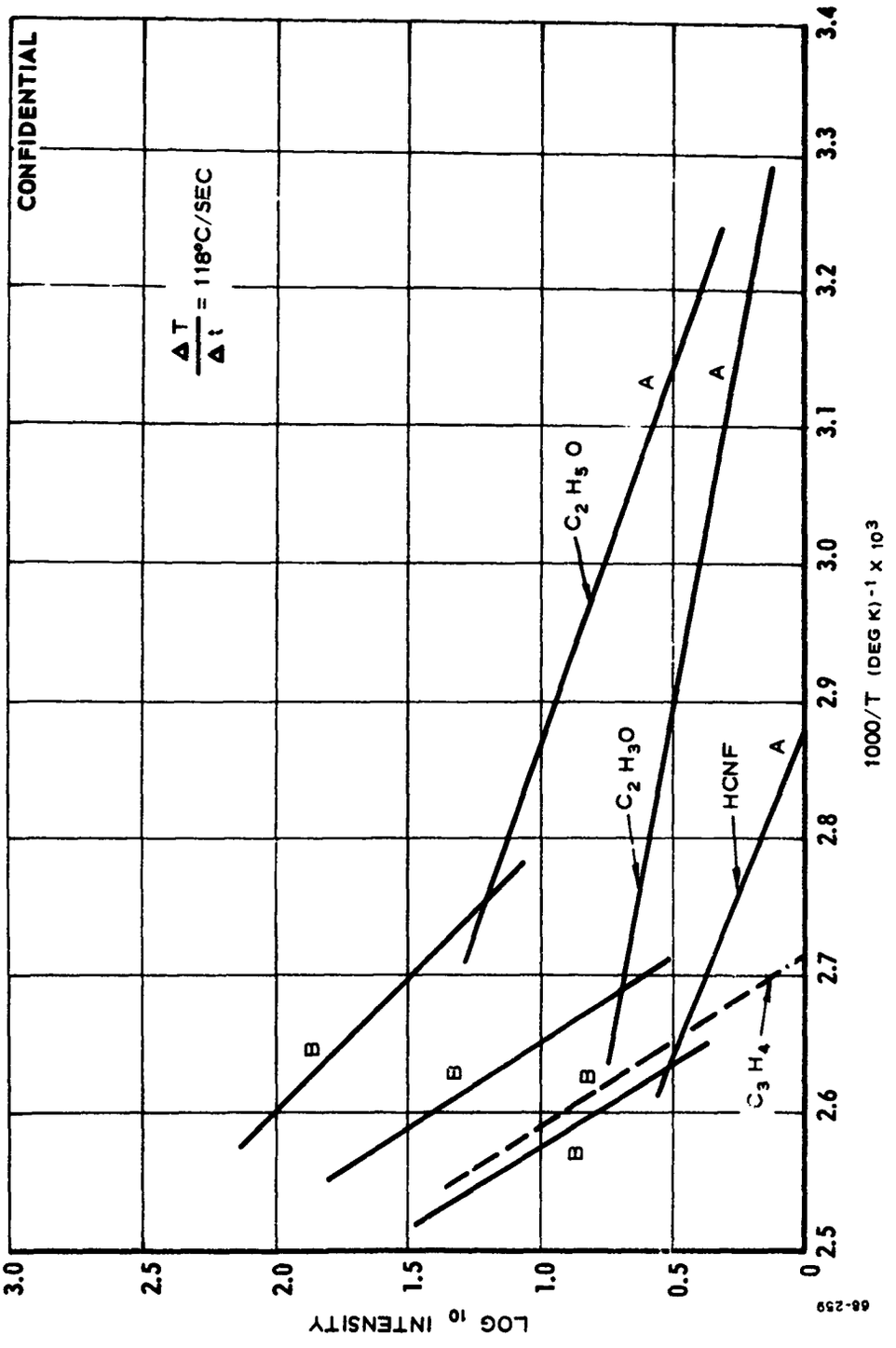

Figure 42 Arrhenius Plot for Initial PBEP Pyrolysis Species, Dynamic FMTA, Sample 9557-90

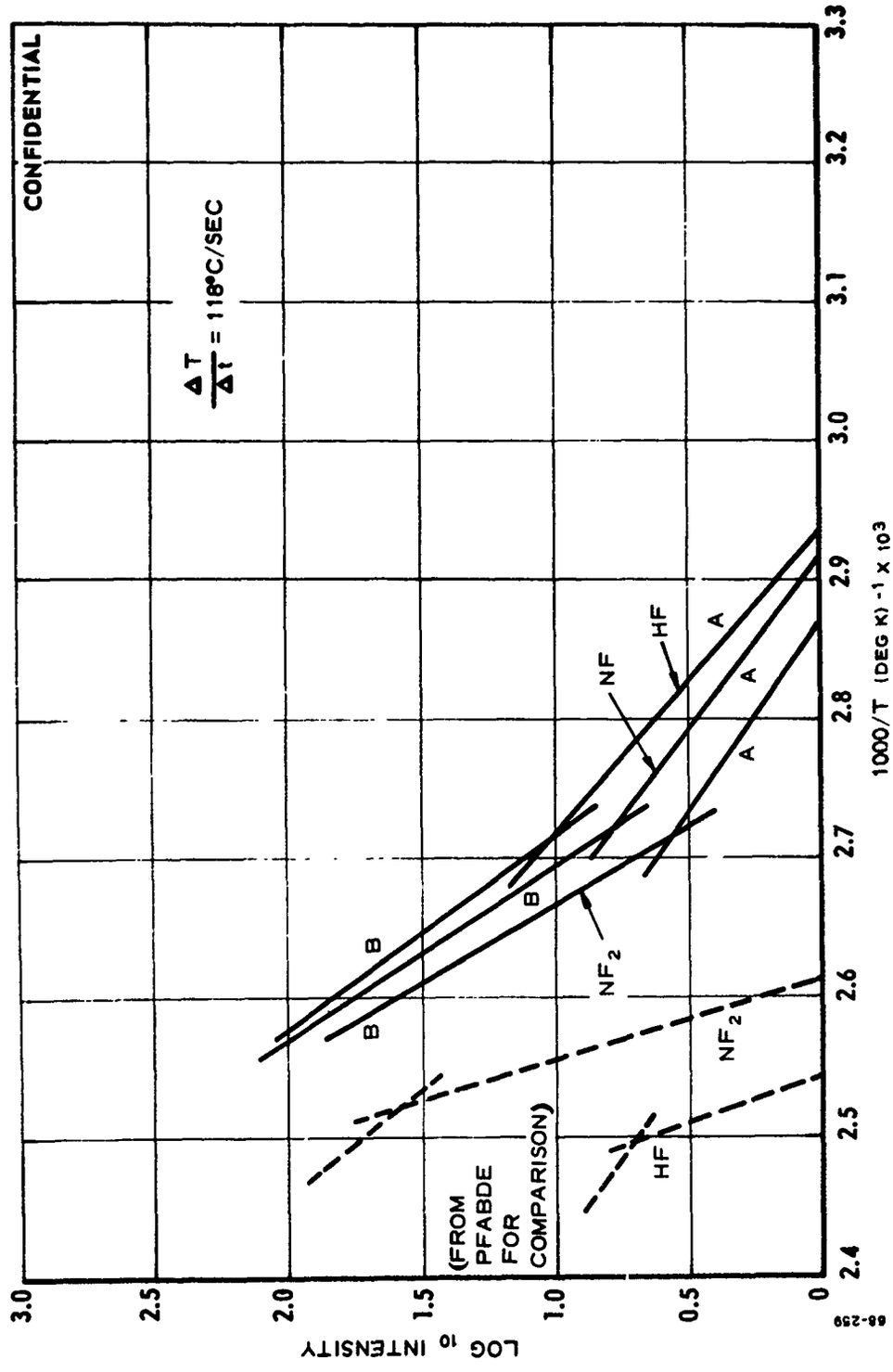

Figure 43 Arrhenius Plot for Later PBEP Pyrolysis Species, Dynamic FMTA, Sample 9557-90

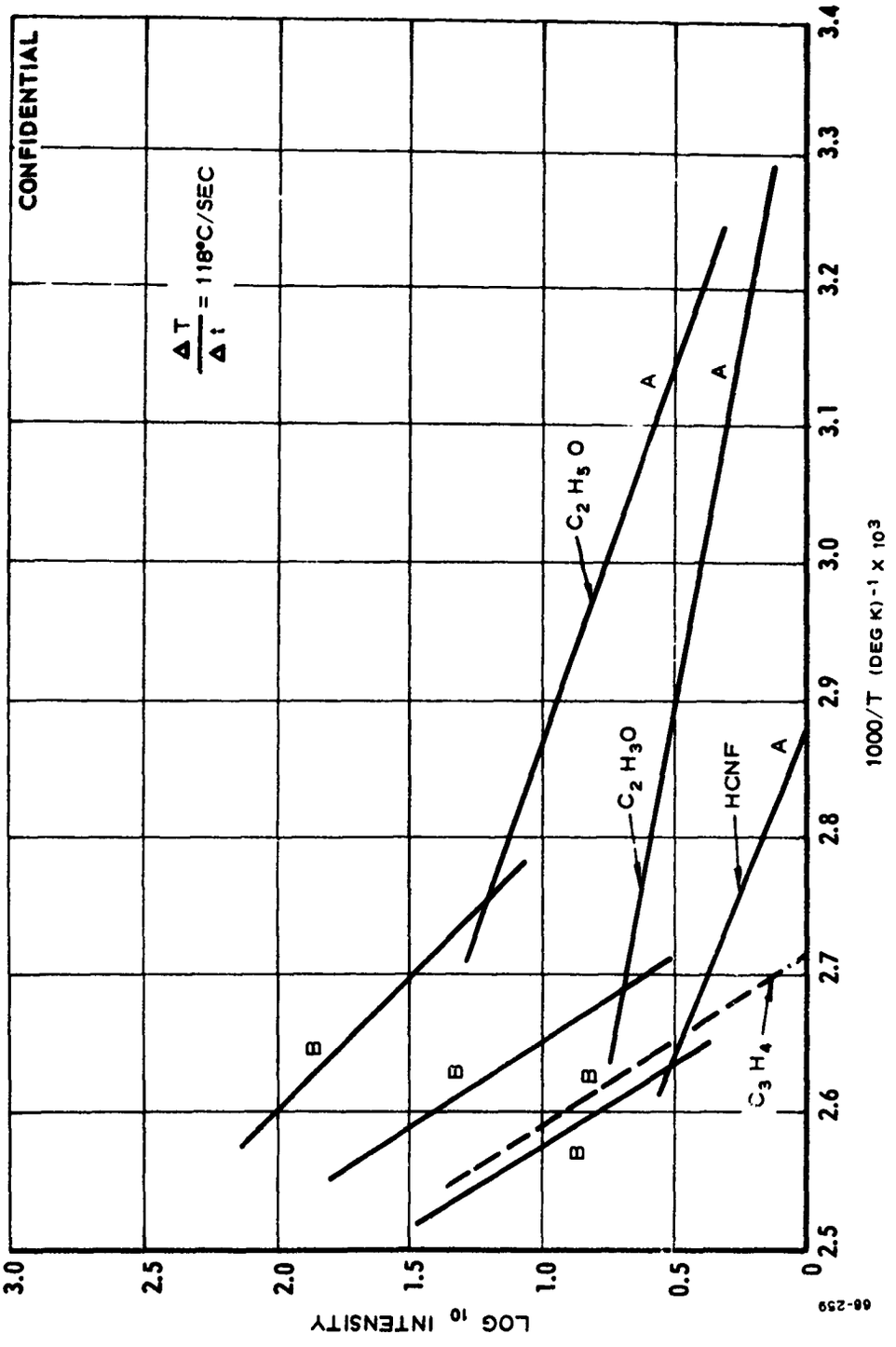

Figure 42 Arrhenius Plot for Initial PBEP Pyrolysis Species, Dynamic FMTA, Sample 9557-90

(U) In the following discussions, data from the previous section on PBEP sample number 9557-90 (-90) will be included for comparison. This sample was prepared by the "batch" process.

(C) Table XIII shows the temperatures of appearance of the first eight species from the pyrolysis of the fractions and the seven key species identified from the previous work, along with the temperatures of appearances of those seven key species from the previous work. Figure 44 presents the intensity histories of several of the species for all the samples. The outstanding feature of the new sample mass spectral histories is the dominant role played by the species responsible for m/e = 57. The remainder of the cracking patterns (not shown) associated with m/e = 57, indicates that this is because of epichlorohydrin (ECH) thermal fragments. Thus, the sample is either incompletely purified, and quantities of ECH and/or poly-ECH (PECH) are residual contaminants, or the precursor material has been incompletely polymerized, resulting in considerable amounts of ECH units in the finished polymer molecules. The presence of ECH in each of the polymer fractions tends to support the latter theory. As the temperature is increased, the 57 peaks for the fractionated polymer accelerate rapidly, and close together. However, the 35A sample proceeds at a slightly lower temperature than the remainder, indicating either a higher decomposition rate or a larger quantity of the ECH impurity.

(C) The m/e = 43, attributed to glycerol end groups in the previous work, appears at higher temperatures from samples -99-4, 35A, and 35B, than with the previous lot (-90). However, the -90 sample begins accelerating at a higher temperature, and hence would appear to be more stable above 340°K. Of the seven key species determined from the previous work, only m/e = 43 shows up in the first eight species from the fractionated samples. The remainder of the key species begin to appear at temperatures above 340°K.

(C) The methoxy species, responsible for m/e = 45 shows that all the new samples are more stable with respect to methoxy loss than the previous, with 35A being the most stable; -99-4 and 35B intermediate between -90 and 35A. The other four key species, NF, NF_2, and HCNF, all have similar behavior. The most stable towards loss of these species is 35B, with -99-4 nearly the same, while -90 is the least stable and 35A is intermediate between -90 and -99-4. For the HF species, -99-4 is most stable, with 35B approaching -99-4; -90 is the least stable with 35A closer to -90 than to the others.

(C) For the most part, the activation energies for each species production closely resembles that for the same species in the previous work (Table XIV). The notable exception is HF, for which the activation energy of only the high molecular weight fraction 35A was close to that of the original work. This implies that the HF is removed from different sites of the 35A fraction than from the 35B or -99-4 samples. A more detailed analysis of the data will be necessary to resolve this point.

(C) The ECH fragment yielded a much lower activation energy in the "high temperature" regime, than in the "low temperature" regime. This behavior has not been previously encountered in the PBEP studies. In

TABLE XIII

TEMPERATURES OF APPEARANCE OF SOME EARLY PBEP PYROLYSIS FRAGMENTS, DYNAMIC FMTA

Temperature (°K)	Mass Number of Species, from Sample No.: 10316 -99-4	9851 -35A	9851 -35B	9557 -90
304				43, 45
325		57		
325.5		43		
326	57	71		
327.5	43	59		
328	71	69		
328.5	59	55		
329	55	85	57	
330	85	71	43	
330.5	87		71	
331	69		59	
331.5			55	
332			69	
333			70	
334			85	
340		45	45	20, 33, 52
350	45		20	
355	20	20	52	46
360			33	
380	33	33, 46, 52		
395	52			
400	46		46	

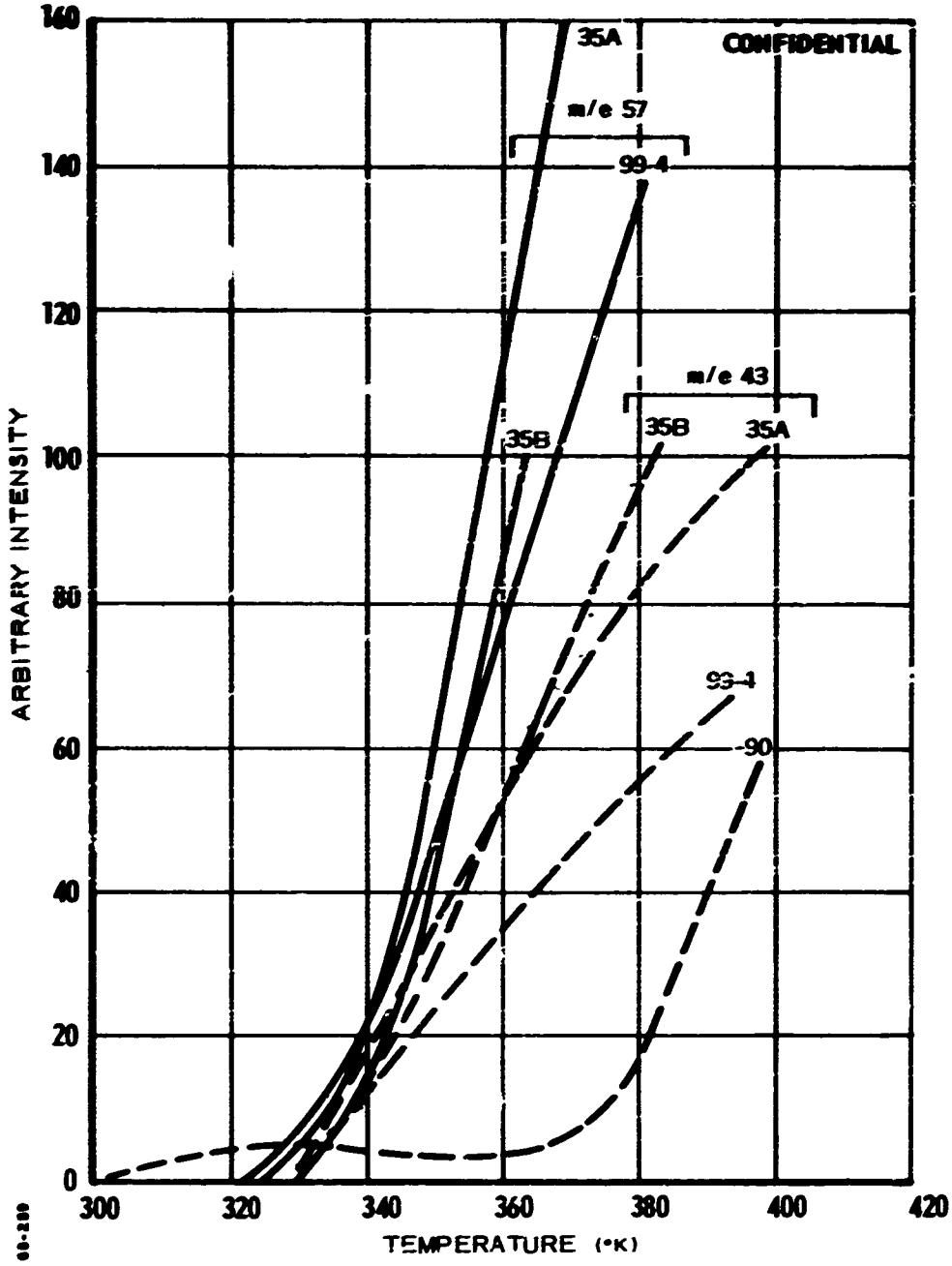

Figure 44 PBEP Fraction Pyrolysis Species, Dynamic FMTA

TABLE XIV

ACTIVATION ENERGIES FOR SEVERAL PYROLYSIS SPECIES FROM DIFFERENT PBEP SAMPLES BY DYNAMIC FMTA

M/e	Probable Species	Activation Energies, K Cal/mole, in the "High Temperature" Regime for Sample Nos:			
		-90	-90-4	-35A	-35B
20	HF	33	19	33	14
43	C_2H_3O	37	35	35	35
45	C_2H_5O	23	23	23	23
46	HCNF	38	40	40	40
52	NF_2	41	40	40	40
57	ECH*		8	8	8

*This species was unique among those PBEP fragments studied so far, because it possesses a much higher (25 K cal/mole) apparent activation energy in the "low temperatue" regime than in the "high temperature" regime.

reference to Table XII, it may be observed that the pyrolysis fragments possess lower activation energy in the "low temperature" regime than in the "high temperature" regime. This may well be a characteristic of the PECH starting material. Resolution of this point awaits the study of the PECH dynamic FMTA. Table XV presents the Shell analysis of Lot Nos. 10316-99-4, 9851-35A, and 9851-35B.

(C) Tables XVI and XVII show the simplest structures fitting the corresponding data. Note that in all cases, the data from Table XV indicates that assumption of only the two terminal groups and an "internal" methoxy besides the PBEP can account for the lot analysis. Because the FMTA data indicate large quantities of ECH, it must be assumed that the analyses were run by Shell on "cleaned up" samples, not on the overall sample. If not, then the Cl from ECH must have been grouped with the F from PBEP in the analysis. In either case, a separate Cl analysis is indicated.

e. Conclusions

(C) As in the PFABDE experiments, there appear to be different mechanisms responsible for the thermal decomposition of PBEP at different heating rates. During isothermal FMTA, important initial steps involve loss of NF_3 and HF, whereas during the dynamic FMTA, loss of end-groups and structural impurities appear to dominate.

(C) Once decomposition is initiated, the PBEP polymer appears to decompose by a free radical induced unzipping mechanism, proceeding smoothly to a maximum rate, without forming a temporarily stable solid product species. At this date, it appears as though the thermal stability of PBEP is strongly affected by impurities. These impurities can be present as structural defects introduced during production, processing or storage, or to "chemically" impure material because of inefficient cleanup of the finished product. In general, the thermal stability of an intermediate molecular weight polymer appears to be superior to either a "high" molecular weight fraction or to the "whole" polymer. However, the cause of instability of the latter may prove difficult to determine.

f. Comparison of PBEP and PFABDE Mechanisms

(U) The conclusions that can be reached by comparing the PFABDE and PBEP pyrolysis data are that PBEP polymer molecules decompose by a less complex, less energy-requiring mechanism than the more complex PFABDE polymer molecules. When decomposition begins, PFABDE decomposes at a faster initial rate than PBEP. The initiating mechanisms for both decompositions appear to involve terminal groups, although this appears to be of much greater importance for PBEP.

(C) Although PBEP is composed of smaller, less complex monomer units than is PFABDE, the decomposing PBEP mass spectrum is more complex and extends to higher mass numbers than does PFABDE. The pattern of species production also is different. HF, NF_3, and C_2H_5O appear to be important product species in the PBEP decomposition, but not in PFABDE decomposition, whereas COF is an important product species from the

TABLE XV

SHELL LOT ANALYSES, PBEP FRACTIONS

		Sample Number		
		10316 -99-4	9851 -35A	9851 -35B
Polymer Fraction (%)		100	29.6	21.9
Average Molecular Weight		3800	6700	5200
Weight percent of:				
	C	25.9	26.1	26.1
	H	3.2	3.2	3.3
	N	15.7	15.9	16.0
	F	41.4	41.1	41.4
(by difference)	O	13.8	13.7	13.2
OH equiv. /100 g		0.042	0.038	0.046
OH functionality		1.6	2.5	2.4
Thermal Stability, (cc/g/100 hrs. at 80°C)		4.8	5.4	5.7

TABLE XVI

"AVERAGE MOLECULAR STRUCTURES" FOR PBEP FRACTIONS

Species	Number of Species in "Average Molecule" for Samples 10316 -99-4	9851 -35A	9851 -35B
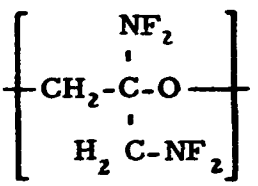	19	31	30
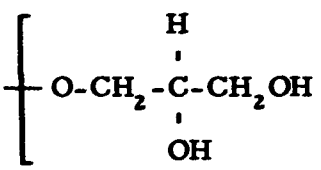	1	1	1
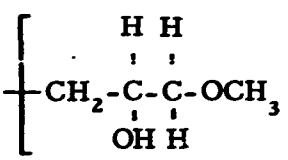	1	1	1
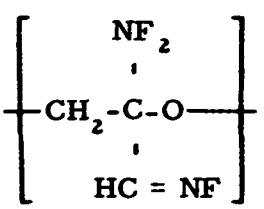	2	7	6
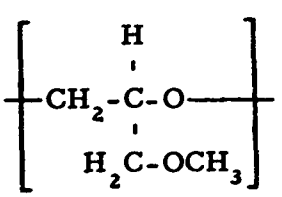	3	6	4

TABLE XVII

MASS BALANCES FOR "AVERAGE MOLECULAR STRUCTURES" OF PBEP FRACTIONS

Sample No.	Moles Atomic Species Required per Mole of "Average Polymer Molecule" C	H	O	N	F
10316-99-4					
a) from "Structure"	82	122	32	42	82
b) from Lot Analysis	82	122	33	42	82
9851-35A					
a) from "Structure"	145	216	55	76	145
b) from Lot Analysis	145	214	57	76	145
9851-35B					
a) from "Structure"	113	168	43	60	113
b) from Lot Analysis	113	172	43	60	113

decomposition of PFABDE, but not from PBEP. Some important similarities are that both NF^+ and NF_2^+ are important ions in the mass spectra from the decomposition of both PFABDE and PBEP, and NF^+ appears in both compounds to come from the parent species NF_2^+, and also from some other independent source.

(C) Some important qualitative differences in the decomposition modes were immediately noticeable. PFABDE decomposition began autoacceleration at approximately 120°C, whereas PBEP began at approximately 80°C -- 40°C lower. The PFABDE decomposition curves are characterized by double peaks, indicative of two different mechanisms.

(C) Decomposition mechanisms may be postulated that appear to account for the thermal decomposition behavior of PFABDE and PBEP. For PFABDE, the tris (NF_2) methoxy groups first lose one NF_2 per group, followed by loss of one methoxy group per pair, followed by a temporary stabilization through cyclization. A simultaneous attack at the end groups provides continuing decomposition at a relatively high activation energy with resulting relatively small decomposition fragments. For PBEP, no such stabilization is possible. The initial attack leaves free valencies on the backbone and at the ends, resulting in polymer "unzipping" and relatively large thermal fragments. Much of the PBEP instability appears to be due to "impurities" consisting of HCNF and methoxy groups on the polymer chain and of polymer terminating groups.

(C) It is of interest to compare PBEP activation energies (Table XII) with those of PFABDE (Table VI) obtained from similar treatments. PFABDE is another polymeric species containing a different structural arrangement of the NF_2 groups, and is more sensitive to impact than PBEP. The tables show that the activation energies for appearance of similar species are indeed different, especially in the lower temperature region. It is of interest to note that the higher activation energy of PFABDE results in a higher rate of acceleration of the reaction in the lower temperature region. For each degree centigrade temperature rise, the rate of acceleration of PFABDE decomposition is more than a thousandfold greater than that of PBEP.

(U) The activation energies estimated from the present data are consistent with the energies required to break the bonds associated with the polymer decomposition mechanism. These data are also consistent with Ubbelohde's (Ref. 9) observations that materials with high activation energies are more sensitive to detonation than material with low activation energies. Thus, it would appear that the only path open for PFABDE to decompose is by detonation, whereas PBEP can absorb energy by literally falling apart without detonation.

6. HYDRAZINIUM DIPERCHLORATE (HP_2) PYROLYSIS

(U) Dynamic FMTA of HP_2 (hydrazinium diperchlorate) show that the pyrolysis occurs in two distinct stages, similar to PFABDE and NC decompositions. The time-intensity curves shown in Figure 45 illustrate the double peaks typical of all ion fragments associated with the perchloric acid parent thermal decomposition fragments. The single peaks occurring

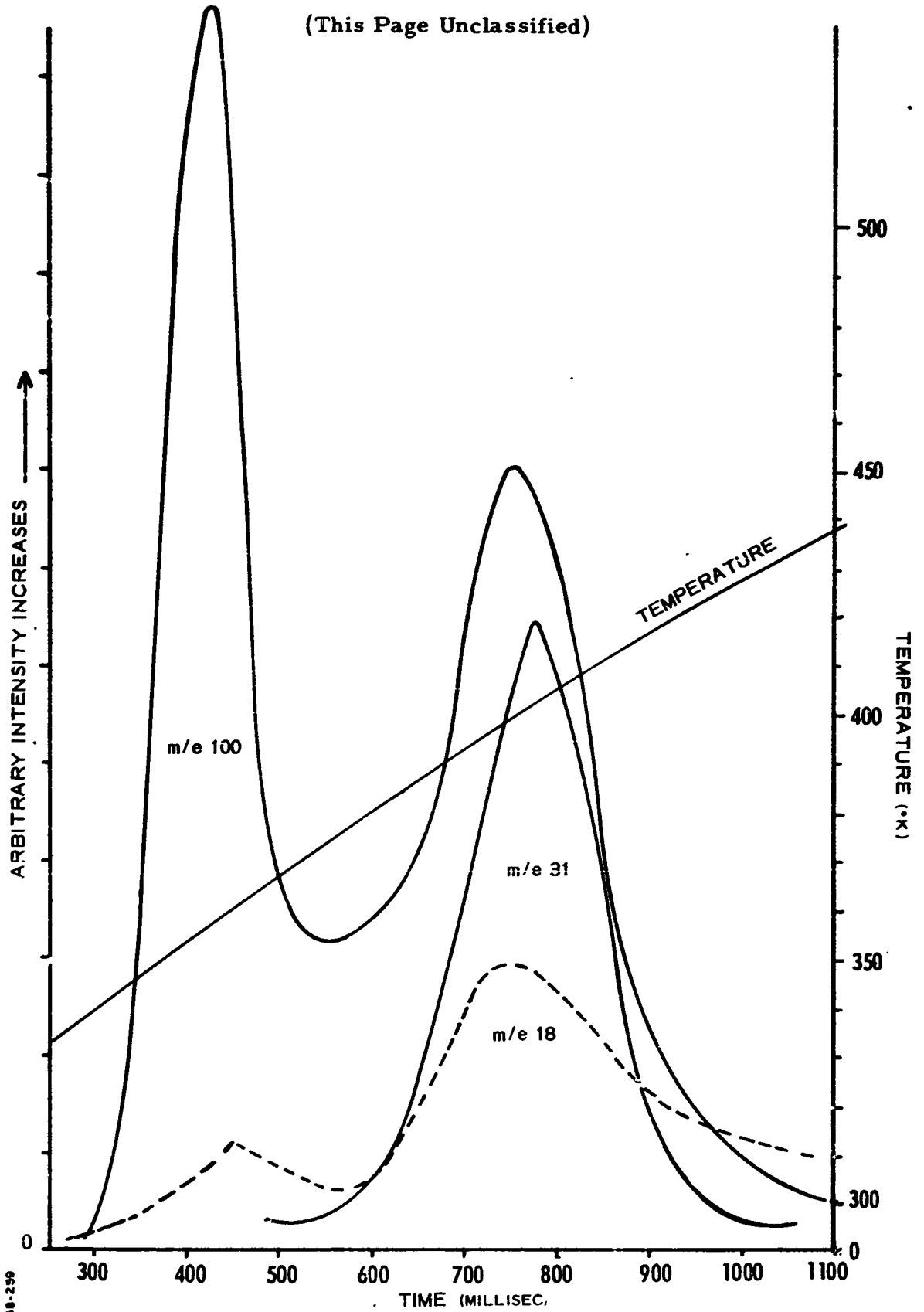

Figure 45 HP_2 Pyrolysis Fragment Histories, Dynamic FMTA

subsequently are typical of all ion fragments associated with the hydrazine thermal fragment. This behavior indicates that the first process involves splitting off $HClO_4$, followed by complete disruption of the molecule at still higher temperatures.

(U) Arrhenius plots for the $HClO_4$ (m/e 100) fragment and the hydrazine fragment $N_2H_3^+$ (m/e 31) are presented in Figures 46 and 47. The activation energies calculated from these plots are presented in Table XVIII. The activation energies and the Arrhenius plots show that the initial loss of $HClO_4$ begins with a low energy requirement, and converts to a high energy requirement at higher temperatures (somewhat similar to the behavior of PBEP). Subsequent production of $HClO_4$ at the second peak then proceeds with an activation energy approximately the same as that for the low temperature stage of the initial decomposition. Production of m/e 31 overlaps the first and second $HClO_4$ peaks and appears to require an intermediate, constant activation energy.

(U) As discussed previously, this activation energy of 23 Kcal/mole compares well with that obtained at RMD (Ref. 8). The mass spectral data obtained from the dynamic FMTA also are consistent with the reaction mechanism postulated by the RMD workers -- the initial peak is most likely caused by the loss of one $HClO_4$ moiety, leaving hydrazinium monoperchlorate (HP). The HP then vaporizes at the higher temperature, and yields its characteristic mass spectral cracking pattern.

7. NITROCELLULOSE (NC) PYROLYSIS

(U) The Arrhenius-type data treatment, previously used with PFABDE and PBEP thermal decomposition studies has been applied to the initial species found in the dynamic FMTA decomposition of NC. Figure 48 shows the intensity/time history of NC. The two-stage reaction mechanism is evident, as is the transposition of the roles of the ions at m/e 46 and 30. As before, the portions of the curves labeled "A" are obtained at early times (low temperature) and the portions labeled "B" are obtained at later times (higher temperatures). However, in the case of NC, these portions are for the first stage only.

(U) Figure 49 shows the results of the Arrhenius plot for portions A and B of the NC decomposition curve. The activation energies of 95 ± 5 Kcal/mole for the A portion and 16 ± 2 Kcal/mole for the B portion are in excellent agreement with the values of 100 Kcal/mole and 14 Kcal/mole reported by R. Musso (Ref. 18) of Hercules (ABL) for these same portions. This agreement with other data again confirms the correctness of the experimental approach and the validity of the assumptions made in the calculation of the activation energies.

(U) Because the NC "molecule" is very complex, and results in very complex mass spectra, the deduction of the decomposition mechanism was deferred.

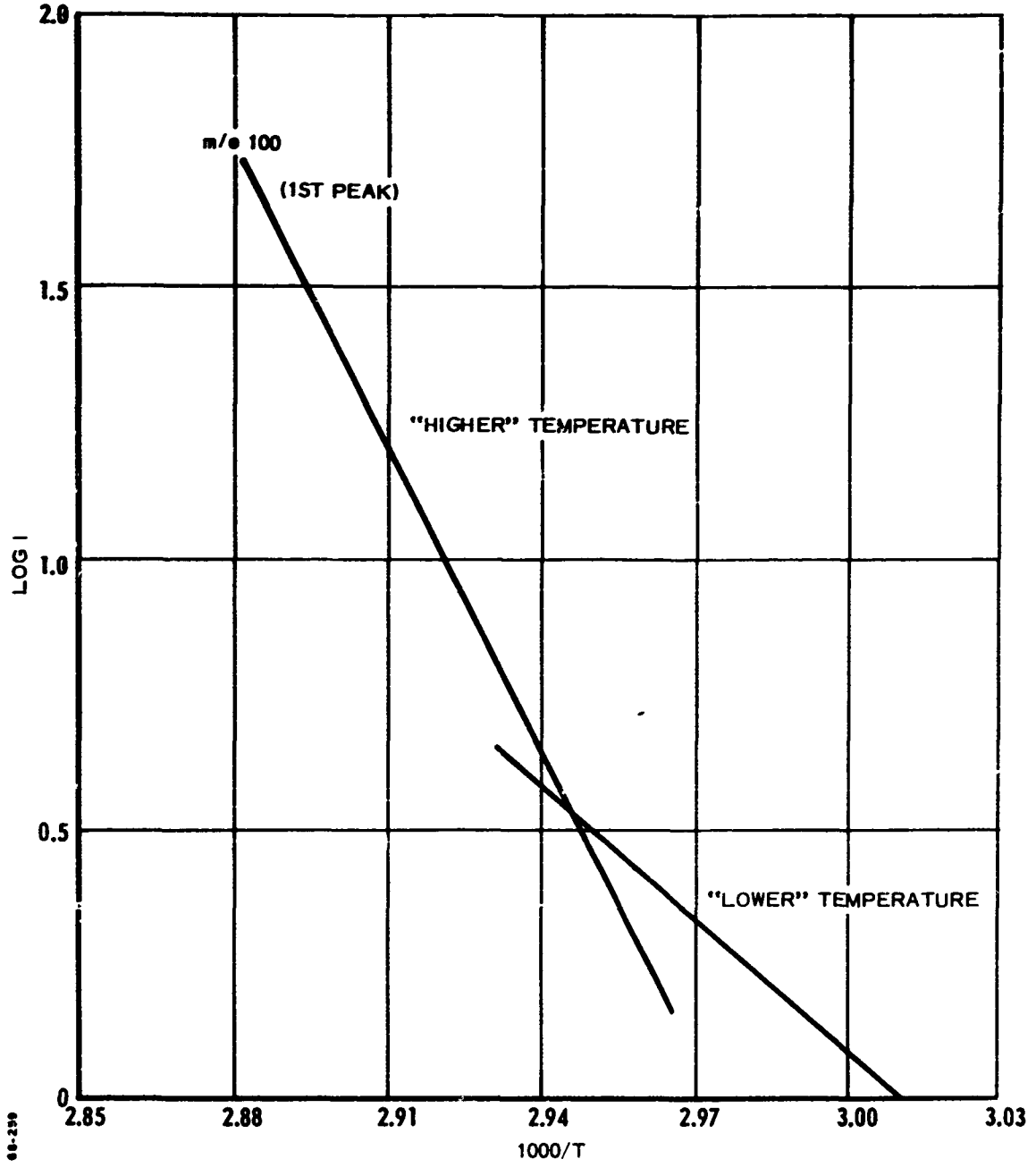

Figure 46 Arrhenius Plot of $HClO_4^+$ from Dynamic FMTA of HP_2

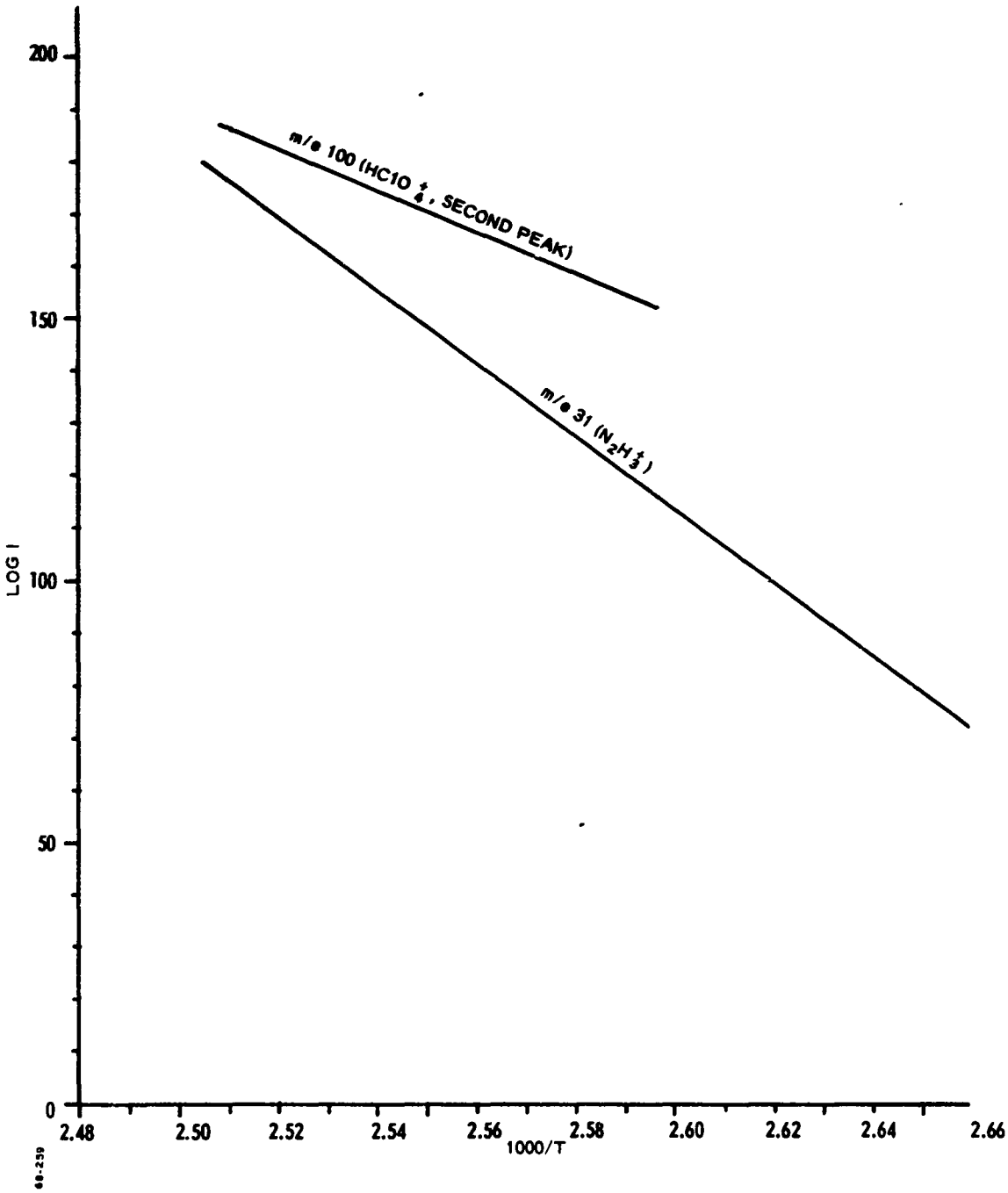

Figure 47 Arrhenius Plots for $HClO_4^+$ and $N_2H_3^+$ from Dynamic FMTA of HP_2

TABLE XVIII

ACTIVATION ENERGIES FOR HP_2 DECOMPOSITION SPECIES FROM DYNAMIC FMTA

Species	m/e	Activation Energies (K cal/mole) First Peak "Low T"	First Peak "High T"	Second Peak
$HClO_4^+$ (parent)	100	23	86	18
$N_2H_3^+$ (from $N_2H_4^+$)	31		32	

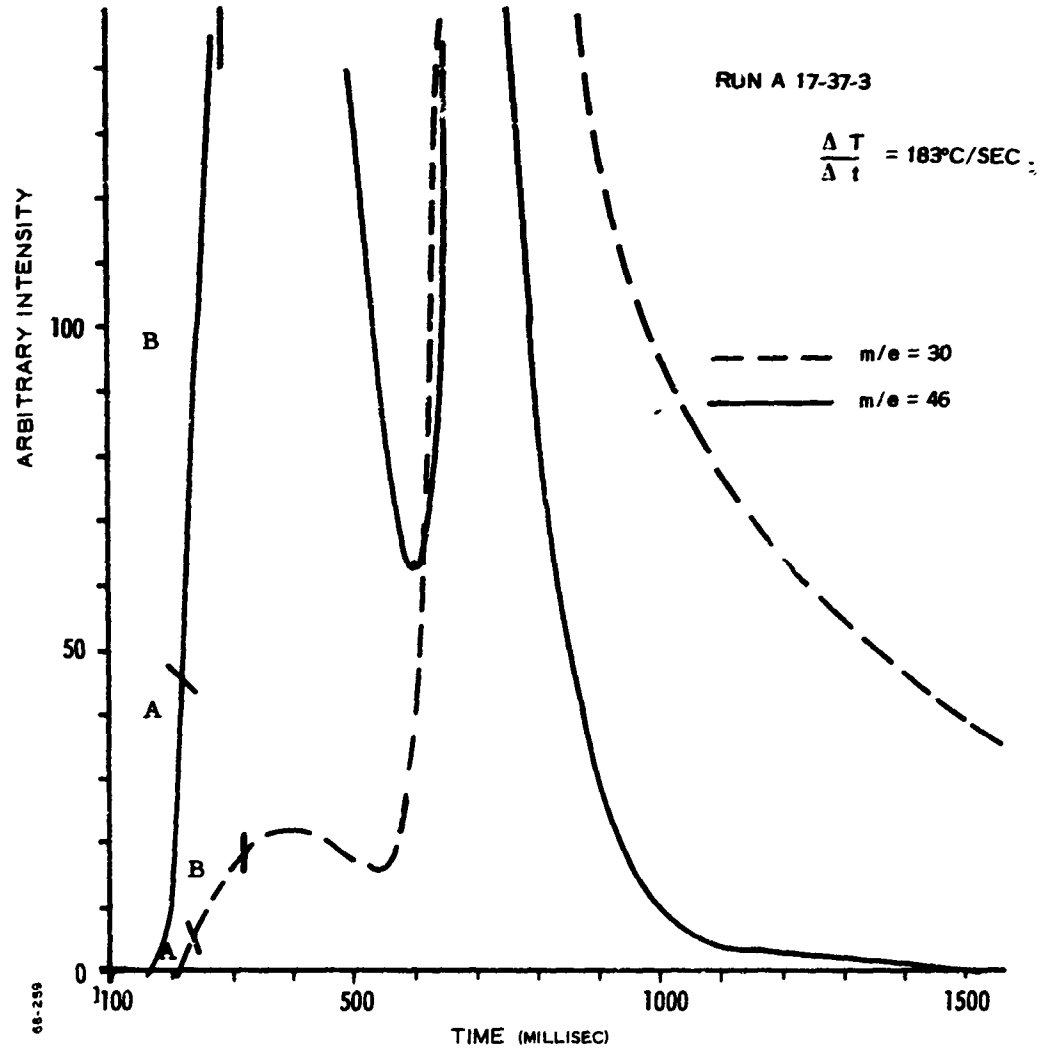

Figure 48 Dynamic FMTA of Nitrocellulose, Showing m/e 30 and 46

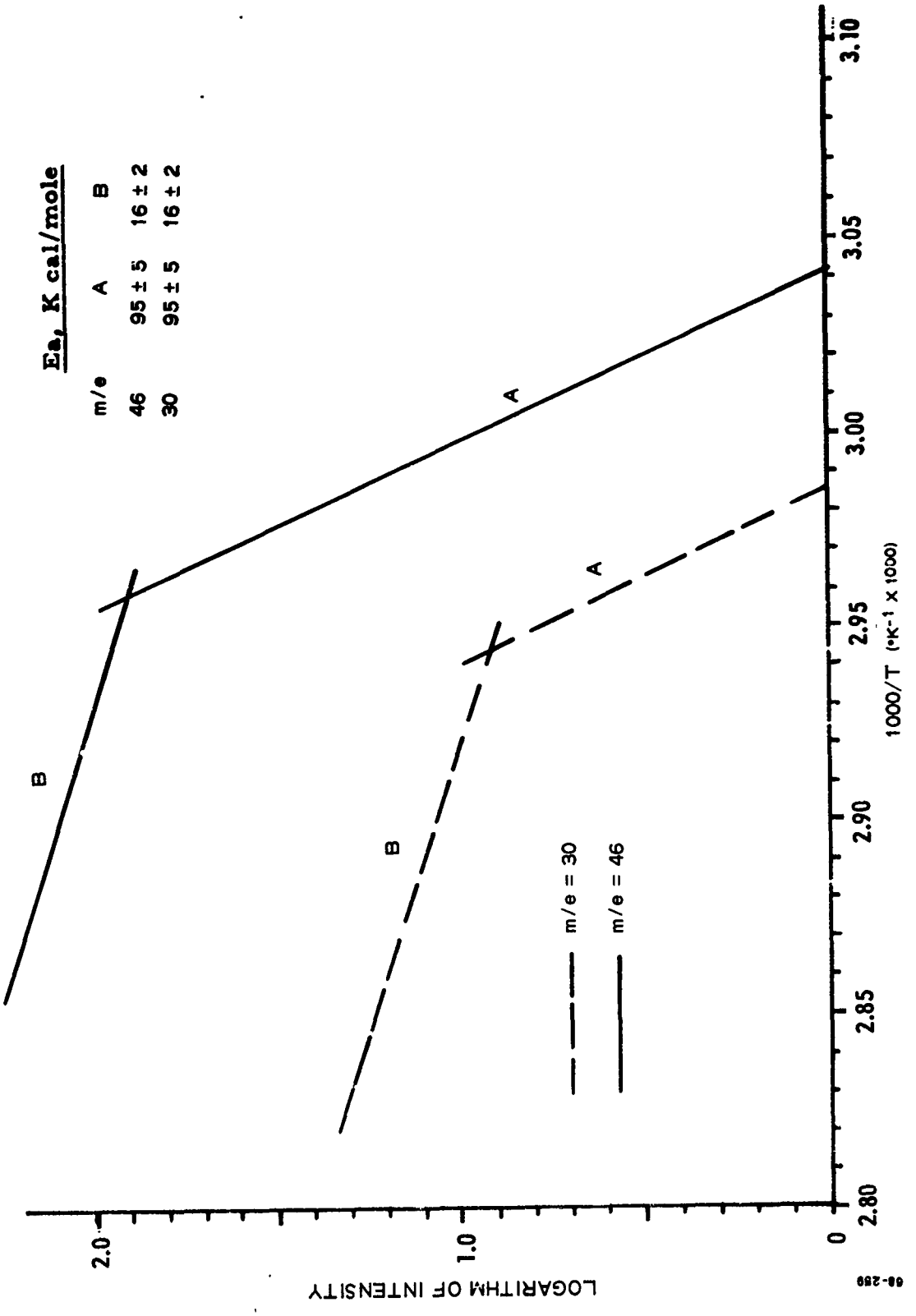

Figure 49 Arrhenius Plots for m/e 46 and 30 from Nitrocellulose Dynamic FMTA

REFERENCES

1. Lockheed Propulsion Company Final Report No. 641-F, Contract No. DA-04-495-AMC-239(R), 30 Dec 1965

2. Lincoln, T., NRDL TR-731, Mar 1964

3. O'Halloran, G.J., Fluegge, R.A., Betts, J.F., and Everett, W.E., Bendix Report No. 644, Apr 1964

4. Carslaw, H.S., and Jaeger, J.C., "Conduction of Heat in Solids," Oxford University Press, London, 1959

5. Clem, J.D., Jr., and Groetzinger, W.H., III, "An Analysis of Some Aspects of the Wenograd Thermal Stability Experiment," Rohm & Haas, Redstone Arsenal Research Division Report No. S-44, Mar 1964

6. Dergazarian, T.E., Dow Chemical Corporation, Private Communication, Dec 1967

7. Flynn, J.P., "Thermal Decomposition Studies on Poly FA-BDE," 4th Sensitivity Seminar on N-F Compounds, CPIA Publication No. 126, pp. 65-76, Sep 1966

8. Grelecki, C.J., and Cruice, W., "Thermal Decomposition of Hydrazinium Monoperchlorate and Hydrazinium Diperchlorate," Advanced Propellant Chemistry, ACS Advances in Chemistry Series 54, pp. 73-81, Washington, D.C., 1966

9. Ubbelohde, A.R., Trans. Roy. Soc. (London) 241 (A831) pp. 198-203, (1948)

10. Wenograd, J., "The Behavior of Explosives at Very High Temperatures," U.S. NOL, NAVWEPS Report No. 7328, Oct 1960

11. "Kinetics of Decomposition of Solid Oxidizers," Quarterly Technical Report No. 2, Dow NF-2Q-66

12. Heath, G.A., and Majer, J.R., RPE TN-219, Apr 1963

13. Gallegas, E., and Kiser, R.W., J. Am. Chem. Soc. 65, 1177 (1961)

14. Mass Spectra Data, API Research Project 44

15. Dinsmore, H.L., Meiklejon, R.A., and Weiblen, D.G., CPIA/ICRPG WGAC MB-21, Mar 1965

16. Schoenfelder, C.W., J. Chromatography 7, 281-7 (1962)

17. Hunter, L., and Ryder, E.E., "Energetic Binder Production," Shell Development Co., Emeryville, Cal., Report No. AFRPL-TR-67-131, Feb 1967

18. Musso, R., Hercules ABL, Private Communication, Oct 1967

(The reverse is blank)

CONFIDENTIAL
Security Classification

DOCUMENT CONTROL DATA - R & D

(Security classification of title, body of abstract and indexing annotation must be entered when the overall report is classified)

1. ORIGINATING ACTIVITY (Corporate author)	2a. REPORT SECURITY CLASSIFICATION
Lockheed Propulsion Company A Division of Lockheed Aircraft Corporation P.O. Box 111, Redlands, California 92374	CONFIDENTIAL 2b. GROUP

3. REPORT TITLE

Kinetics of Decomposition of Solid Oxidizers

4. DESCRIPTIVE NOTES (Type of report and inclusive dates)

Final Report 720-F; 1 December 1965 to 31 January 1968

5. AUTHOR(S) (First name, middle initial, last name)

Baumgartner, W.E.; Myers, G.; Stapleton, G.; Koehler, W.;
Tajima, Y.A.; and Hammond, J.A.

6. REPORT DATE	7a. TOTAL NO. OF PAGES	7b. NO. OF REFS
February 1968		18

8a. CONTRACT OR GRANT NO.	9a. ORIGINATOR'S REPORT NUMBER(S)
AF 04(611)-11385	LPC 720-F
b. PROJECT NO.	
c.	9b. OTHER REPORT NO(S) (Any other numbers that may be assigned this report)
d.	

10. DISTRIBUTION STATEMENT Qualified requesters may obtain copies of this report from DDC. This document is subject to special export controls and each transmittal to foreign governments or foreign nationals may be made only with prior approval of AFRPL (RPPR/STINFO), Edwards, California 93523.

11 SUPPLEMENTARY NOTES	12. SPONSORING MILITARY ACTIVITY
	Air Force Rocket Propulsion Laboratory Research and Technology Division Air Force Systems Command United States Air Force, Edwards, Calif.

13. ABSTRACT

This document is the final report on work performed under Air Force Contract AF 04(611)-11385 during 1966 and 1967. Fast vacuum pyrolysis techniques were combined with a Bendix Time-of-Flight mass spectrometer for the study of the initial reactions occurring during Thermal decomposition in INFO-635, PFABDE, PBEP, NC, and HP_2. Primary decomposition mechanisms were postulated, and activation energies calculated. Indications for a heating rate dependence of the decomposition mechanisms were found for INFO-635, PFABDE, and PBEP.

DD FORM 1 NOV 65 1473

CONFIDENTIAL
Security Classification

14. KEY WORDS	LINK A		LINK B		LINK C	
	ROLE	WT	ROLE	WT	ROLE	WT
INFO-635						
PFABDE						
PBEP						
Nitrocellulose						
Hydrazinium Diperchlorate						
High Energy Oxidizers						
Mass Thermal Analysis						
Pyrolysis						
Decomposition Kinetics						
Activation Energy						
Flash Heating						
Mass Spectrometry						
Reaction Mechanisms						
Primary Species						
Vacuum Degradation						
Thermal Stability						